LBL-28981

Lawrence Berkeley Laboratory
UNIVERSITY OF CALIFORNIA

Nuclear-Decay Studies of Neutron-Rich Rare-Earth Nuclides

R.M. Chasteler
(Ph.D. Thesis)

April 1990

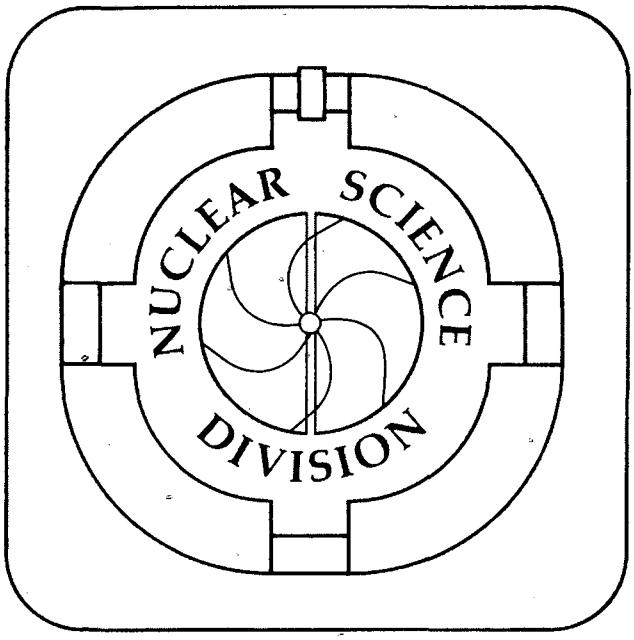

Prepared for the U.S. Department of Energy under Contract Number DE-AC03-76SF00098.

DISCLAIMER

LBL-28981

Nuclear-Decay Studies of Neutron-Rich Rare-Earth Nuclides

by

Robet Mark Chasteler

Ph.D. Thesis

(April 26, 1990)

Department of Chemistry

University of California, Berkeley

and

Nuclear Science Division

Lawrence Berkeley Laboratory

1 Cyclotron Road

Berkeley, CA 94720

This work was supported by the Director, Office of Energy Research, Division of Nuclear Physics of the Office of High Energy and Nuclear Physics of the U.S. Department of Energy under Contract No. DE-AC03-76SF00098.

Nuclear-Decay Studies of Neutron-Rich Rare-Earth Nuclides

Robert Mark Chasteler

ABSTRACT

Neutron-rich rare-earth nuclei were produced in multinucleon transfer reactions of ^{170}Er and ^{176}Yb projectiles on ^{nat}W targets at the Lawrence Berkeley Laboratory SuperHILAC and their radioactive decays properties studied at the on-line mass separation facility OASIS. Two unknown isotopes, ^{169}Dy ($t_{1/2} = 39 \pm 8$ s) and ^{174}Er ($t_{1/2} = 3.3 \pm 0.2$ m) were discovered and their decay characteristics determined. The decay schemes for two previously identified isotopes, ^{168}Dy ($t_{1/2} = 8.8 \pm 0.3$ m) and ^{171}Ho ($t_{1/2} = 55 \pm 3$ s), were characterized. Evidence for a new isomer of 3.0 m ^{168}Ho^{g}, ^{168}Ho^{m} ($t_{1/2} = 132 \pm 4$ s) which decays by isomeric transition (IT) is presented. Beta particle endpoint energies were determined for the decay of ^{168}Ho^{g}, ^{169}Dy, ^{171}Ho, and ^{174}Er; the resulting Q_{β^-} values are: 2.93 ± 0.03, 3.2 ± 0.3, 3.2 ± 0.6, and 1.8 ± 0.2 MeV, respectively. These values were compared with values calculated using recent atomic mass formulae. Comparisons of various target/ion source geometries used in the OASIS mass separator facility for these multinucleon transfer reactions were performed.

DEDICATION

This thesis is dedicated to my two best friends who supported me during the writing stage. Their words of encouragement convinced even me that I could finish it. If it wasn't for their support and encouragement, I wouldn't have received any and this thesis would never have been completed. Lauren and Lisa, I thank you both from the bottom of my heart and am indebted to you for the rest of my life.

ACKNOWLEDGEMENTS

This work was supported by the Director, Office of Energy Research, Division of Nuclear Physics of the Office of High Energy and Nuclear Physics of the U.S. Department of Energy under Contract No. DE-AC03-76SF00098. The support of the Nuclear Science Division of Lawrence Berkeley Laboratory and the Chemistry Department of the University of California, Berkeley.

I would like to thank Prof. Darleane Hoffman for the opportunity given to me in learning nuclear chemistry and graduate research. The first three years of my six year graduate career were spent under Darleane's guidance. Even though the research I performed during that time is not contained in this thesis, the tools and skills I learned then were invaluable in compiling this work. I would like to thank the other members of the LBL Heavy Ion Radiochemistry Group I worked with (D. Lee, M. Nurmia, K. Gregorich, R. Henderson, C. Gannett, D. Bennett, and R. Chadwick) for their assistance.

I am indebted to the OASIS group (M. Nitschke, P. Wilmarth, K. Vierinen, R. Firestone, and A. Shihab-Eldin) for helping me perform the experiments of this thesis. The last three years of my graduate career were spent working with and learning from these fine scientists. A special thanks goes to Phil W. and Kari V. for their guidance and direction when I first joined the group. If it wasn't for their help I would have floundered around for at least a year and delayed this work by at least as much time. Also, I wish an extra thanks to Phil W. for the help preparing this thesis in running the Macintosh and providing some figures.

The outstanding technical support of L. Archambault and A. Wydler in keeping OASIS running whenever it was needed is acknowledged. I would also like

to extend an extra thanks to L. Archambault for providing the CAD drawing of the OASIS ion source used in Figure 3.4. The assistance of the staff and crew of the SuperHILAC is also noted.

Last, but not least, I owe a thanks to all my friends, family, and roommates (past and present) for their friendship and support during my graduate career. I will not even try to name you all, for I will certainly forget someone. A big thank-you is sent to you all for helping keep my sanity in Berkeley.

TABLE OF CONTENTS

LIST OF FIGURES

LIST OF TABLES

1. INTRODUCTION

This investigation is concerned with the synthesis and decay studies of neutron-rich rare-earth nuclei. Nuclear-decay information for neutron-rich isotopes has important applications to astrophysical problems and reactor technology. Neutron-binding energies and nuclear half-lives are the most important parameters needed for calculations of astrophysical nucleosynthesis. Nuclear half-lives of neutron-rich isotopes are particularly critical in the case of rapid neutron capture (the *r*-process). During the *r*-process, in the enormous neutron flux inside of stars, the time required for a nucleus to capture a neutron is very short compared to beta decay times and the neutron exposure time is many times longer than the beta decay half-lives so that successive beta decays can take place during bombardment. During supernova explosions, neutron fluxes reach high enough levels, for short periods of time, that "prompt" capture processes occur in which neutrons are quickly added to a nucleus until the product is at the neutron-drip line (point where the neutron-binding energy equals zero). Both the *r*-process and "prompt" capture process result in the flow of nucleosynthesis along the neutron-drip line [Cow70]. Peaks in the mass abundance distribution occur around masses 80, 130, 165, and 194 where the *r*-process reaches magic neutron shells and further neutron capture is hindered due to the low neutron-binding energy. The mass flow moves along these neutron numbers because of β^- decay and subsequent neutron capture back towards the magic neutron numbers.

With the neutron-drip line approximately 50 mass units away from the known isotopes in the rare-earth region, astrophysicists have to depend heavily on half-life predictions for their calculations. At the start of this research, two sets of half-life

estimates for large numbers of neutron-rich nuclei existed. Takahashi, Yamada, and Kondoh [Tak73] calculated beta decay half-lives using the gross theory of beta decay. Klapdor, Metzinger, and Oda [Kla84] used calculations incorporating a detailed treatment of beta strength functions. In general, the calculations of Takahashi, Yamada, and Kondoh overestimate and the calculations of Klapdor, Metzinger, and Oda underestimate half-lives of nuclei in the neutron-rich rare-earth region. The deviations from the experimental half-lives at times approach an order of magnitude resulting in large uncertainties in the calculation of astrophysical nucleosynthesis.

Decay information for these neutron-rich isotopes is also important in developing and testing nuclear theory. Theoretical calculations of nuclear level energies [Nil69, Möl89] and deformations [Möl81] are used in predicting β strength functions and ground-state spins and parities. Also numerous calculations of atomic masses have been made [Möl81, Hau88 (and references therein)] with varying results. Since most of these calculations depend on measured masses, spins, and parities to determine the best parameter sets for their models, new decay information is always needed. Also, half-life prediction codes [Tak73, Kla84] are dependent on the atomic masses used.

The present investigation is concerned with the decay properties of neutron-rich rare-earth nuclei with masses greater than A~160. There is very little information known about nuclei in this important region. Prior to about 1980, nuclei of only two neutrons more or two protons less than the most neutron-rich stable isotopes were known for this region. These were made using relatively simple reactions (i.e. (n,γ), (n,α), (n,p), (γ,p), (p,2p), (p,3p), and (t,p)) which could be performed with nuclear reactors, neutron generators, and Van de Graaff accelerators.

After approximately 1980, two new methods of producing neutron-rich rare-earth isotopes with A>160 were investigated; fission of heavy actinides and multinucleon transfer reactions.

The fission of heavy actinides proves to be very efficient in producing new neutron-rich isotopes of the rare-earth elements from Ce (Z=58) to Tb (Z=65) [Mac86, Gre87, Kaw88, and references therein]. Thermal neutron fission of ^{235}U has been used at Brookhaven National Laboratory (BNL) to produce isotopes with masses up to A=161 [Mac86]. However, their research is limited by the mass yields from thermal neutron fission of ^{235}U which drops drastically above mass A=160 (Figure 1.1). Researchers at Idaho National Engineering Laboratory (INEL) have used the spontaneous fission of ^{252}Cf as a production source of neutron-rich rare-earth nuclei [Gre87]. The extra 16 nucleons in ^{252}Cf as compared to $^{235}U + n_{thermal}$, shifts the heavy mass tail up about 10 atomic mass units as seen in Figure 1.1. This shift has allowed INEL to investigate neutron-rich rare-earth isotopes up to mass A=168 [Geh82].

In the early 1980's, researchers at Gesellschaft für Schwerionenforschung (GSI) started using multinucleon transfer reactions to produce new neutron-rich nuclei of heavy rare-earths and nuclei lighter than the group of light fission products (A=52-79) [Run85]. In the case of heavy rare-earths, $^{nat}W/Ta$ or $^{186}W/Ta$ targets were bombarded with ^{136}Xe and ^{238}U ions at 11.5 MeV/u [Ryk89]. Since ^{136}Xe is an N=82 nuclide with six stable N=82 stable isotones with atomic numbers greater than 54 (Xe), one expects some preference for the pick-up of protons from the target nucleus. The increased N/Z-ratio of the ^{238}U projectile should enhance the production of neutron-rich nuclei compared with lighter projectiles. Both projectiles, ^{136}Xe and ^{238}U, have been successful in producing neutron-rich rare-earth nuclei

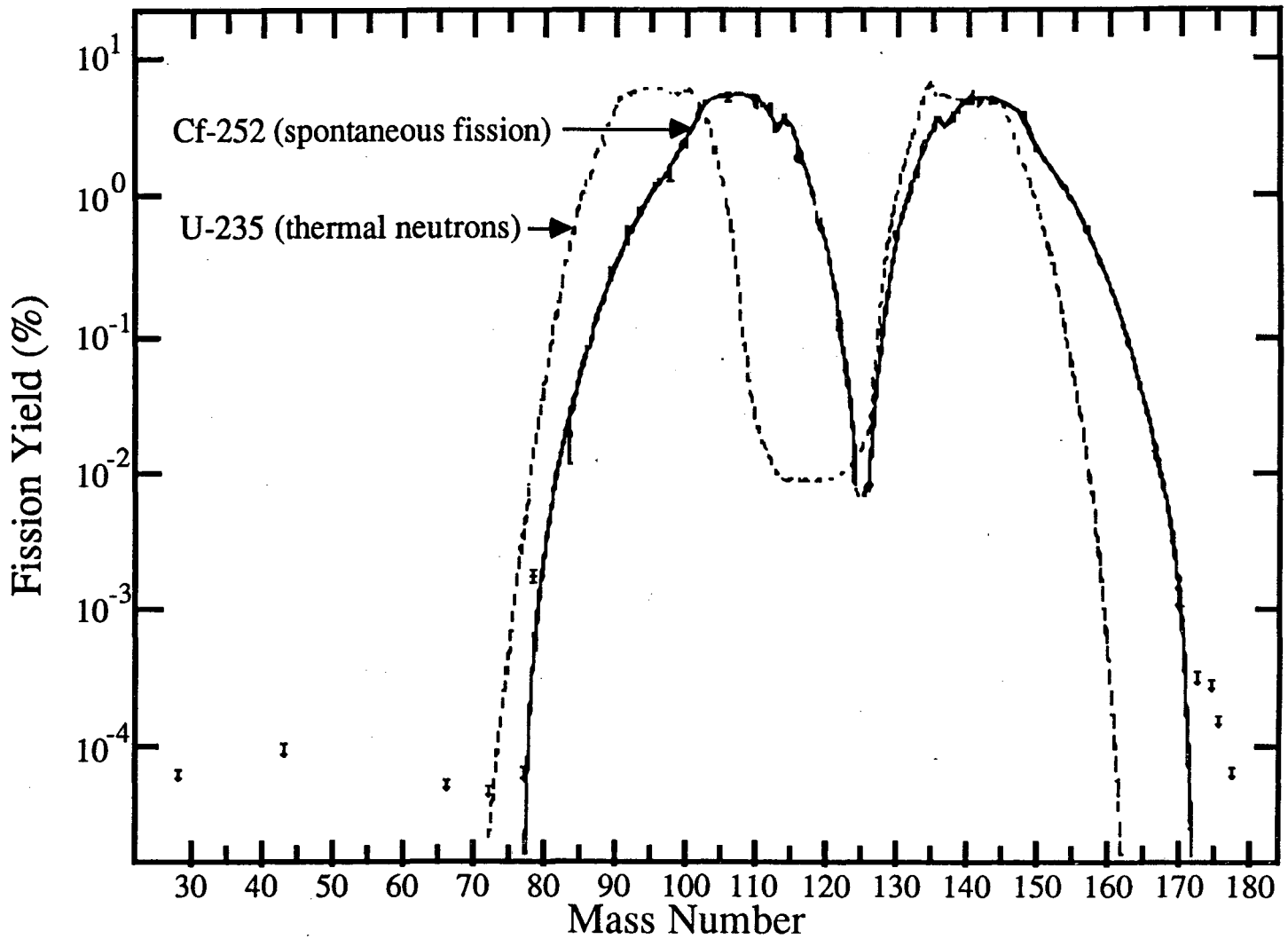

Figure 1.1. Spontaneous fission yield from Cf-252 as compared with the yield curve for the thermal neutron fission of U-235. Curves are taken from Hyde [Hyd71].

having masses A=177-184 with similar production yields [Ryk89]. ^{136}Xe has proven to be the only projectile to produce the lighter masses A=171, 172, and 174 [Ryk89, Mei89]. For the production of nuclei below the group of light fission products [Run85], a different method of isotope production was used. Because GSI's mass separator ion source requires heavy refractory materials, like W or Ta, for non-compound nucleus reactions, target-like fragments in the A~65 region can not be produced. However, using neutron-rich beams, near the desired nuclei, on $^{(nat\ or\ 186)}$W/Ta targets, neutron-rich projectile-like fragments can be produced. In these reactions, the target picks up protons from the projectile, though, not with the same affinity as ^{136}Xe. Researchers at GSI has used ^{76}Ge and ^{82}Se beams to produce ^{60}Cr, ^{61}Mn, ^{64}Fe, ^{65}Co, ^{69}Ni, and ^{73m}Zn [Run85, Bos88] using this method of projectile-like fragment production.

In the current investigation, multinucleon transfer reactions were used to produce new neutron-rich rare-earth nuclei. However, instead of looking at the target-like fragments in this region as did researchers at GSI, projectile-like fragments of ^{170}Er and ^{176}Yb [Cha89] beams were produced as was done at GSI in the A=60-73 region with ^{76}Ge and ^{82}Se beams. Using the OASIS facility [Nit83] on-line at the Lawrence Berkeley Laboratory SuperHILAC for mass separation and detection of the products, two new isotopes, ^{169}Dy and ^{174}Er, and one new isomer, ^{168}Ho^{m}, were identified. Also, the decay schemes for two previously identified isotopes, ^{168}Dy and ^{171}Ho (one at INEL and one at GSI, respectively), were determined. Figure 1.2 shows the region of the chart of the nuclides studied with the various nuclei produced at GSI, BNL, INEL, and OASIS marked. As can be seen in the figure, this research fits between the upper limits at INEL and the lower limits at GSI.

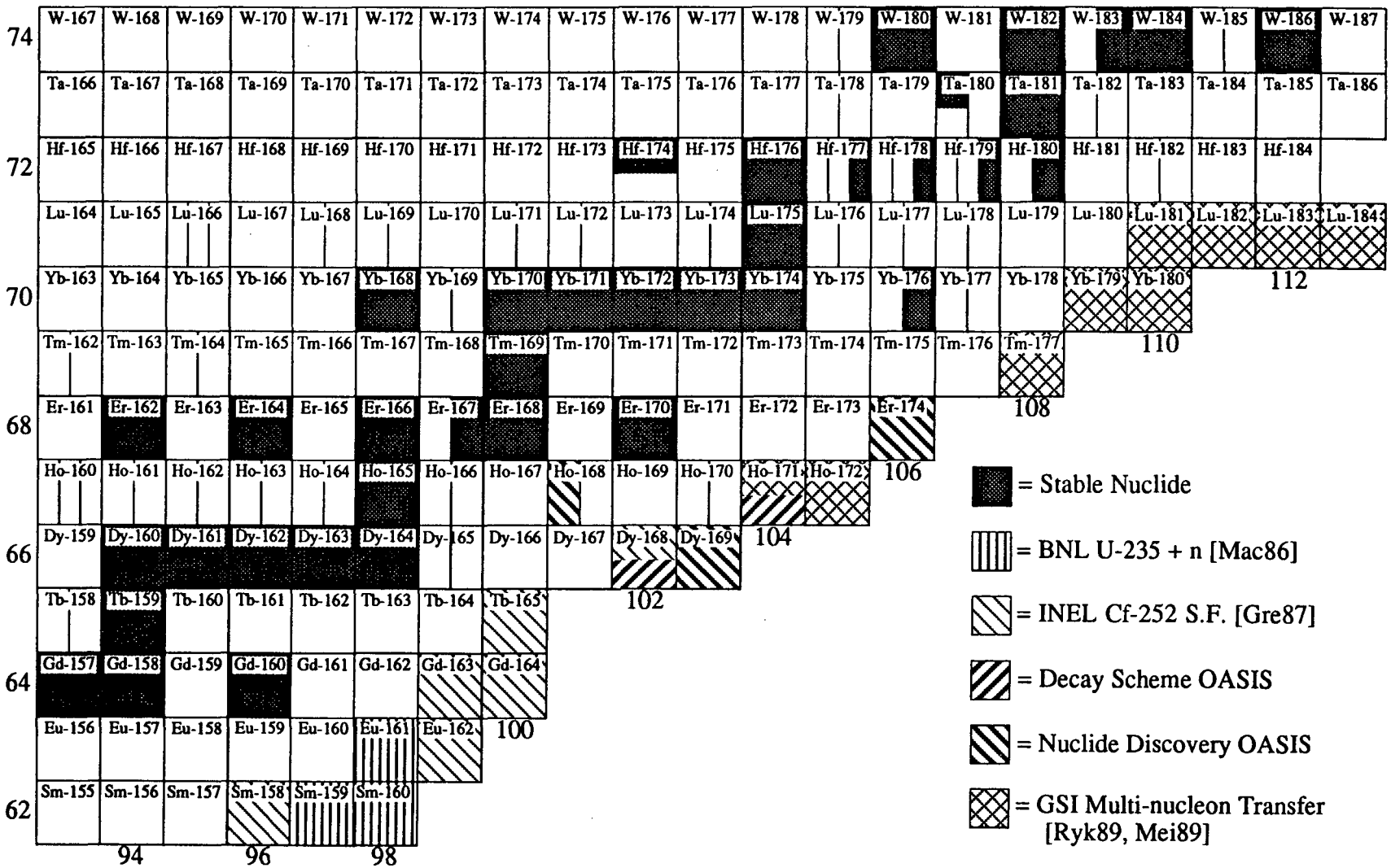

Figure 1.2. Region of the chart of nuclides showing the various nuclei produced in this study (OASIS) and at Gesellschaft für Schwerionenforschung (GSI), Idaho National Engineering Laboratory (INEL), and Brookhaven National Laboaratory (BNL).

A short discussion of the physics of multinucleon transfer reactions and their application to this study is presented in chapter 2. A description of the experimental conditions and parameters is given in chapter 3. A brief discussion of the data analysis techniques and computer programs used is presented in chapter 4. The results of the experiments are presented in chapter 5. These results will be presented in order of increasing mass number rather than the chronological order in which they were produced. Conclusions from this study are discussed in chapter 6.

2. MULTINUCLEON TRANSFER REACTIONS

Some of the mechanisms and properties of multinucleon transfer reactions and their application to this research study are discussed in this chapter. Heavy-ion nuclear reactions can be broadly classified into five types of reactions: "distant", "touching", "solid contact", "deeply penetrating", and "fusion" collisions [Sch77a]. "Distant" collisions, elastic scattering and Coulomb excitation reactions, and "touching" collisions, inelastic scattering and few nucleon transfer reactions, are classified as reactions with little or no energy damping (loss of kinetic energy between the entrance and exit channels). "Fusion" collisions, compound nucleus reactions, are associated with full energy damping. "Solid contact" collisions, fragmentation and multinucleon transfer reactions, and "deeply penetrating" collisions, deep inelastic reactions, are classified as reactions with large, but not complete, energy damping. These last two reaction types are of interest to this study, where penetration depths are deep enough to allow substantial mass transfer, yet not so deep as to have complete loss of projectile and target identities. Mechanisms and properties of these damped heavy-ion collisions will be discussed below.

In strongly damped reactions, where several hundreds of MeV of kinetic energy can be lost, numerous reaction channels are energetically possible and there is no obvious preference for a binary reaction mode. Yet, in-plane kinematic coincidence of correlated fragments from reactions of ^{84}Kr (600 MeV) on ^{209}Bi indicate a preference for a binary reaction mode. The experimental results were consistent with a binary fragmentation of the intermediate system followed by neutron evaporation [Sch77a]. Studies using lighter heavy-ions, ^{12}C, ^{16}O, ^{20}Ne, ^{32}S, ^{35}Cl, ^{40}Ar, and ^{63}Cu, also lend support to the two-body nature of strongly

damped reactions. There are indications that sequential fission of the heavy fragment is an important decay mode for reactions involving very heavy targets [Sch77a].

Assuming a binary reaction mechanism, damped heavy-ion reactions can be broken into a four-step process: formation of the dinuclear complex; charge, mass and energy exchange in the dinuclear complex; break-up of the dinuclear complex; and deexcitation of the product fragments. Evidence of the existence of the dinuclear complex has been found in reactions of $^{209}Bi + ^{136}Xe$ (1130 MeV) [Sch76, Sch77a]. Double-differential cross-section contour plots, with respect to lab angle and total kinetic energy of the products, produced a ridge that moved down in energy at an almost constant angle. This indicates strong angular focusing of an intermediate double nucleus which decays at approximately the same angle, independent of angular momentum [Sch77a]. The charge, mass, and energy exchange in the dinuclear complex becomes the important step in determining the products of damped heavy-ion reactions. It has been found for reactions of ^{84}Kr ions on ^{165}Ho and ^{209}Bi targets and ^{136}Xe ions on ^{209}Bi targets that interaction times of 10^{-22} s to several times 10^{-21} s were obtained for the dinuclear complex of damped collisions [Sch77b]. Relaxation times for equilibration of the N/Z distribution, kinetic energy damping, and charge distribution of dinuclear complexes have been measured as approximately 1.3×10^{-22} s, 3×10^{-22} s, and 60×10^{-22} s respectively [Mor81]. A relaxation time of the N/Z distribution on the order of 10^{-22} s has also been measured for Xe projectiles on Au targets [Kra79]. It can be seen from these times that the N/Z distribution and kinetic energy damping are almost completely equilibrated in the dinuclear complex, while the charge distribution is not equilibrated.

Much research has been performed on the dependence of the differential cross section on bombarding energy, charge, mass, product angle, and energy damping. It

has been found that the lab-frame angular distribution for reactions of ^{84}Kr on ^{208}Pb exhibits a strong peak that moves forward and sharpens with increasing bombarding energy [Van76]. In reactions of ^{209}Bi with 1130-MeV ^{136}Xe ions, the differential cross section was very strongly peaked at an angle of 29.8° in the laboratory frame, inside of the measured quarter-point angle of 33.1° [Sch76]. There was essentially no recoil intensity at $\theta_{lab} = 0°$. The width of the angular distribution for projectile-like fragments for the above reaction increases substantially with larger energy damping [Sch77a]. The width of the charge distribution also increases with larger energy damping [Sch76]. The last two facts indicate that large mass transfers are associated with a large degree of energy damping and wide angular distributions. Measurements of the most probable mass number for each product Z in reactions of ^{129}Xe (761 MeV) with ^{197}Au indicate that, for projectile-like products, the most probable mass number decreases by ~2 for each Z below the projectile charge (A_{prob}≈129 for Z=54 (Xe)) [Kra79]. This indicates that the N/Z equilibration tends to follow the line of beta stability.

The results mentioned above indicate that the desired products from these damped heavy-ion reactions recoil with non-zero lab frame angles centered close to the quarter-point angle. For large energy damping, associated with large mass transfers, the angular distribution becomes quite wide. These large angles presented problems for performing these reactions using the OASIS mass separator, since previous ion sources were designed for compound-nucleus reactions. Further discussion of this problem will be presented in the experimental and results chapters. The quoted results indicate that large energy damping is desirable for increasing the yield of projectile-like products with a few (2-4) protons removed. These studies did not address the problem of the disposition of this lost kinetic energy. The energy

loss is assumed to appear as excitation energy of the recoiling products. The normal modes of deexcitation for this region would be by neutron evaporation, or gamma emission for excitation energies below the last neutron binding energy. This hinders this research since neutron-rich nuclei are of interest. A balance between maximizing the width of the charge distribution, i.e. increasing the energy damping, and minimizing the amount of recoil excitation, i.e. decreasing the energy damping, is desired.

A modeling code was sought that would help determine the optimum target, projectile, and beam energy to use for these reactions and also serve as a guide for possible nuclei which could be studied. A computer code originally used to predict cross sections for $^{136}Xe + ^{249}Cf$ reactions [Gre85] was used. This code assumed that the unequilibrated charge distributions took on the features described by Wollersheim [Wol84]. After calculating the $\partial^2\sigma/\partial Z\partial E$ distribution [Wol84], the neutrons and excitation energy were distributed among the products. Since equilibration of the N/Z distribution and kinetic energy is fast compared to the interactions times, a statistical procedure based on the calculated level densities of the dinuclear complex and all possible exit channels was used. This would yield the triple differential cross section distribution $\partial^3\sigma/\partial Z\partial N\partial E^*$, where E^* is the excitation energy of the target-like product. This distribution was then deexcited by neutron emission, the fission deexcitation channel of the original code being neglected for this region. The original code, designed for target-like product calculations, was modified to calculate projectile-like products. Figure 2.1 shows some sample cross-section calculations for $^{170}Er + ^{nat}W$ using the modified computer code. The cross sections are listed for beam energies 10%, 20%, and 50% above the Coulomb barrier. Cross sections were calculated for ^{170}Er projectiles on the various stable W

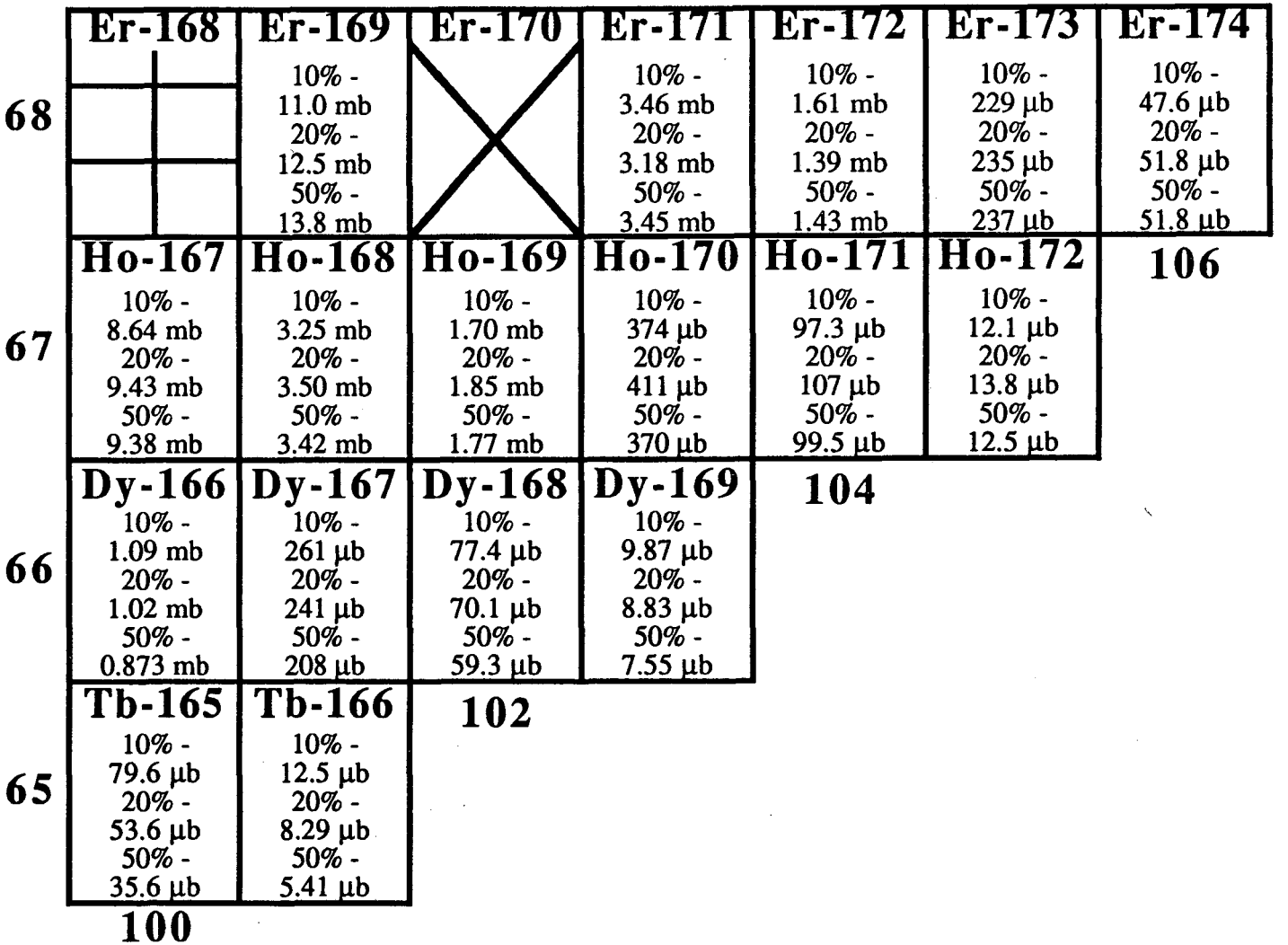

Figure 2.1. Cross-section calculations [Gre85] for Er-170 projectiles (at energies 10%, 20%, and 50% above the Coulomb barrier) on W(natural) targets.

isotopes and then added together using the isotopic abundances as weighting factors to give the numbers in Figure 2.1. There is a smooth energy dependence of the Er and Ho cross sections, while for Dy and Tb isotopes the cross sections drop off rapidly with larger beam energies, and hence larger energy damping, as expected. Zycor *et al.* [Zyc83] measured yields for isotopes of hafnium and lutetium isotopes from reactions of ^{40}Ar, ^{84}Kr, and ^{136}Xe beams on thick ^{nat}W targets and found them to be similar to cross sections from thin targets for projectiles with energies of ~1.3 times the Coulomb barrier.

In the current study, production of the strongest sources of new neutron-rich isotopes was desired. Selection of the most neutron-rich projectiles enhances the production of neutron-rich projectile-like products. The calculations predicted that ^{170}Er and ^{176}Yb were the best projectiles and these were chosen as the bombarding particles to produce neutron-rich isotopes of Dy, Ho, and Er. Target selection was limited to either Ta or W due to ion source construction, and the modeling code favored W. The question of optimum beam energy to use was actually a simple problem. The thickness, of the W anode endplate that served as the target, 1471 mg/cm^2, was far thicker than the thickness required to degrade the energy of the 8.5 MeV/u, ^{176}Yb or ^{170}Er ion beams (from the SuperHILAC) below the Coulomb barriers for interactions with W of ~12-14 mg/cm^2 thickness. The cross-section calculations for all the desired isotopes showed at most a 50% decrease in cross sections (for the Dy isotopes) at the full beam energy versus 10% above the Coulomb barrier. Therefore the maximum SuperHILAC beam energy, 8.5 MeV/u, was chosen to increase the amount of target encountered by the beam at energies above the barrier.

3. EXPERIMENTAL

The neutron-rich nuclei studied in this research were produced at the Lawrence Berkeley Laboratory's SuperHILAC which provided the ^{170}Er and ^{176}Yb ion beams. A few specifics about this machine will be presented in section 3.1. The OASIS mass separator, including the devices used to produce and ionize, mass separate, and transport the desired nuclei, and the detector system used to observe their decays, will be discussed in section 3.2. The various electronics, computers and other data acquisition hardware and software used during the experiments will be presented in section 3.3. The final section will explain the specific experimental parameters for each experiment.

3.1. THE SUPERHILAC

The SuperHILAC at the Lawrence Berkeley Laboratory delivered ion beams of ^{170}Er and ^{176}Yb to the OASIS mass separator located in Cave N, see Figure 3.1, of the experimental area. Full energy beams (~8.5 MeV/u) were used to maximize the amount of target material the beam would encounter before being decelerated below the Coulomb barrier. The beam-line optics and OASIS orientation used in this study are shown in Figure 3.1. The E42 beam-line can deliver full-rigidity beams as heavy as ^{238}U into Cave N and OASIS. The new beam apertures were of sufficient size to deliver two charge states simultaneously (probably 33^+ and 34^+) of the ^{170}Er beams on target inside of OASIS.

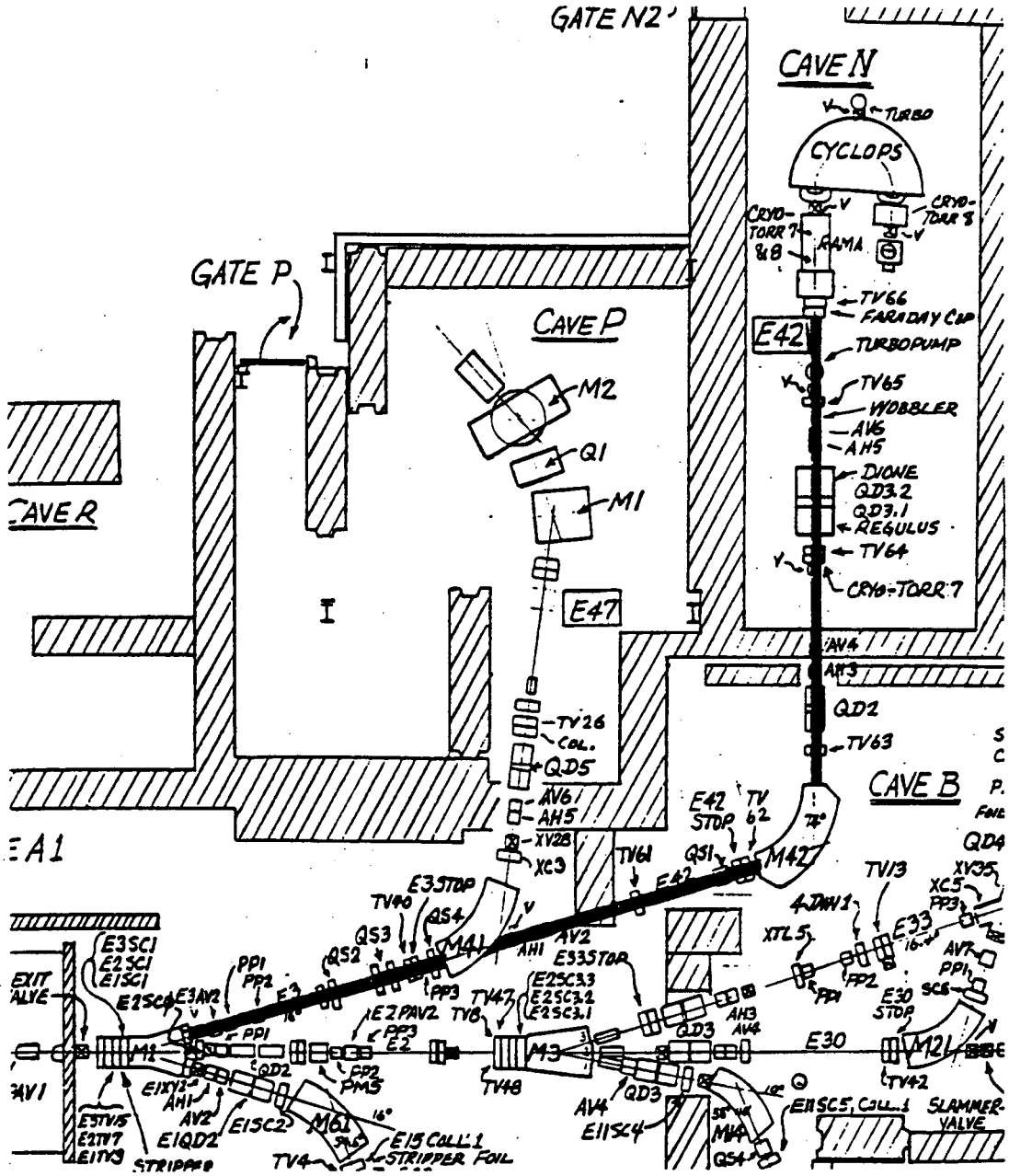

Figure 3.1. Beam optics used at the SuperHILAC for this research study. The path of the ions between bending magnets from the end of the accelerator to OASIS is shaded.

3.2. OASIS

The On-Line Apparatus for SuperHILAC Isotope Separation [Nit83] consists of four main parts discussed in the following sections: target/ion source system, the separator, transport systems, and the detector system. A modified diagram [Wil88] of the complete system is shown in Figure 3.2.

3.2a. TARGET/ION SOURCE SYSTEMS

The SuperHILAC beam was transported via standard ion optical elements to the OASIS "cave". There, the beam encountered a "wobbler" (a three phase motor with the beam-line replacing the rotor) that moved the beam spot uniformly on the target to allow even heating. This "wobbler" was located ~1-1/3 meters upstream of the OASIS ion source. About six inches downstream from the "wobbler", a beam scanner was located for the ^{170}Er experiments. This scanner consisted of a helical wire perpendicular to the beam-line, that when rotated about the helix axis, would cause the wire to fist scan across the beam vertically and then horizontally. By measuring the current on the wire and using a digital oscilloscope for display, both horizontal and vertical beam profiles could be obtained without interrupting the beam. This information, along with electrometer readings from the collimator and an RF pickup electrode (to measure the beam intensity entering the ion source) close to the target, determined the path of the ions into the OASIS ion source. In the case of the ^{170}Er ion beams, two distinct peaks were seen in the horizontal scan, while only one was seen in the vertical scan. This can be explained assuming that two charge states of the ^{170}Er ion beam left the M42 bending magnet (Figure 3.1) with slightly different trajectories. The beam-optics downstream of M42 were tuned to place the

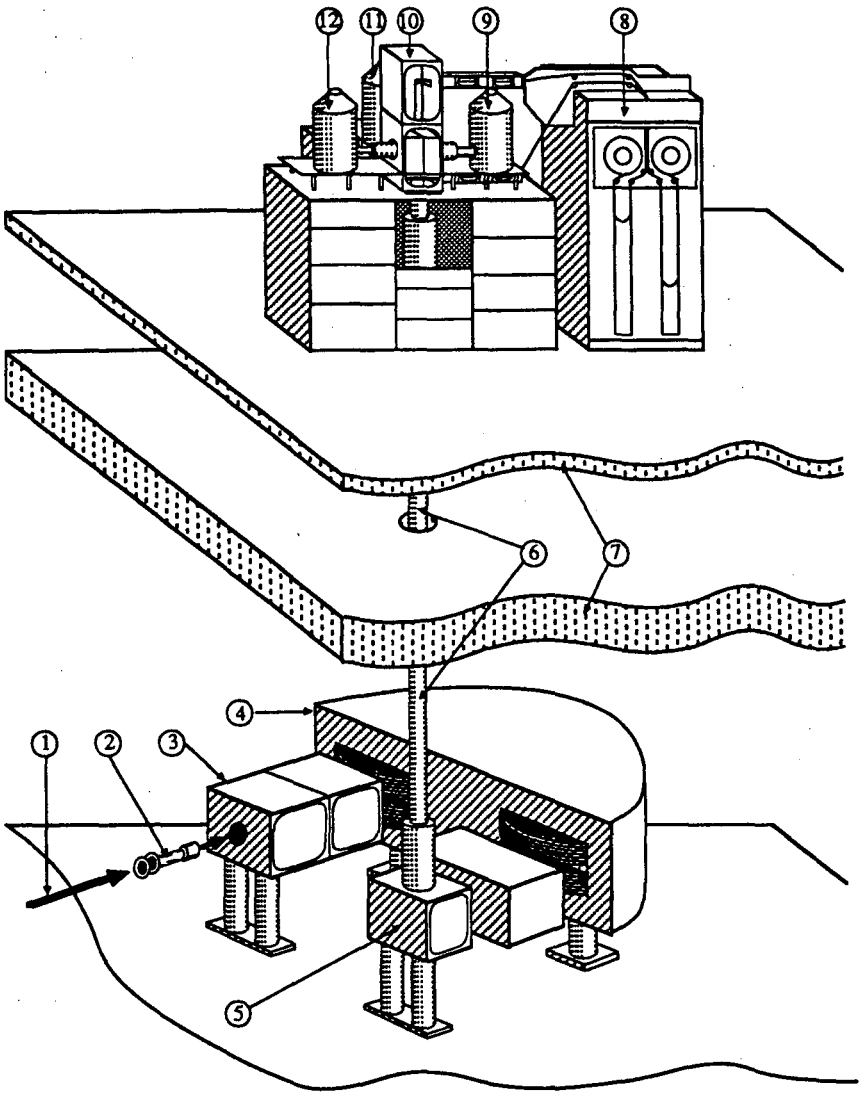

1. SuperHILAC Beam
2. Target/Ion Source
3. Extraction and Focusing
4. Analyzing Magnet
5. Electrostatic Mirror
6. Transfer Line
7. Concrete Shielding
8. Tape Drive (IBM 729)
9. Ge Detector (52%)
10. Detector Box
11. Ge Detector (24%)
12. HPGe Detector

Figure 3.2. Simplified representation of the OASIS mass separator on-line at the LBL SuperHILAC. The major components are labeled. Figure is a modified diagram from Wilmarth [Wil88].

valley between the two peaks of the horizontal scan on the beam-line center of the scanner, while simultaneously producing the largest beam-to-collimator signal ratio. Figure 3.3 shows a graphic representation of the digital oscilloscope display obtained while two charge states of ^{170}Er ions were delivered to OASIS.

The normal target/ion source used in OASIS for compound nucleus reactions is shown in Figure 3.4. Due to the large recoil angles for the multinucleon transfer reactions performed in this study, the normal target position with the small Ta capillary tubes (22.23 mm in length with ~1 mm inner diameter) would not allow the recoil products to enter the surface ionization region of the ion source. The capillaries are used to allow compound-nucleus products (small recoil angles) to enter the ionization region, but limit the amount of products diffusing back upstream to the cooler regions of the ion source. In this study, the problem of the large recoil angles and the extreme temperature(~2500 C) in the ionization region of the ion source coupled with the desire to not have to redesign the entire ion source allowed very few solutions. The Havar window, N_2 cooling gas, and compound-nucleus target were removed and the beam was allowed to pass through the carbon heat shields and the Ta capillaries and impinge upon the anode endplate. The anode endplate was used as the target and the Ta material which normally acted as the recoil catcher was replaced with W since the large number of neutrons in W compared to Ta should enhance production of neutron-rich products. This was the standard target/ion source geometry used in these multi-nucleon transfer reactions. A few other target/ion source geometries were tried in hopes of increasing the yield of the products. These included using a Ta endplate with a thin layer (~20mg/cm^2) of evaporated W, since Ta shows better diffusion of ions than W, or installing a thin (~12-17mg/cm^2) W window/targets at the end of the capillary section with and without capillaries.

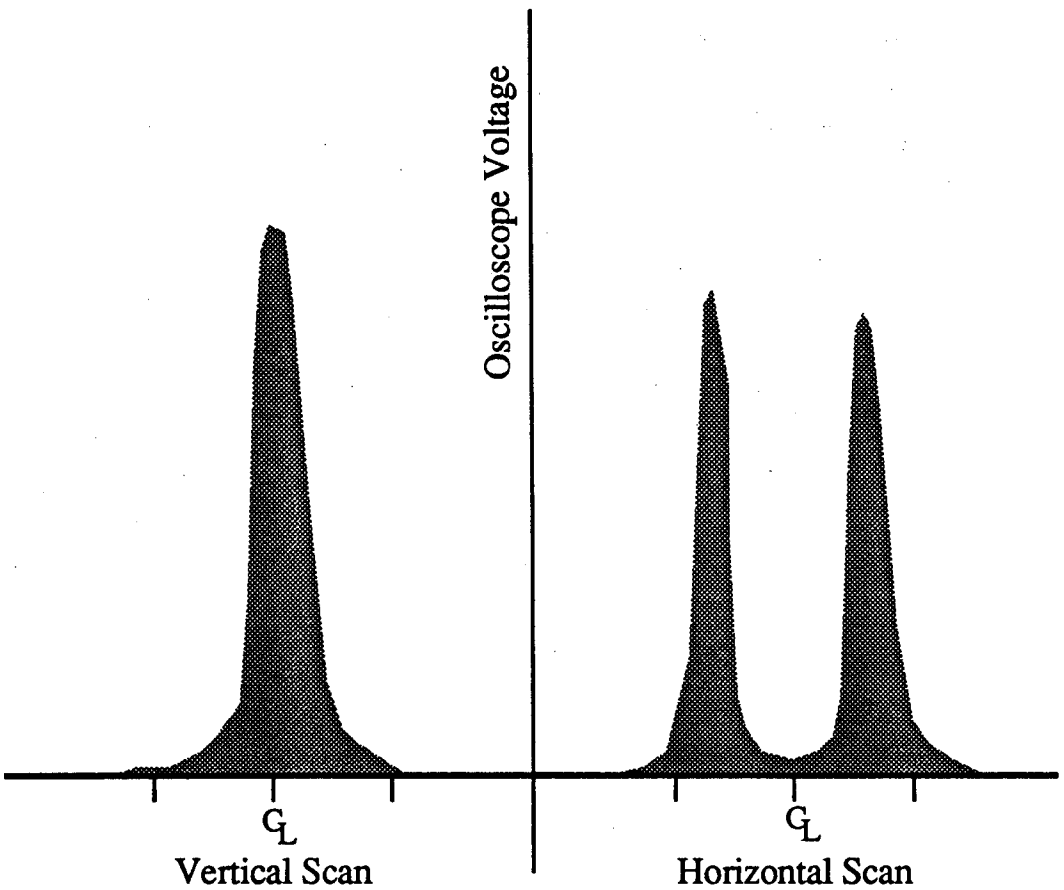

Figure 3.3. Graphic representation of the oscilloscope display for the beam scanner obtained while two charge states of Er-170 where being delivered to OASIS. The beam-line center for each scan is marked. The extra marks on each side of the center are for 1 cm off the beam-line center.

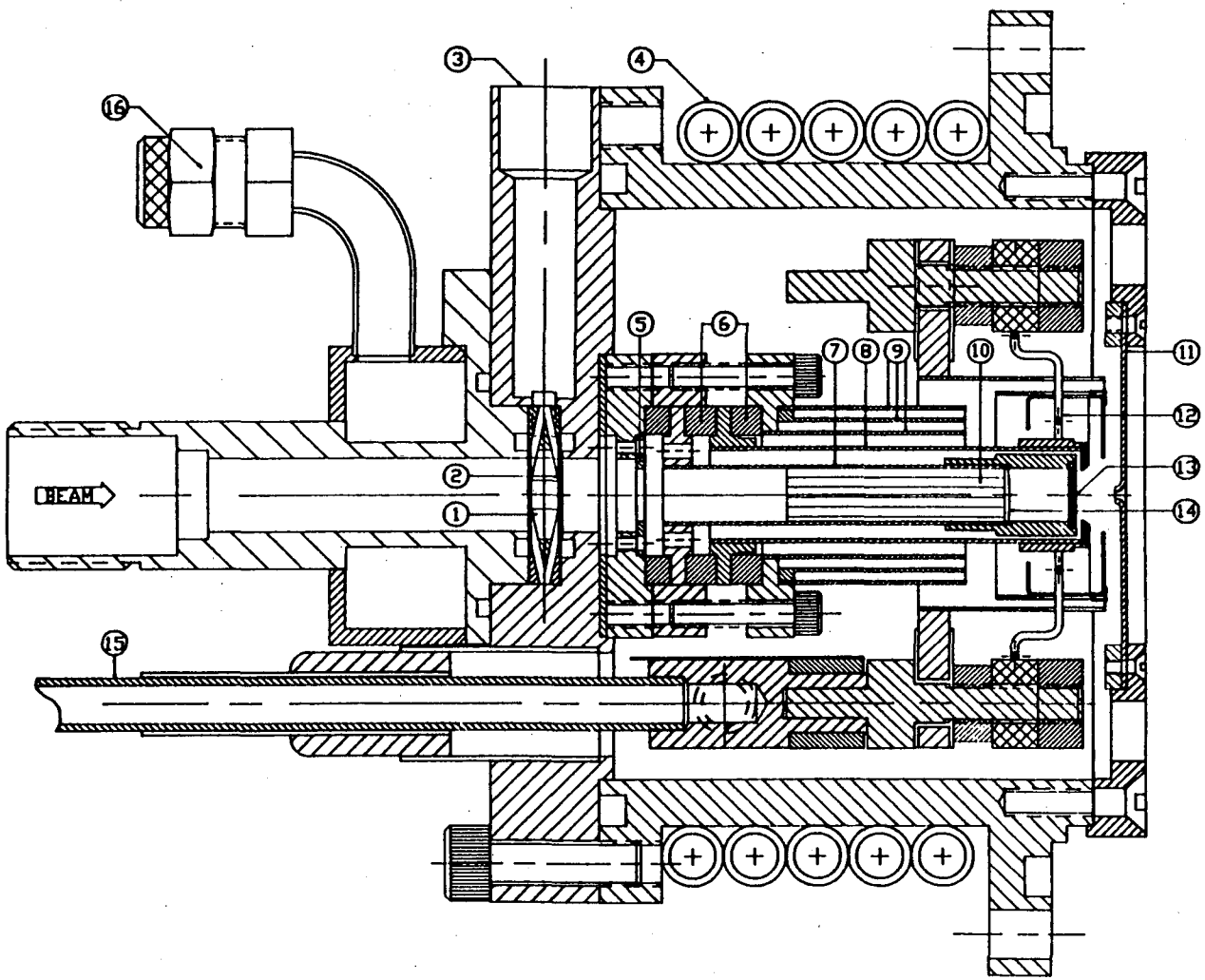

1. Havar Window
2. Compound-Nucleus Target
3. Nitrogen Gas Inlet
4. Cooling Water
5. Heat Shields (C)
6. BeO Insulators
7. Anode
8. Cathode
9. Heat Shields (Ta)
10. Capillaries (Ta)
11. Heat Shield (Mo)
12. Filament
13. Extraction Slit
14. Winow/Target Position
15. Filament Cooling Water
16. Cooling Water Inlet

Figure 3.4. Normal compound-nucleus OASIS target/ion source.

Results of these target/ion source tests will be discussed in chapter 5. The recoils produced (and caught in the case of the W window/target ion source) in the anode endplate diffused from the catcher and were surface ionized by heating the ionization region of the ion source to temperatures near the melting point of Ta (~3000 C) by electron bombardment (EB). Most target/ion sources lasted ~24 hours before most of the Ta cylinder wall of the anode had been evaporated by the EB, except for the W window/target source where the W window was melted through by the SuperHILAC beam in about six hours. Any of these problems caused a noticeable drop in the ion source output at which time a new ion source would be installed.

3.2b. THE SEPARATOR

After being ionized, recoils in the ion source would be extracted axially and accelerated to a 50 keV potential. The ion beam was then focused with an einzel lens and a quadrupole triplet onto the entrance slit of the separator magnet. This magnet had the following basic parameters: sector angle ϕ=180°, mean radius of curvature r_o=0.66 m, first field index α=0.5, and a mass resolving power R_m=880 (for 1.5 mm object slit). With the 50-kV acceleration, masses from 45 to 380 amu were separable with a transmission of ~95%. The magnetic field was measured with an NMR probe located at the 135° position inside a small homogeneous magnetic field section. A Hall probe was located next to the NMR probe to tune the NMR probe as the magnetic field was changed. The ion energy was accurately determined by measuring the accelerating potential with a 6-1/2 digit digital voltmeter (DVM). A PDP 11/10 minicomputer was used for control of the accelerating voltage. Using the NMR probe and DVM reading, the computer calculated the mass that would come through the magnet and then applied a correction voltage (-8 volts to +8 volts) to the

accelerating potential to separate the desired mass with an accuracy of ± 0.01 u. Mass calibrations were accomplished after each ion source change by introducing a small amount of a suitable rare earth oxide into the ion sources. This allowed a stable mass marker either at the desired mass or a few mass units away to be produced. The PDP 11/10 minicomputer also monitored and controlled all other important instrumental parameters of the separator.

3.2c. TRANSPORT SYSTEMS

After the recoil products had been mass analyzed, the ion beam was deflected 90° vertically to the counting room four meters above the cave. The deflection was performed via an electrostatic mirror operated at ~80% of the accelerating potential. The transfer line from the electrostatic mirror to the counting room contained two quadrupole triplets and two Faraday cups at the midpoint and counting room end for tuning the beam optics. The counting room was shielded from the radiation produced in the cave by the cave ceiling (~18 inches of concrete), large quantities of polyethylene for neutron thermalization, the counting room floor (~6 inches of concrete), and ~4 inches of lead on the counting room floor.

After transport to the counting room, the recoils were collected on a fast cycling tape system. This system consisted of an IBM 729 tape drive modified to bring a tape loop through an evacuated chamber where the recoils were collected and counted. To bring the tape from the atmosphere into a vacuum of ~10^{-6} torr, it was guided through three differentially-pumped feed-through chambers. The activities were then implanted in the magnetic tape directly above the transfer line. After the appropriate collection time, the tape was moved 6.88 inches to bring the activity into the detector array. The tape, after leaving the detector chamber, went through a

second set of vacuum feed-through chambers, identical to the first, and was then wound up by the IBM 729 drive. Magnetic computer tape with a conductivity of 3-4 kΩ per square (Scotch 700) was used to prevent electrostatic build-up from the 50-keV ion beam. For the ^{176}Yb beam experiment, a tape travel time of ~70 msec was used to move the activity from the collection point to the detector array. For the ^{170}Er beam experiments, this travel time was increased to ~200 msec, by using a different gear ratio in the IBM 729 drive to assure better activity positioning in the detector array.

The tape drive was controlled by an Intel 8085 microprocessor. The system was run in a stepping mode where by the activity was collected for a set time and then moved to the detectors to be counted while the next sample was being collected. The collection/counting time intervals were selected based on the known or predicted half-lives [Kla84, Tak83] of the desired activities. The tape control computer inhibited counting during the tape movement plus ~10 msec settling time and also reset and started a digital timer used for time-tagging of each decay event during the counting interval for half-life determinations.

3.2d. THE DETECTOR SYSTEM

Beta decay of neutron-rich rare-earths produces measurable electrons, x rays, γ rays, and conversion electrons. X-ray and γ-ray singles data were of the most importance in identifying new isotopes. However, βγ, γγ, and xγ coincidence information and β^- endpoint energy determinations were essential for synthesizing decay schemes. The normal detector set-up used at OASIS for neutron-deficient studies, shown in Figure 3.5, was used for these studies also. The only element of this array not required for this research was the 10.4 μm Si detector normally used as

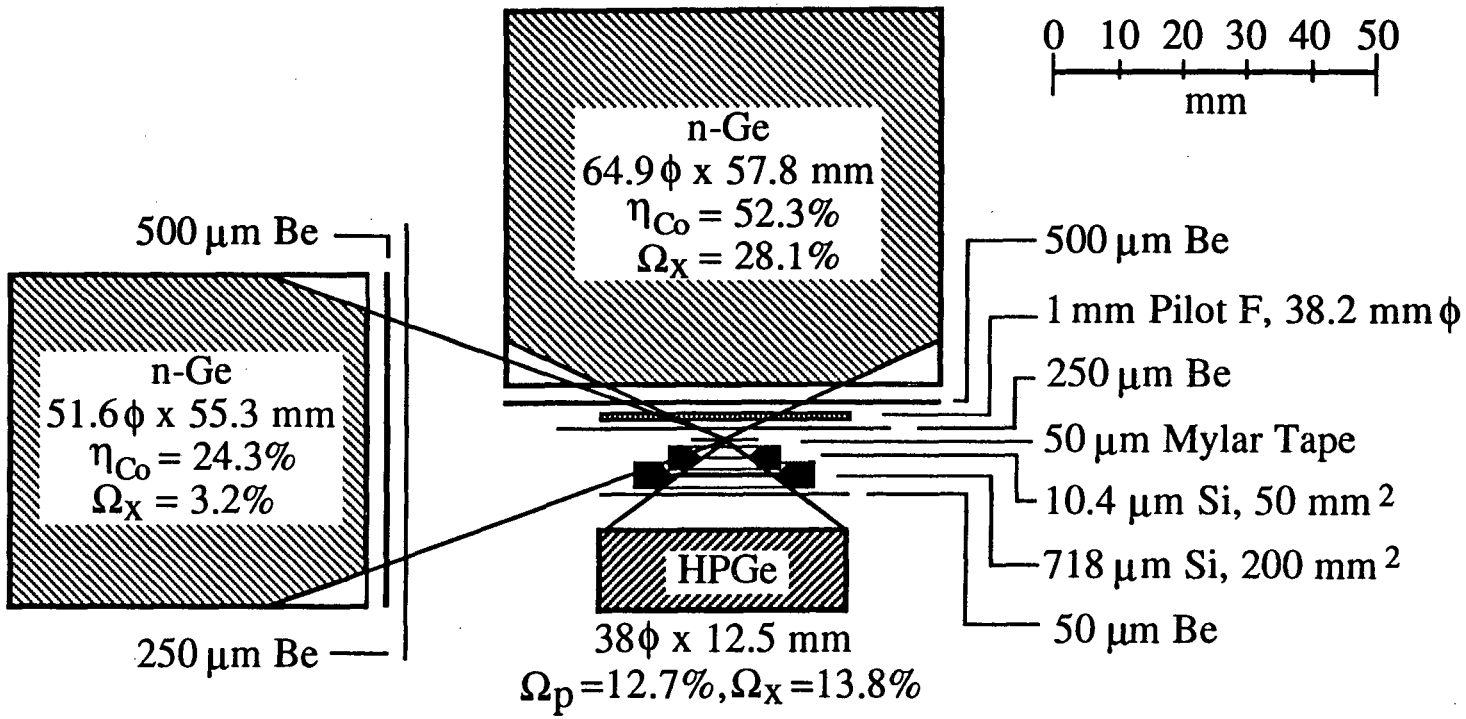

Figure 3.5. Detector configuration used at the OASIS mass separator for neutron-rich rare-earth nuclei.

a ΔE particle detector of a particle telescope. It was not removed due to its fragile nature. Its effect on β^- energies is to absorb ~3.6 keV for a 1 MeV electron and ~4.1 keV for a 5 MeV electron [Pag72], a negligible effect in these experiments.

A beta telescope and low-energy (10-400 keV) γ-ray detector, consisting of a 718 μm Si detector and a planar hyperpure Ge (HPGe) detector, faced the radioactive layer on the tape. The 718 μm Si detector was capable of stopping electrons of 0.40 to 0.55 MeV [Pag72] depending on the direction of the electron thru the Si. The remaining energy of a high energy electron would be detected in the HPGe. A large solid angle (~35%) 1-mm thick plastic scintillator, for electron and positron detection, and a large (52% relative efficiency) Ge detector, for γ-ray detection were located on the opposite side of the tape. A third Ge detector (24% relative efficiency) was located ~4.5 cm from the source at 90° to the other detectors. All five detectors used were surrounded by at least 2 inches of lead to shield against background radiation and activities on the tape being collected for the next counting cycle or from previous counting cycles.

Energy calibrations were performed before and after each experiment. In the case of the two-week long ^{170}Er beam experiment, a mid-run calibration was performed. Calibrations of the germanium detectors were performed using standard γ-ray sources (^{152}Eu, ^{241}Am, ^{226}Ra). The silicon detector was calibrated with a precision pulser which was periodically calibrated using standard α sources. The long term stability of the pulser was very good. Special thin sources attached to the computer tape and moved to the actual counting position were used to determine the absolute efficiencies of the Ge detectors about once per year. Calibration of the plastic scintillator was not necessary since output from this detector was used only

for coincidence information to determine βγ and βx coincidences with much higher β efficiency than with the β telescope.

3.3. DATA ACQUISITION

Data acquisition for OASIS consisted of the electronics, computers , and various software discussed in the following sections.

3.3a. DETECTOR ELECTRONICS

The pulsed optical preamplifier signal from the HPGe detector was electronically split into a low gain amplifier, for β^- particle detection (0-5 MeV range), and a high gain amplifier, for low energy photons (0-400 keV range). The low gain signal and the amplified signal of the 718 μm Si made up the β telescope signals. The 52% Ge preamplifier signal was also split into a low gain (0-4 MeV range) amplifier and a high gain (0-400 keV range) amplifier. Single amplifiers were used for the 718 μm Si, plastic scintillator, and 24% Ge detectors.

Singles data were acquired for the high gain HPGe, low gain 52% Ge. and the 24% Ge detectors for determining intensity information of γ and x rays. Multiparameter event-by-event data were acquired for βγ, xγ, and γγ coincidences. The fast timing signals from each detector, after going through appropriate shaping amplifiers and constant fraction discriminators, were used to define coincident events of interest. Timing information between detector pairs was also generated from the fast timing signals using time to amplitude convertors (TAC's). In the ^{176}Yb beam experiment, coincidences (~2 μs overlap) between the 718 μm Si and HPGe detectors (β telescope), the plastic scintillator and the 52% Ge detector, and pairs of the three germanium detectors defined a coincidence event. These five coincidence

signals were logically OR'ed to obtain one master event trigger. In the ^{170}Er beam experiment, the same coincidence criteria as in the ^{176}Yb experiment were used plus additional coincidences between the plastic scintillator and the other two germanium detectors (HPGe and 24% Ge) were added since these would add $\beta\gamma$ coincidences with a large β efficiency. High quality linear electronic components were used for amplification, shaping, and gating of all energy signals, resulting in good resolution and stability. Extreme efforts were made to prevent ground loops in electronics, and these efforts were generally successful.

All coincident energy signals, TAC's, and timing information, after the above mentioned electronic processing, were routed to a single CAMAC crate. In the CAMAC crate, the energy and TAC analog signals were converted to digital information with high resolution LeCroy 3511 or Ortec AD811 ADC's. Timing information was digitized using LeCroy scalers. Analog singles data from the HPGe and 52% Ge detectors were digitized with LeCroy 3512 Buffered ADC's, time-routed (8 equal time bins per counting cycle) with LeCroy 3587 Routers, and histogrammed in CES HM2161 64K histogramming memories (8 by 8192 channel spectra).

3.3b. COMPUTERS AND DATA ACQUISITION SOFTWARE

The main data acquisition computer was a ModComp Classic computer. Interfacing between the computer and various ADC's, scalers, and memories was achieved with a CAMAC branch controller and a differential branch driver and transceiver. The CDAS software package [Bel86] was used to read the various event parameters, store the data on magnetic tape, and also supply some on-line sorting and display. The data acquisition architecture allowed a data rate of >30,000 parameters

per second. However, the data rate never approached that level in this study. The histogramming memories (HPGe and 52% Ge singles data) could be read either into the on-line graphics display memory or directly to magnetic tape, with a task running at a lower priority than the CDAS software on the ModComp Classic computer. A Tracor Northern 1750 multichannel analyzer was used for pulse-height analysis of the singles data from the 24% Ge detector. An Apple Macintosh Plus was used to read out the data from the Tracor Northern and store it on floppy disk.

3.4. EXPERIMENT SPECIFICS

This research study consisted of two major experiments: a six-day experiment of ^{176}Yb projectiles which was run in the first week of November 1987, and a two-week run (longest continuous run for OASIS to date) of ^{170}Er ions that was performed in the first two weeks of August 1989. The details for these two runs will be discussed in the following sections. A five-day run was attempted in December 1988, but due to technical difficulties with the SuperHILAC, no ^{170}Er beam was delivered to OASIS.

3.4a. ^{176}Yb EXPERIMENT

The SuperHILAC delivered 25-45 particle nanoampere beams of 8.40 MeV/u ^{176}Yb ions on W targets using natural ytterbium in the ion sources (^{176}Yb abundance=12.7%). The purpose of this experiment was to produce new isotopes at masses A=171 and 174. The OASIS mass separator was mass calibrated using Yb_2O_3, which provided mass markers at A=171 and 174. Most of the target/ion sources used in OASIS were of the normal geometry (capillaries, W endplate, no windows). One special ion source was used which had capillaries, a Ta endplate,

and a 17mg/cm^2 W window/target at the end of the capillaries (position 14 in Figure 3.4). The event-by-event data consisted of 15 parameters (event tag, clock parameter, time (from last tape movement), 7 energy parameters and 5 TAC's) per event.

3.4b. ^{170}Er EXPERIMENT

The SuperHILAC provided 50-125 pnA of 8.5 MeV/u ^{170}Er ions on W targets using natural erbium ion sources (^{170}Er abundance=14.9%) and ion sources with ^{170}Er enriched strips spot-welded to natural erbium backings. The purpose of this experiment was to produce new isotopes at mass A=169 and construct decay schemes of ^{168}Dy and ^{171}Ho. The OASIS mass separator was mass calibrated using Yb_2O_3 for masses A=168 and 171. Mass A=169 was calibrated by interpolating between the A=168 and 170 mass calibrations of the Yb_2O_3. Two special target/ion source geometries were run in OASIS besides the normal geometry (capillaries, W endplate, no window): one geometry with capillaries, W coated Ta endplate, and no window and the other geometry with no capillaries, Ta endplate, and a 12 mg/cm^2 target/window at position 14 in Figure 3.4. The event-by-event data consisted of 17 parameters (event tag, clock parameter, time (from the last tape movement), beam parameter (for ion source test normalization), 7 energy parameters, and 6 TAC's) per event.

4. DATA ANALYSIS

The data acquired in the experiments performed can be grouped into three subsets: the gamma singles data, the event-by-event coincidence information, and the beta telescope spectra.

4.1. GAMMA SINGLES DATA

The singles data (ModComp tapes or Macintosh floppy disks) were first transferred to Digital Electronic Corporation (DEC) computers. In the case of the Macintosh data, commercial Kermit file transfer programs were used. The ModComp tapes were read with software developed in the OASIS group. The two DEC computers used in the analysis of the singles data were a VAX 8650 Cluster at LBL or a μVAX-II Workstation owned by the OASIS group. The 8650's cpu and I/O were almost an order of magnitude faster for the analysis programs used than the μVAX, however, due to the 8650 being a time-sharing machine, their speed increase was not realized under actual conditions. All spectra were converted to an identical binary format to minimize disk memory usage.

The main program used to analyze the singles spectra was a VAX version of SAMPO [Rou69]. This version allowed for the fitting of up to eight γ rays, as compared to only six in the original code, in a single fitting region. This new option was very useful in fitting of K_α and K_β x-ray regions, where four adjacent elements were detected. The shape parameters, the key variables in SAMPO to assure good fits, were generated from the calibration spectra of each experiment. Separate shape parameters were used for γ rays and x rays due to slightly different shapes of their

peaks. Efficiencies used were from the once per year calibrations and are shown in Figure 4.1.

Intensity versus time information, from the 52% Ge and HPGe detectors, was fit with a least-squares error-weighted decay program [Gre85]. This program allowed either up to five independent components, or growth and decay with up to four independent components, or two growth and decay components with up to one independent component. However, since the hardware used created only eight time-binned histograms for these detectors, no more than three half-lives were fit at one time. The program would calculate a χ^2 goodness of fit parameter and a reduced χ^2, χ^2/(# of points - # of free parameters - 1). Both of these parameters will be shown with the decay curves presented in chapter 5.

For the determination of absolute γ-ray intensities, information from the 52% Ge had to be treated with caution. Due to the large size of the crystal and the proximity of the source, summing problems were noted. This was not a count rate problem ("pile-up"), but a true gamma cascade summing problem. The errors this introduced were at the largest when one of the γ rays in a cascade was at at an energy near the peak of the 52% Ge detectors efficiency (~150 keV in Figure 4.1). Summing problems were not seen in the HPGe detector, and the 24% Ge detector was far enough from the source to avoid this problem. Gamma intensities reported in this study are from the HPGe and 24% Ge detectors, unless noted. In a few cases, the order of magnitude difference in the efficiencies of the the two Ge detectors (Figure 4.1), would cause the desired gamma ray to be undetectable in the 24% Ge detector above the various backgrounds and the intensities from the 52% Ge were used.

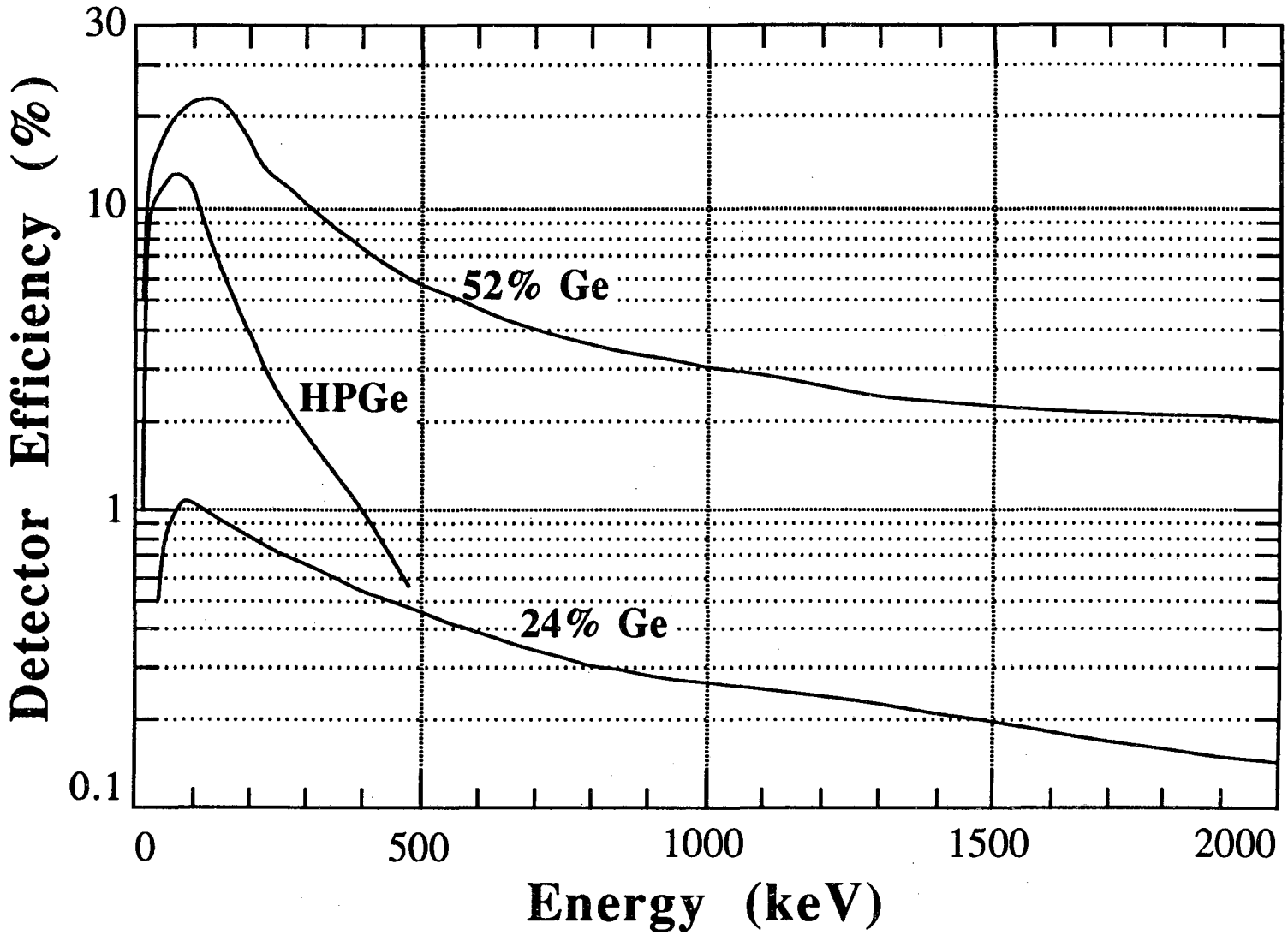

Figure 4.1. Absolute efficiencies from 15 to 2000 keV for the germanium detectors in the geometry used.

4.2. COINCIDENCE DATA

The event-by-event data were analyzed with a ModComp Classic computer. The EVA software package [Bel87a] was used exclusively to produce the various histograms. Appropriate peak and background gates would be set in a chosen detector and coincidence spectra from the other detectors would be generated. Beta telescope spectra were produced based on the following requirements: energy signals above 0.18 MeV in the 718 μm Si detector and 0.15 MeV in the HPGe low gain signal plus a very narrow gate on the prompt TAC peak of the 718 μm Si/HPGe TAC. These gates were used to avoid noise in both detectors and to obtain clean signals with the narrow TAC. Other coincidence spectra were normally produced with "wide-open" TAC gates. After $\gamma\gamma$, $x\gamma$, or $\beta\gamma$ coincidences were found, TAC spectra were generated after gating on both signals of the coincidence pair to determine if the intermediate level in the decay was delayed.

The peaks in the histograms generated with EVA were fit with the SUSIE graphics software package [Bel87b]. The program gave graphic displays of the histograms plus arithmetic functions to operate on the spectra. Background-gated spectra could be subtracted from peak-gated spectra and stored on disk or tape. Simple peak-fitting calculations could also be performed and hardcopy plots could be quickly generated.

After use of the one-dimensional features of the software mentioned above, two-dimensional features were noticed and used. Two-dimensional energy spectra were generated for any pair of detector signals (the beta telescope is only one signal in this discussion) with EVA. The SUSIE software package allowed for quick interactive background-subtracted gates to be set in one direction of the 2-D spectrum

and produce the resulting 1-D projection. This procedure allowed for quicker results once the 2-D spectra were generated. Generation of the 2-D spectra was about an order of magnitude slower than generating 1-D spectra due to the size difference in the spectra. The flexibility of the 2-D histogram more than made up for this speed difference, since all possible gates in either detector could be tested without having to resort the event-by-event data.

Spectra generated with either software package could be read into the DEC computers and fit with SAMPO, in the case of γ spectra, or the β analysis software (to be described below), in the case of β spectra.

4.3 BETA TELESCOPE SPECTRA

The spectra measured with the beta telescope in this study proved to contain extremely important information. Unlike the neutron-deficient studies normally done at OASIS, where K x rays were seen in a large fraction of the decays due to the large electron-capture branches, neutron-rich decays only produce x rays if a γ transition in the decay is internally converted. Thus, the elemental assignment from the K x rays was almost absent as a means to identify a specific isobar in the mass chain separated. However, electrons from β^- decay could be detected with good resolution in the beta telescope. The electrons of a particular decay become hard to distinguish from beta particles of other decays due to the energy of β^- decay being randomly split between the electron and the electron antineutrino. However, in odd mass chains, the total beta decay energies, Q_β, generally increase with the neutron number in an isobaric chain. This fact coupled with possible ground state or low excitation energy level beta feedings yields for the lowest Z isobar a portion of the beta spectrum beyond the beta endpoints of isobars closer to the line of beta stability. The increase

in Q_β values for more neutron-rich nuclei is not always seen in even mass chains due to the odd-even affect of nucleons on masses. The Q_β value for an even-even isotope is generally less than the Q_β values of it's two neighboring odd-odd isobars. However, if an odd-odd decay was studied, it's Q_β value was generally greater than the isobars closer to beta stability.

Being able to determine new beta decays and intensities from only the upper part of a beta spectrum was needed. Integration of regions of the time-binned beta spectra beyond known beta endpoints would yield half-life information for the beta decay. Background subtraction was performed by using an identically sized window at the higher energy part of the beta spectrum (background region) normalized with a ratio factor determined for the same windows in a 15-hour beta background spectrum. A computer code was written to calculate Fermi-Kurie plots in order to determine beta endpoints. Examples of this calculation are shown in Figures 4.2 and 4.3, where endpoints of β^- particles coincident with gamma rays seen in the 52% Ge detector from the decay of ^{168}Ho are calculated. An error-weighted least-squares fit was used to determine the best linear fits shown in the figures and the corresponding endpoints.

Determination of absolute beta intensities was not as simple as determining gamma intensities. A large fraction of beta counts were lost in the determination of the beta telescope energy below ~0.35 MeV (due to the 0.18 and 0.15 MeV threshold gates in the 718 μm Si and HPGe low gain signals). Also for ground state beta branches, no gamma-ray gating could be used, so only the part of the beta spectrum beyond the known beta endpoints (the very low statistics portion of a beta spectrum) could be used. Using some subroutines from a code to calculate the response of Ge detectors to positrons [Avi81], a computer program was written that would generate

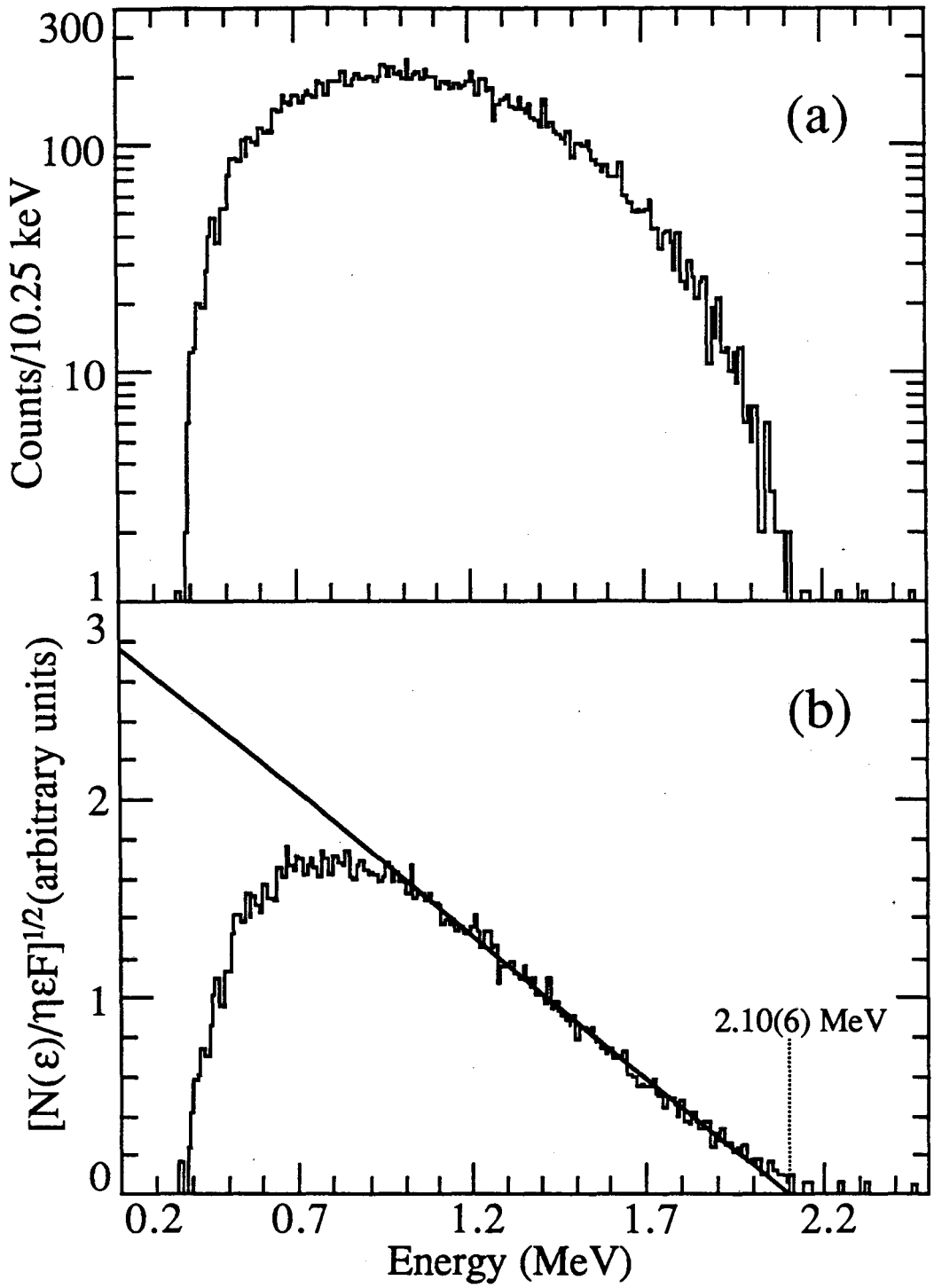

Figure 4.2. Beta decay data coincident with 741-keV gamma rays in the 52% Ge detector for the A=168 mass chain; (a) beta particle spectrum measured wth the beta telescope and (b) Kurie plot and least-squares linear fit from 1.1 to 2.0 MeV.

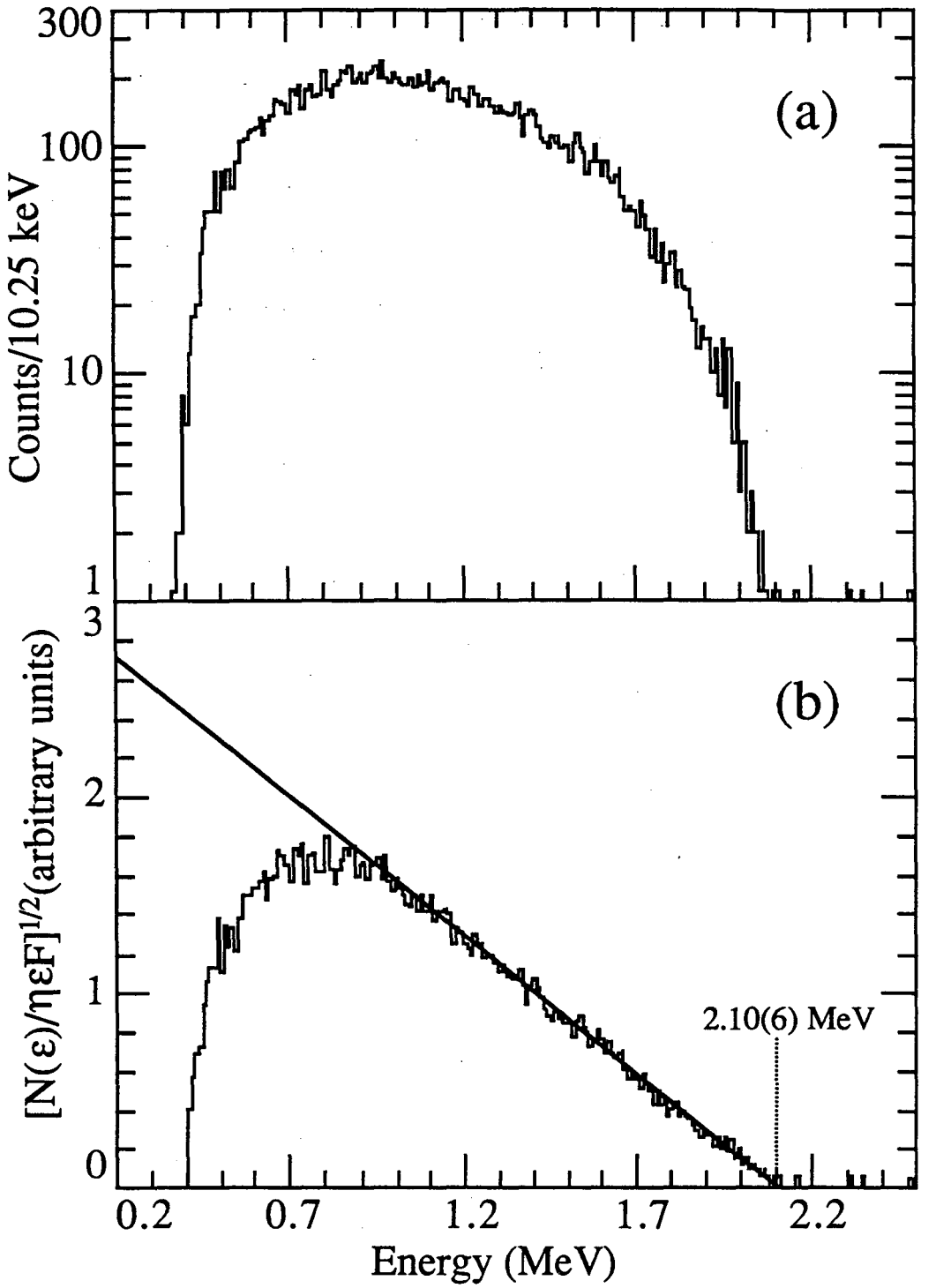

Figure 4.3. Beta decay data coincident with 821-keV gamma rays in the 52% Ge detector for the A=168 mass chain; (a) beta particle spectrum measured wth the beta telescope and (b) Kurie plot and least-squares linear fit from 1.1 to 2.0 MeV.

an ideal allowed β^- spectrum. It required only the Z, A, endpoint energy, and energy calibrations to generate a calculated β spectrum. A copy of the source code used to calculate these calculated β spectra is given in Appendix A. A calculated spectrum would then be renormalized to the measured spectrum such that the number of the counts in the clean upper region of the measured spectrum equaled the number of counts in the calculated spectrum over the same region. Figure 4.4 shows the fit of calculated spectra to the measured β spectra in Figures 4.2 and 4.3. The absolute efficiency of the beta telescope was determined from these calculated spectra. The total counts of these two calculated spectra were divided by the number of gamma rays seen in the 52% Ge singles data, used as gates to generate the measured beta spectra. A β^- detection efficiency of 8.47% was determined by this method for the energy and TAC gates used. The dependence of this efficiency on different endpoint energies was not determined.

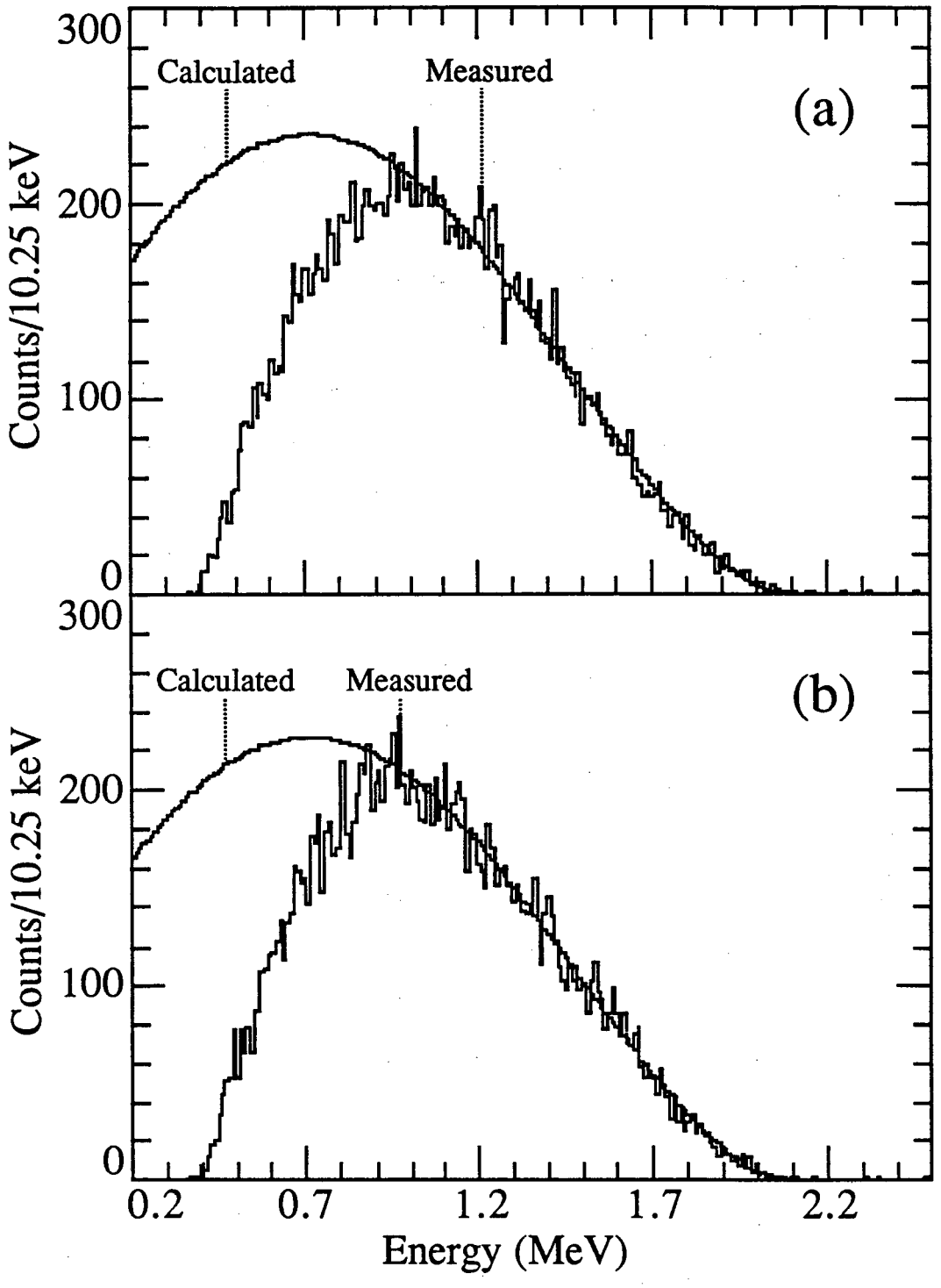

Figure 4.4. Beta decay data and calculated spectra fits in the A=168 mass chain coincident with gamma rays in the 52% Ge detector at; (a) 741 keV and (b) 821 keV.

5. RESULTS

In the course of this research, two new isotopes, ^{169}Dy and ^{174}Er [Cha89], and the isomer ^{168}Ho^{m} were discovered. In addition, the decay schemes of two previously identified isotopes, ^{168}Dy [Geh82] and ^{171}Ho [Ryk89], were determined. Figure 5.1 shows location of these isotopes in the chart of the nuclides. These results will be discussed in the following sections in increasing mass number. The A=168 isotopes will all be discussed in one section due to the related data analysis. For historical purposes, the chronological order of the production of these isotopes is as follows: ^{174}Er - 11/6/87, ^{171}Ho - 11/8/87 and 8/7/89, A=168 isotopes - 8/2/89, and ^{169}Dy - 8/4/89. The results of the various OASIS target/ion source tests are also presented.

A few standard short-hand notations used in decay scheme studies are followed in this presentation. Internal conversion coefficients (ICC) will be denoted by α_{tot}, α_K, α_L, etc. to represent the total, K-shell, L-shell, etc. conversion coefficients. All ICC's listed in tables are theoretical values [Rös78]. Only α_K values could be measured with the equipment. Experimental values followed by numbers in parenthesis have an experimental error equal to the value of the number(s) in parentheses on the last digit(s) of the listed value. Errors are one sigma limits (68% confidence limits). All beta endpoints determined from Fermi-Kurie plots were calculated using a least-squares fitting program with error-weighting. β^- decays in this region are Gamow-Teller allowed ($\Delta I = 0$ or 1, $\Delta\pi$ = no) or first-forbidden ($\Delta I = 0$ or 1, $\Delta\pi$ = yes) decays. The relevant selection rules for electromagnetic multipole radiation [Seg77] are reproduced in Table 5.1. The original computer code used by Takahashi *et al.* [Tak73] to calculate nuclear half-

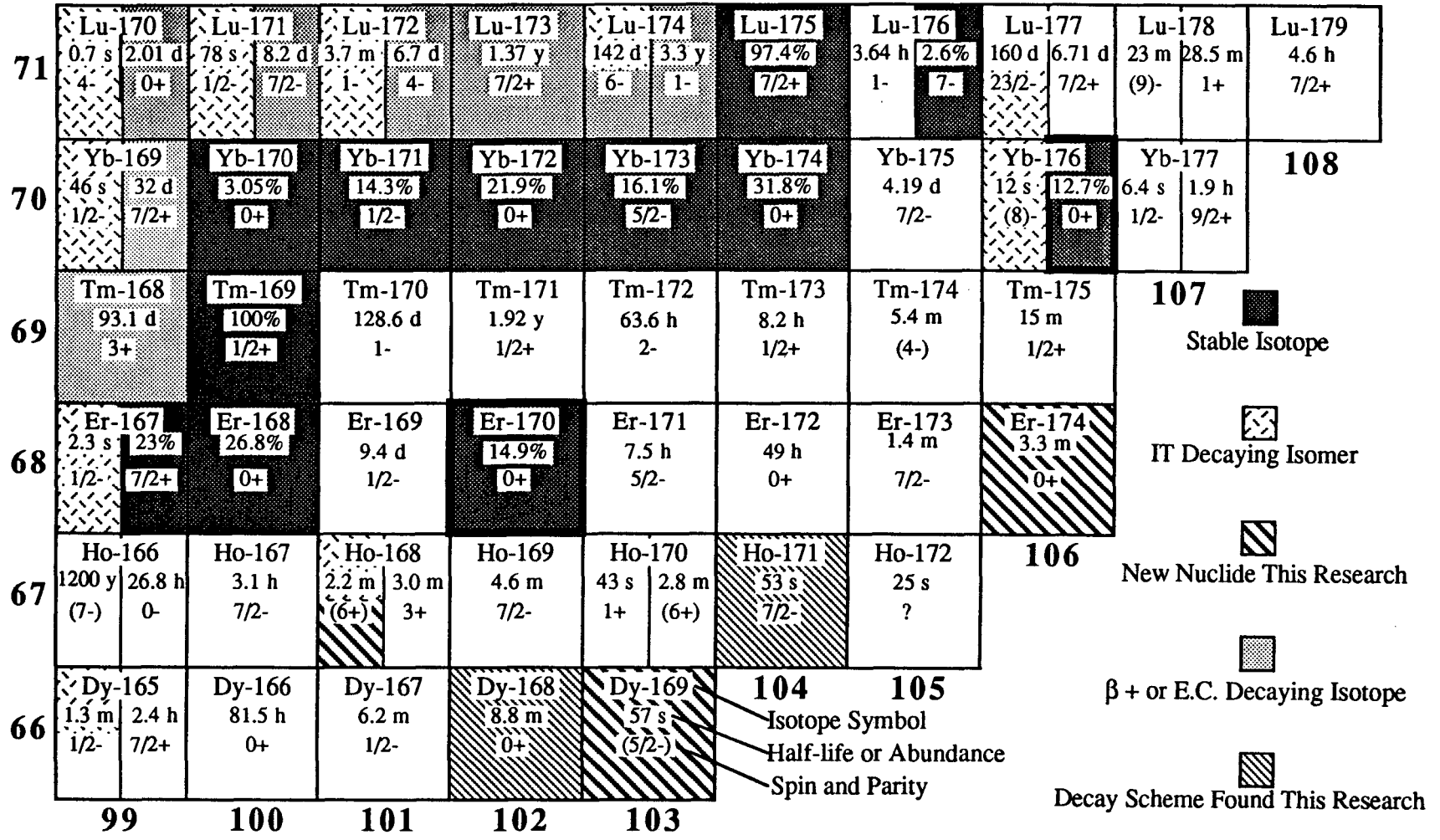

Figure 5.1. Chart of nuclides for the region studied. Isotopes investigated in this research are indicated. All unshaded nuclides decay by beta emission. The two projectile ions used in this research have bold borders.

Table 5.1. Selection rules for electromagnetic multipole radiation [Seg77] used in this research.

	E1	E2	E3	E4
$\Delta\pi$	yes	no	yes	no
$\Delta I \leq$	1	2	3	4
	M1	M2	M3	M4
$\Delta\pi$	no	yes	no	yes
$\Delta I \leq$	1	2	3	4

lives was obtained from the author [Tak88]. Using Q values calculated with more recent nuclear mass formulae [Hau88] this Gross Theory of Beta Decay (GTBD) code predicted half-lives with better accuracy than before.

5.1 A=168 MASS CHAIN

The A=168 mass chain was studied using ^{170}Er projectiles with various OASIS target/ion source geometries. The discussion of the different sources used and the results will be presented in a later section. Natural erbium was used as the source material for the SuperHILAC ion sources. Beam intensities of 33 to 75 particle nanoamperes on target were delivered for about 30 hours. This experiment was performed to determine the decay scheme of the 8.5(5) m ^{168}Dy [Geh82] and investigate the affect of various target/ion source geometries on the production of 3.0 m ^{168}Ho [Wil60]. Thus, a tape cycle time of 1024 s (17.1 m) was used to study ^{168}Dy, and 512 s (8.5 m) was used to study ^{168}Ho. During the analysis of the ^{168}Dy data, evidence of a new isomer ^{168}Ho was seen. Also a new Q_{β^-} value for ^{168}Ho [Kaw73] was determined.

5.1a ^{168}Dy DECAY SCHEME

^{168}Dy was identified by researchers at Idaho National Engineering Laboratory from the spontaneous fission of ^{252}Cf and assigned a half-life of 8.5(5) minutes [Geh82]. They used a rapid chemical separation system, ESOL (Elemental Separation On-Line) to prepare Ho/Dy fraction samples. Five new gamma rays at 143, 192, 443, 487 and 630 keV were seen to decay with the average half-life given above and were assigned to the decay of ^{168}Dy. They also assigned an emission probability per beta decay of 0.22(4) for the 487-keV gamma ray from intensity ratios with the 821-keV gamma ray from ^{168}Ho at various decay times.

In the 1024-s tape cycle time data of this research, all five of the gamma rays previously reported were observed to decay with the reported half-life. In addition, two new gamma rays, with energies of 43.8 and 437.0 keV, were identified to decay with the same half-life. A weighted average value of 8.8(3) m was determined for the half-life of these seven gamma rays. In the x-ray singles data, Ho $K_{\alpha 1}$ and $K_{\alpha 2}$ x rays were observed. However, these x rays exhibited a two-component decay behavior. Figure 5.2 shows the decay curves of the Ho $K_{\alpha 1}$ and $K_{\alpha 2}$ x-ray activities. The long half-life had to be held fixed or the fitting program would diverge. The short-lived activity deduced from these curves will be discussed in the section on the ^{168}Ho^{m} isomer. The intensities of the 8.8 m Ho $K_{\alpha 1}$ and $K_{\alpha 2}$ activities were determined by integrating the long-lived component of the decay curves.

The absolute decay intensity of ^{168}Dy could be determined by observing the growth and decay of its daughter activity, 3.0 m ^{168}Ho. However, this was complicated by the short-lived activity observed in the x-ray singles analysis. This

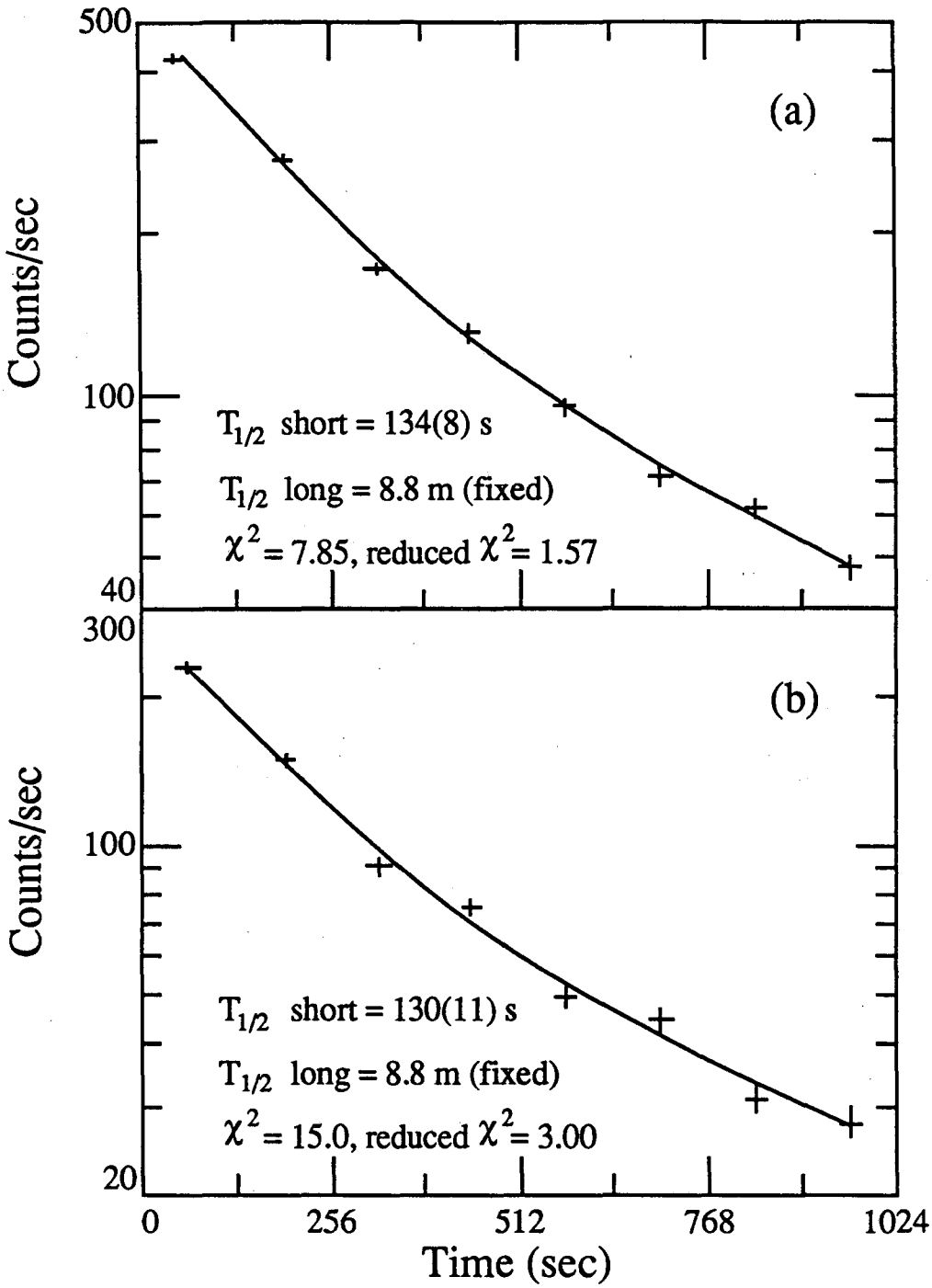

Figure 5.2. Two-component decay curves fit to the Ho x-ray data for the 1024-s run; (a) Ho $K_{\alpha 1}$(47.5 keV), and (b) Ho $K_{\alpha 2}$(46.6 keV). Vertical bars are indicative of the error in the activity at each point. Horizontal bars are for plotting purposes only and have no relationship to the uncertainty in time (which was assumed to be negligible).

short-lived activity also decays to ^{168}Ho and adds another growth component to the gamma rays of ^{168}Ho. Figure 5.3 shows the decay curves of the two strongest gamma rays (741 and 821 keV) in the decay of ^{168}Ho. Double growth and single decay fits of the ground (^{168}Dy) and isomeric (^{168}Ho^{m}) parent decays feeding the single daughter activity (^{168}Ho), with all half-lives held fixed, are shown in the figures. (The choice of 132 s for the short-lived parent will be justified in the next section.) This fit was performed using two growth and decay components with one of the daughter's initial activity held fixed at zero to help convergence. The decay fit in Figure 5.3 may look like only one-component decay, but the fit shown gave a better χ^2 value than single- or double-component decay or one growth and decay component. The ratio of the initial intensities for the short- to long-lived parent activities was ~7.2 for the fit in Figure 5.3 during the 1024-s run. The intensity of the 8.8-m parent, ^{168}Dy, was integrated over the counting interval and corrected for the known branching ratios of the 741- and 821-keV γ rays in ^{168}Ho decay, 35.9(8)% and 34.7(8)%, respectively [Led78]. An emission probability per beta decay of 0.225(16) was determined for the 487.0-keV gamma ray in ^{168}Dy decay in good agreement with the reported value 0.22(4) [Geh82].

Coincidence gates were set for the seven γ rays and the Ho $K_{\alpha 2}$ x ray in the HPGe or 52% Ge detectors and the corresponding spectra were generated for coincidences in the other Ge detector without the gate, the β telescope, or the plastic scintillator. A "clean" gate for the Ho $K_{\alpha 1}$ x ray could not be set due to interference from Er $K_{\alpha 2}$ x rays (48.2 keV) of the ^{168}Ho decay. Table 5.2 lists the seven gamma- and Ho K_{α} x-ray energies, absolute intensities, multipolarities, conversion coefficients (α's), and gamma-ray coincidences assigned to the decay of 8.8 m ^{168}Dy. The proposed partial decay scheme, put together from the coincidence and

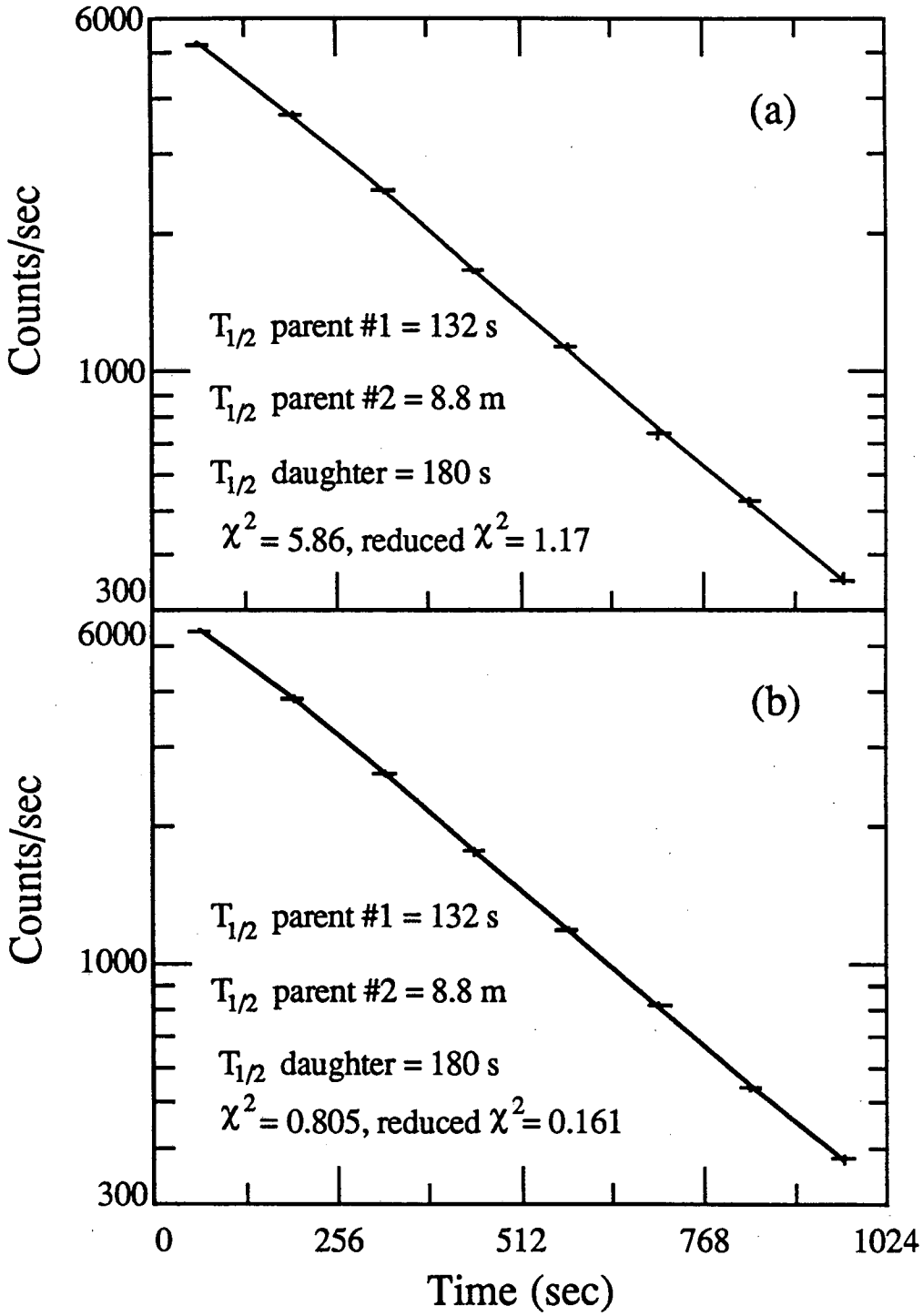

Figure 5.3. Calculated double growth and decay curves of ground and isomeric parent decay feeding one daughter activity, 3.0-m Ho-168, for the 1024-s run; (a) 741-keV gamma-ray decay and (b) 821-keV gamma-ray decay. All half-lives were held fixed.

Table 5.2. Gamma-ray energies, E_γ, absolute intensities, I_γ, multipolarities, M, theoretical conversion coefficients [Rös78], α_K and α_{tot}, and gamma coincidences in the decay of ^{168}Dy.

E_γ (keV)	I_γ (abs.)	M[a]	α_K	α_{tot}	Coincident γ rays[b]
43.8(2)	0.044(4)	(M1)	0	4.90	X, (143), 443
46.6 Ho $K_{\alpha 2}$	0.122(14)				43.8, X, (143), 443, 487
47.5 Ho $K_{\alpha 1}$	0.213(23)				c
143.5(2)	0.065(5)	(M2)	5.12	6.72	43.8, 487
192.5(2)	0.328(20)	E2	0.180	0.279	(X), 437
437.0(7)	0.085(11)	(M1)	0.0398	0.0465	X, 192
443.3(2)	0.155(11)	(E1)	0.00600	0.00703	43.8, X, (143)
487.0(2)	0.225(16)	(E1)	0.00486	0.00569	X, (143)
630.4(3)	0.136(11)	(E2)	0.00730	0.00897	d

[a] ( ) indicates the multipolarity was not measured but inferred from the decay scheme.
[b] X = Ho K x rays. ( ) indicates a weak coincidence.
[c] Due to Er $K_{\alpha 2}$ interferences, no clean coincidence gate could be set.
[d] No coincidences were measured.

intensity information, is shown in Figure 5.4. The gamma intensities listed in Table 5.2 were obtained from the 52% Ge detector due to the masking of the ^{168}Dy gammas by ^{168}Ho activity in the 24% Ge detector. The intensity of the ^{168}Ho activity was orders of magnitude greater than that of ^{168}Dy in these experiments. All the gamma rays assigned to ^{168}Dy decay and the Ho K_α x rays were observed in coincidence with β^- particles in the beta telescope and the plastic scintillator. Due to ^{168}Ho interferences, β^- energy endpoint analysis could not be performed for ^{168}Dy decay. An average value of 1.4 MeV was obtained from the mass formulae

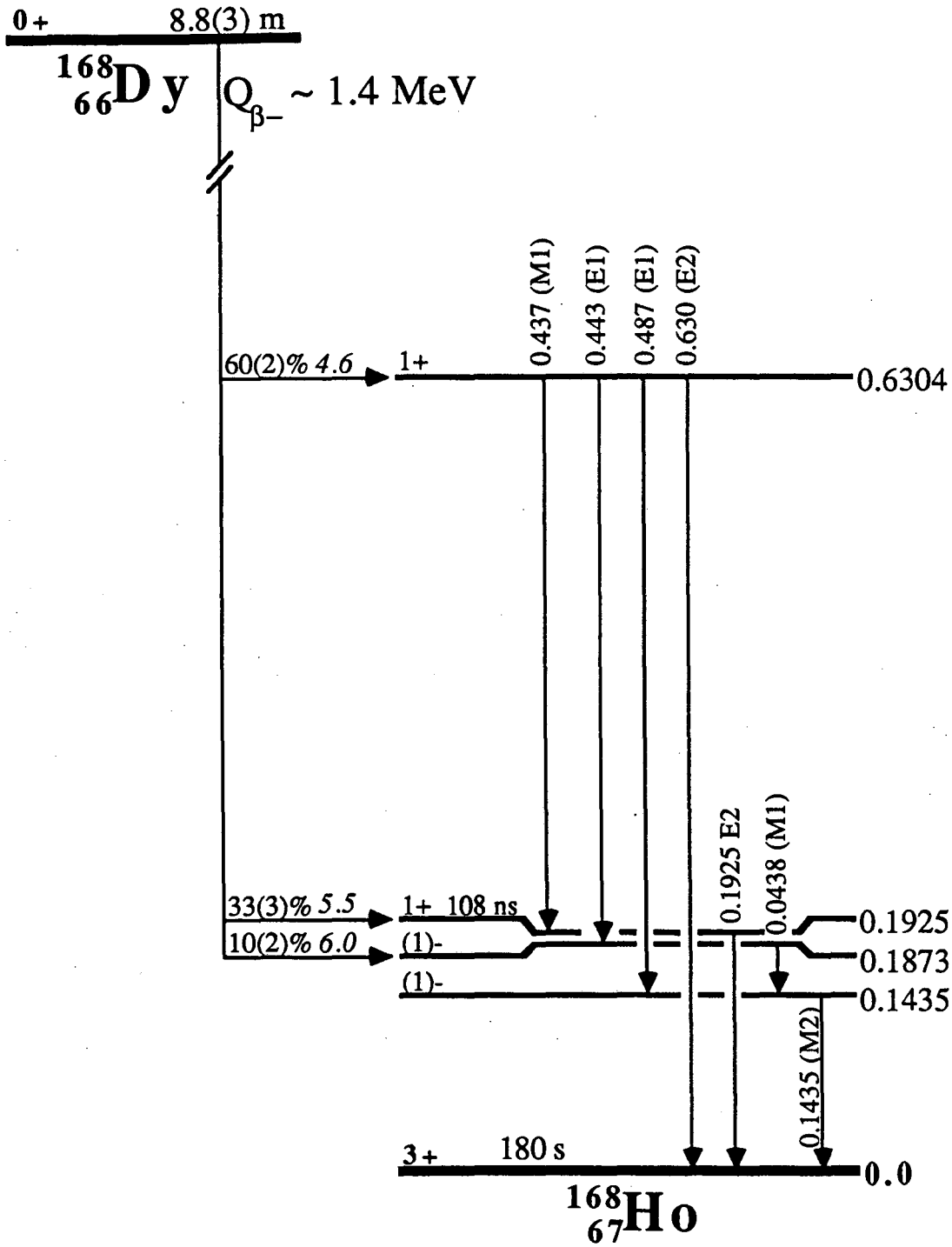

Figure 5.4. Proposed decay scheme for the decay of 8.8(3) m Dy-168. All energies are in MeV. The beta decay energy is an average of the mass formulae compiled by Haustein [Hau88]. Log *ft*'s are in italics. The spin and parity assignments are discussed in the text.

compiled by Haustein [Hau88]. The multipolarities of the 143- and 192-keV transitions were determined from intensity ratios with Ho K x rays (α_K=5.4(4) and 0.22(4), respectively) in coincidence spectra feeding each transition and the use of internal conversion coefficient tables [Rös78]. The multipolarity of the 43.8-keV transition could not be determined since K conversion is energetically impossible and the Ho L x-ray energies were too low for the HPGe detector to measure, but was inferred from the intensity balances in the proposed decay scheme given in Figure 5.4. TAC spectra measured between the 193-keV transition and β^- particles (in the beta telescope or plastic scintillator) indicated that the 192.5-keV level was delayed. Figure 5.5 shows the decay fit of the TAC data for this delayed level and the measured half-life of 108(11) ns. The measured half-life of this level, as compared with the half-life calculated using the single-particle model [Bla52] for an E2 transition and corrected for internal conversion was calculated as 5.0 Weisskopf units. The half-lives of all other levels were prompt (<5 ns). This is inconsistent with the measured M2 multipolarity for the 143.5-keV γ transition which has a calculated half-life of ~1.8 μs [Bla52] after correction for ICC.

The 1+ spin and parity of the 192- and 630-keV levels in the decay scheme are the only assignments that are consistent with their measured log*ft*'s and ground state gamma branches. The negative parity assignments of the 143- and 187-keV levels are consistent with the multipolarity assignments and their low beta feedings. A 0- or 1- spin assignment to the 187-keV level is consistent with the level scheme, but a 0- assignment is inconsistent with the measured log*ft*'s of ~7.2 to ~8.1 for other 0+ to 0- beta transitions in this region [Led78]. The 143-keV level's spin and parity must be the same as the 187-keV level since they are connected by a M1 transition ($\Delta I = 0$ or 1, $\Delta\pi$ = no). From these arguments the spin and parity of the

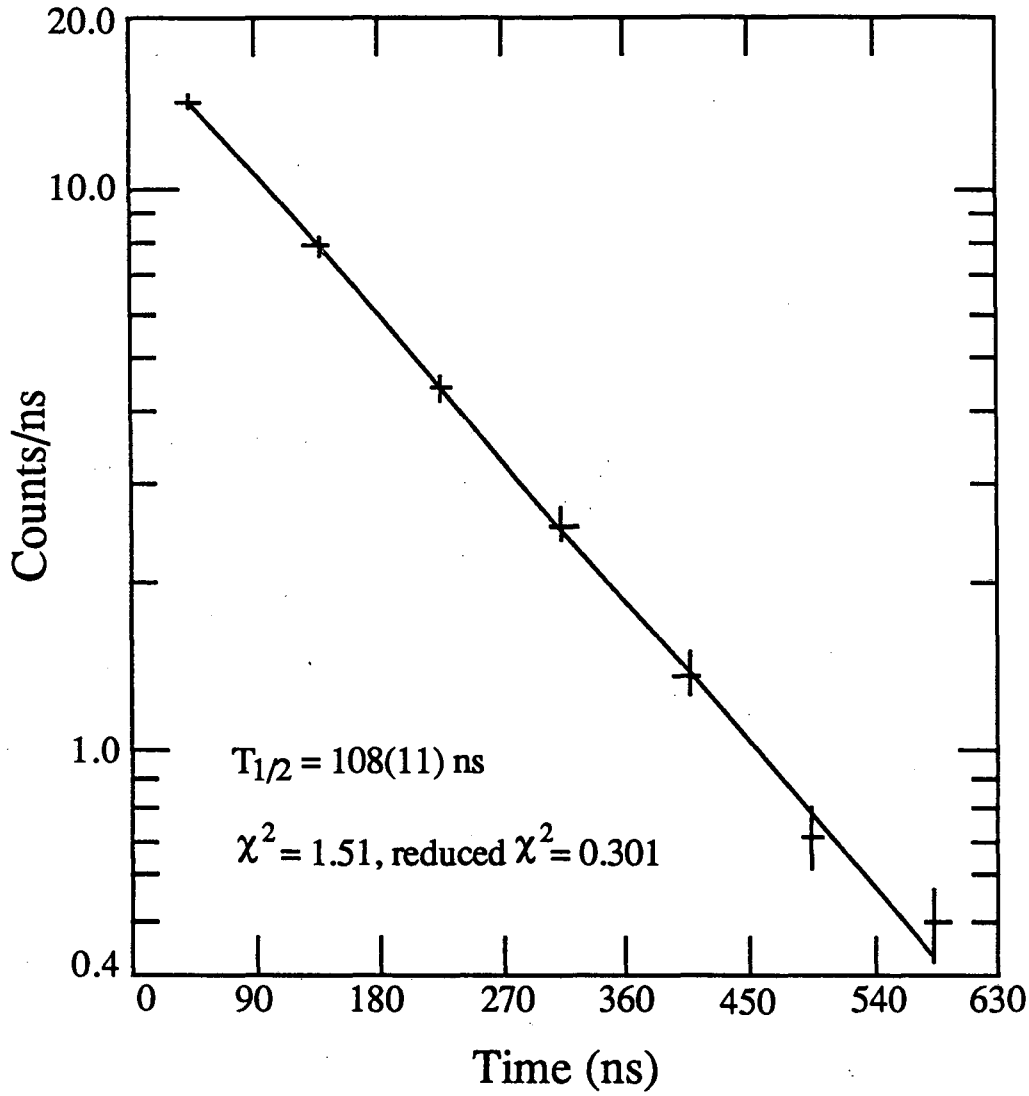

Figure 5.5. Single-component decay fit to the timing information between beta particles (in the beta telescope or plastic scintillator) and 193-keV gamma transitions measured in the A=168 mass chain.

143- and 187-keV levels are tentatively assigned as (1)-. The multipolarities of the 437-, 443-, 487-, and 630-keV transitions in Table 5.2 and Figure 5.4 are based on the level spin and parity assignments. Ground state β^- feeding would be inconsistent with the measured data and the parent and daughter spins and parities. Beta feeding to the 143-keV level had a measured upper limit of $\leq 2(4)\%$; however, with all of the beta intensity (103(5)%) assigned and the large percentage error on this beta branch, no beta feeding to this level is proposed.

5.1b. $^{168}Ho^m$ ISOMER

When a short-lived activity was noted in the 1024-s run data, the 512-s run data were analyzed more thoroughly than originally intended for the target/ion source tests. The Ho $K_{\alpha 1}$ and $K_{\alpha 2}$ x-ray singles activity again exhibited a two component decay behavior as shown in Figure 5.6. A weighted average of 132(4) s was determined for the half-life of the short-lived x-ray activities from both the 512-s and 1024-s runs. The intensities of the 132-s Ho $K_{\alpha 1}$ and $K_{\alpha 2}$ x rays were determined by integrating the short-lived activity of the decay curves. This was also done for the short-lived x-ray activities in the 1024-s run in Figure 5.2.

Two possible explanations of this observation are: a new ^{168}Dy isomer which predominantly β^- decays (^{168}Dy decay showed no growth and decay behavior) with an internally converted γ ray, or a new ^{168}Ho isomer which has an isomeric transition (IT) branch which is internally converted. Isomers of even-even isotopes are not expected in this region and this new activity is assigned to the new isomer $^{168}Ho^m$ with a half-life of 132(4) s.

The decay intensity of this new isomer for decay by isomeric transition was determined by analyzing the growth and decay curves of its daughter activity, 3.0 m

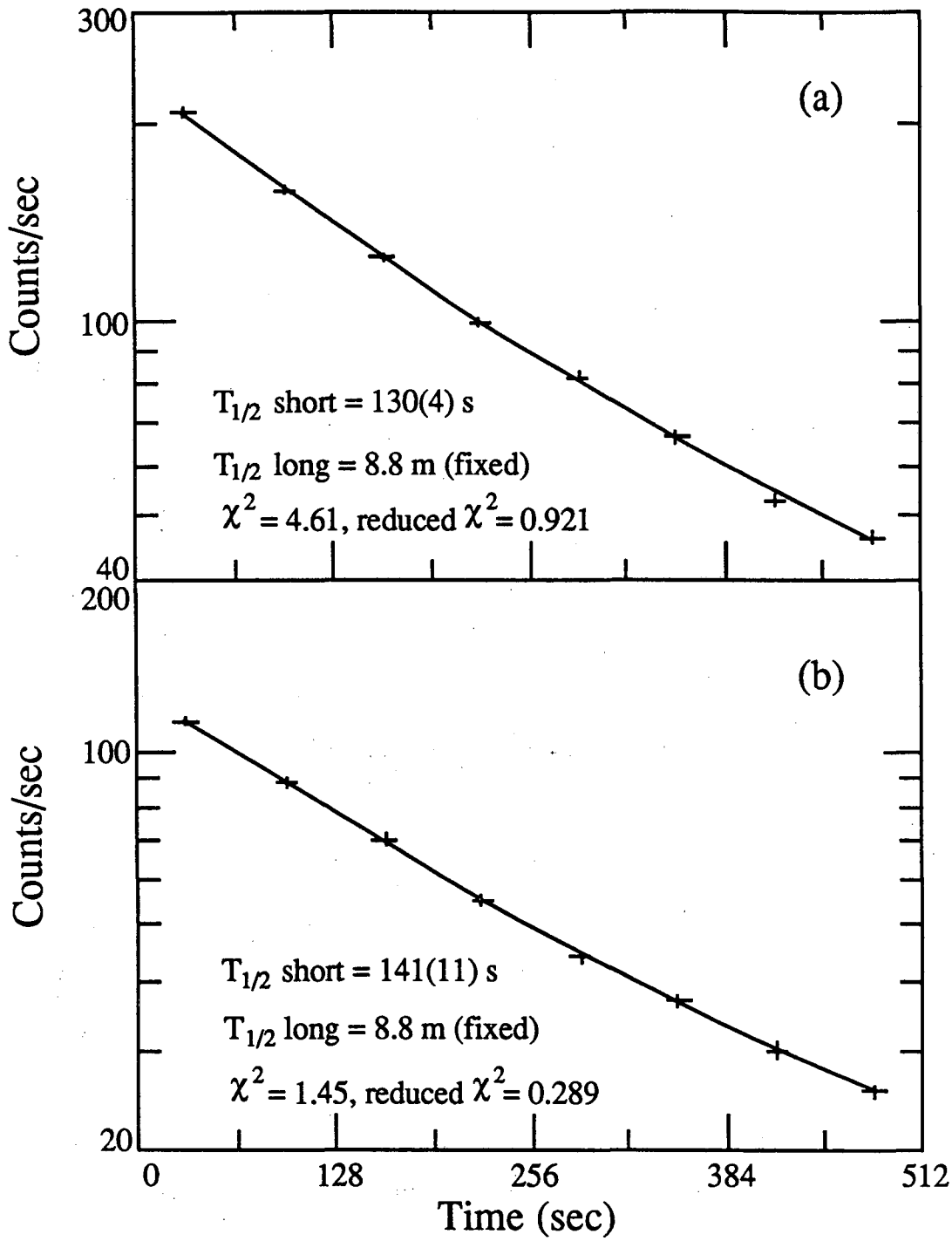

Figure 5.6. Two-component decay curves fit to the Ho x-ray data for the 512-s run; (a) Ho $K_{\alpha 1}$ (47.5 keV), and (b) Ho $K_{\alpha 2}$ (46.6 keV).

^{168}Ho, as was done to determine the decay intensity of ^{168}Dy. Figure 5.7 shows the decay curves of the 741- and 821-keV gamma rays of ^{168}Ho for the 512-s run. A decay curve fit of two growth and decay components with one daughter's initial activity held fixed at zero and the long-lived parent and the daughter half-lives fixed at 8.8 m and 180 s, yielded a ~120 s short-lived parent half-life (fits shown in Figure 5.7). The ratio of the initial activities for the short- to long-lived parent activities was ~11.2 for the fit in Figure 5.7 during the 512-s run. The intensity of the short-lived parent was integrated over the counting interval and corrected for the 741- and 821-keV emission probabilities [Led78]. This was also done for the short-lived parent in the 1024-s run growth and decay curves in Figure 5.3. An absolute Ho K x-ray intensity of 0.133(10) was determined for the IT branch of ^{168}Ho^{m} by dividing the Ho K x-ray intensity, (Ho $K_{\alpha 1}$ + $K_{\alpha 2}$ intensity)/0.79, by the short-lived parent intensity (determined above) for both the 512-s and 1024-s runs.

The HPGe and 52% Ge detectors' singles data did not contain any gamma rays that decayed with this 132-s half-life. All γ rays seen could be assigned to other A=168 activities or background radiations. The γ rays of ^{168}Ho were investigated very closely to determine that their intensities matched those in the literature [Led78] and showed no β^- feeding from the ^{168}Ho^{m} isomer. Based on the above facts, the β^- branch of this new isomer was determined to $\leq$0.5%.

Having found only a half-life and K x-ray intensity, we sought means to identify the IT gamma ray. For internal conversion of Ho K x rays, the gamma transition in the decay of this new isomer must have an energy $\geq$ 57 keV. A high multipolarity is likely for the γ transition depopulating the isomeric level in order to a half-life as long as 132 s. Also, any of the γ rays in the decay of the isomer must be highly converted, or have energies less than 10 keV, or they would have been

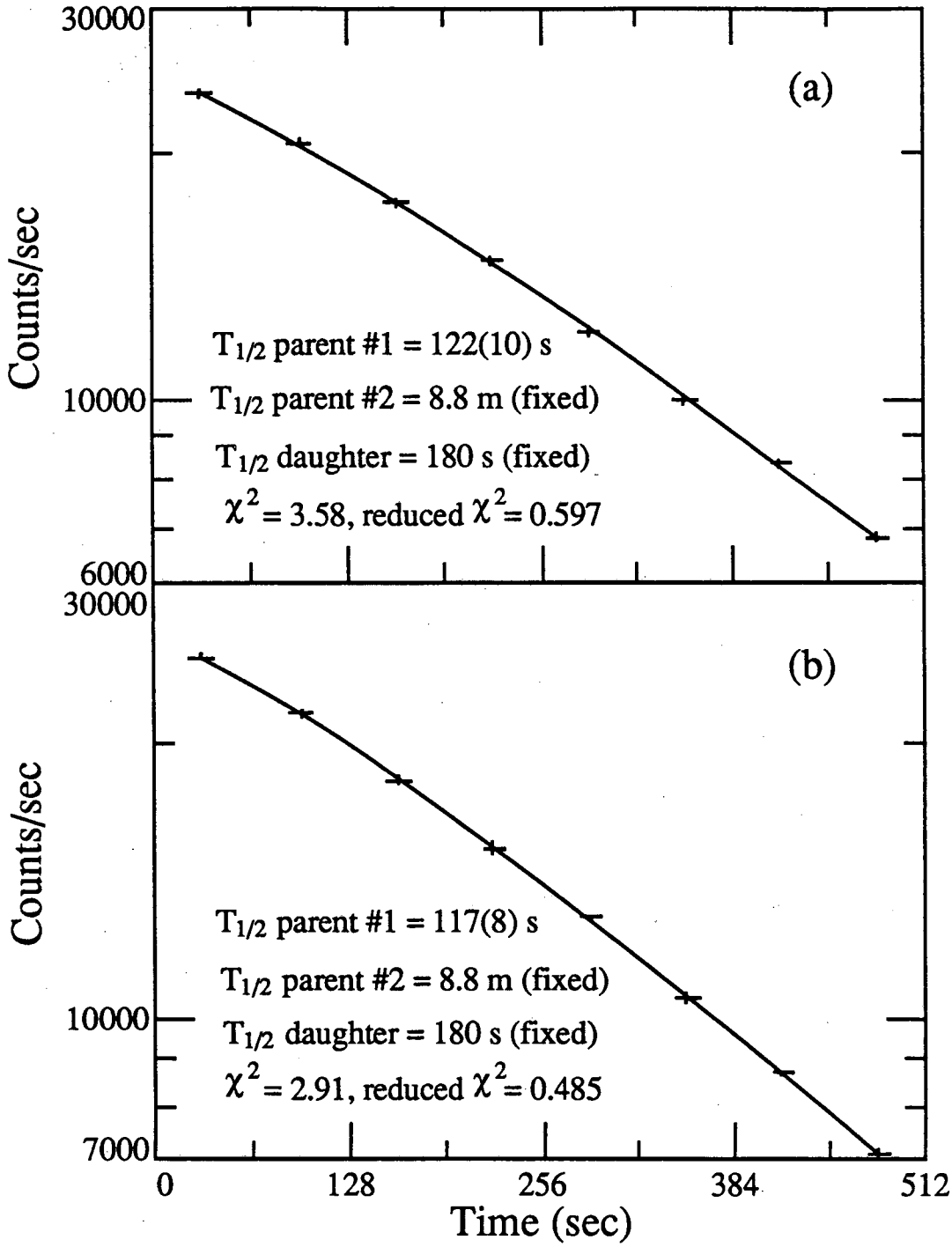

Figure 5.7. Calculated double growth and decay curves of ground and isomeric parent decay feeding one daughter actifity, 3.0-m Ho-168, fit to the data from the 512-s run; (a) 741-keV gamma-ray decay and (b) 821-keV gamma-ray decay.

detected above the background in the singles data. Possible decay schemes are the following: a single, high-multipolarity, and highly-converted γ transition ($\geq$ 57 keV) decaying to the ground state of ^{168}Ho; or a high-multipolarity, highly-converted γ transition that feeds one or more low energy (< 10 keV) or highly-converted γ transitions; or a high-multipolarity, low-energy (< 10 keV) γ transition that feeds a highly-converted γ transition ($\geq$ 57 keV). The prospect of finding the specifics of the last possibility was slim with the existing data due to the myriad of γ energy and multipolarity combinations. The first two possibilities had one feature in common; a high-multipolarity, highly converted γ ray with an energy $\geq$ 57 keV that depopulates the isomeric level. A search for this gamma ray was performed by first calculating the energy and multipolarity of a γ transition that would have a theoretical K x-ray intensity equal to the measured value of 0.133(10). Figure 5.8 was prepared using internal conversion coefficient tables [Rös78] and dividing the K conversion coefficient by the total conversion coefficient plus one (for the γ-ray intensity) for each γ-ray energy and multipolarity. Transitions types E3, E4, M3, and M4 were the only multipolarities shown due to the level half-life requirements. The possible γ-ray energies (59, 91, 127, and 196 keV) for each transition type (M3, M4, E3, and E4, respectively) are indicated in Figure 5.8. Next, again using ICC tables [Rös78], theoretical absolute γ-ray intensities were calculated, $(1 + \alpha_{tot})^{-1}$, for each of the four energies and multipolarities. The E3 and E4 transitions were not possible since their theoretical γ-ray intensities, ~6.0% and ~6.8%, respectively, indicate that the γ ray would have been seen above the measured background. The theoretical γ-ray intensities of the 59-keV M3 and the 91-keV M4 γ transitions, ~0.04% and ~0.03%, respectively, are small enough for the γ ray not to be measured.

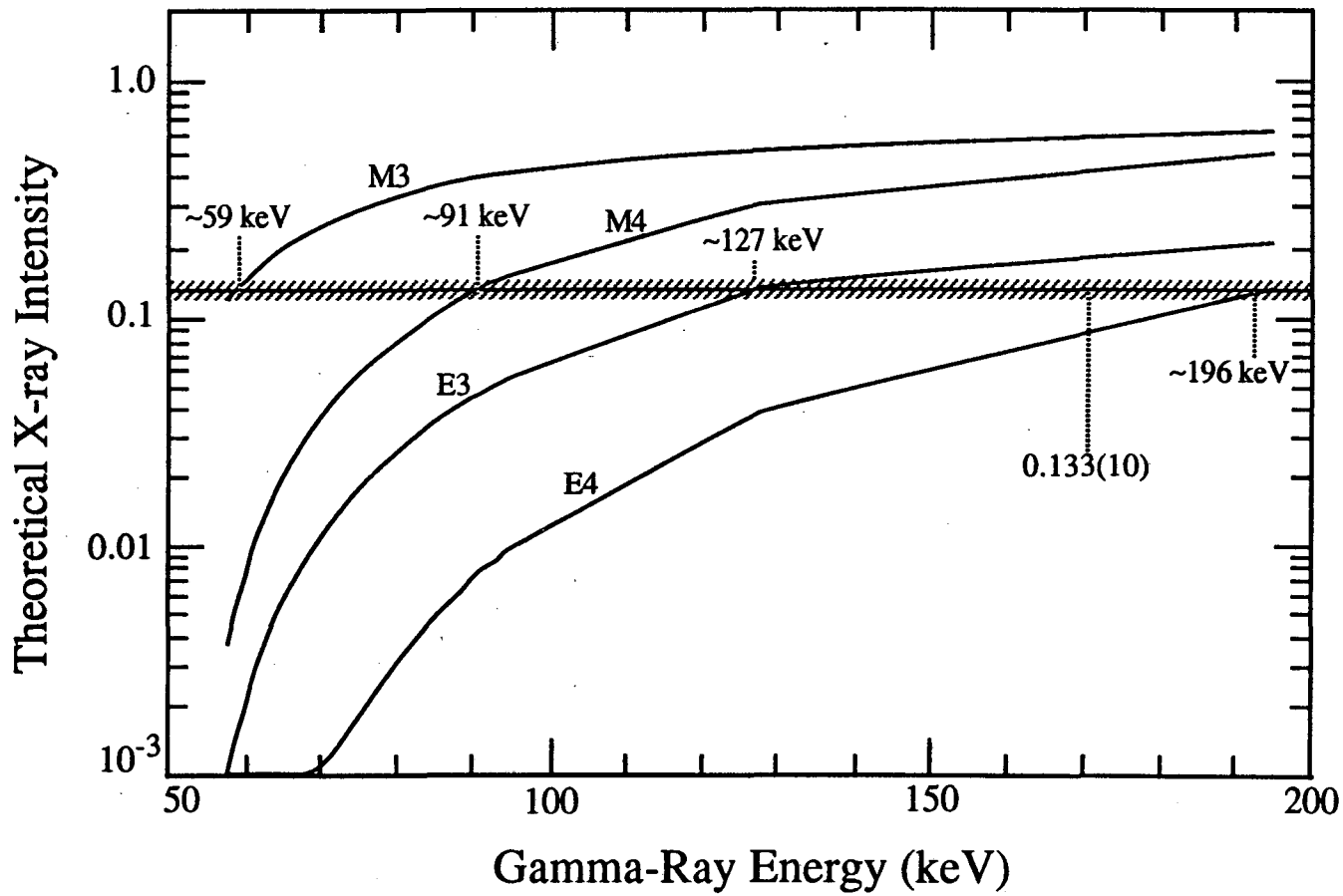

Figure 5.8. Theoretical K x-ray intensities calculated for M3, M4, E3, and E4 gamma tansitions from ICC tables [Rös78] for a Z=67 nucleus. Line at x-ray intensity = 0.133(10) is the measured value for the isomeric decay of Ho-168.

Half-lives of these γ transitions were calculated using the single-particle model half-life formulae from Blatt and Weisskopf [Bla52]. They were corrected for their internal conversion branches by multiplying the calculated half-life by the theoretical γ intensities calculated above. For a Z=67 and A=168 nucleus, a 59-keV M3 γ transition would have a calculated half-life of 8.5 s and a 91-keV M4 γ transition would have a 34-d half-life. The calculated half-life for the M4 transition was too large by four orders of magnitude, clearly in disagreement with M4 transitions, while the M3 transition calculation was too short by a factor of ~15, well within measured distributions for this transition type [Bla52]. Assuming a single IT M3 transition, a spin and parity of 6+ is proposed for the isomeric level since the ground state of ^{168}Ho has a 3+ assignment [Hau71].

Similar isomerism is seen in another N=101 nucleus, ^{172}Lu. This nucleus has an isomeric level that is depopulated by IT via a M3 gamma transition. Valentin *et al.* [Val62] assigned 4- and 1- spins and parities to the ground and isomeric states, respectively. They also proposed that these assignments arose from couplings of the 71st proton level, 7/2+[404], with the 101st, 1/2-[521], and 103rd, 5/2-[512], neutron levels. These levels, assignments and decay of ^{172}Lu isomers are depicted in Figure 5.9a. These assignment of the 1- isomeric level consisting of the 7/2+[404] proton and 5/2-[512] neutron levels has been further justified by the assignment of the ^{174}Lu (71 protons and 103 neutrons) ground state as 1-, also composed of the same proton and neutron level couplings [One72]. Using the same single-particle model half-life formulae as above [Bla52], the calculated half-life after correction for internal conversion for ^{172}Lu was 8.6 s, too short by a factor of ~26.

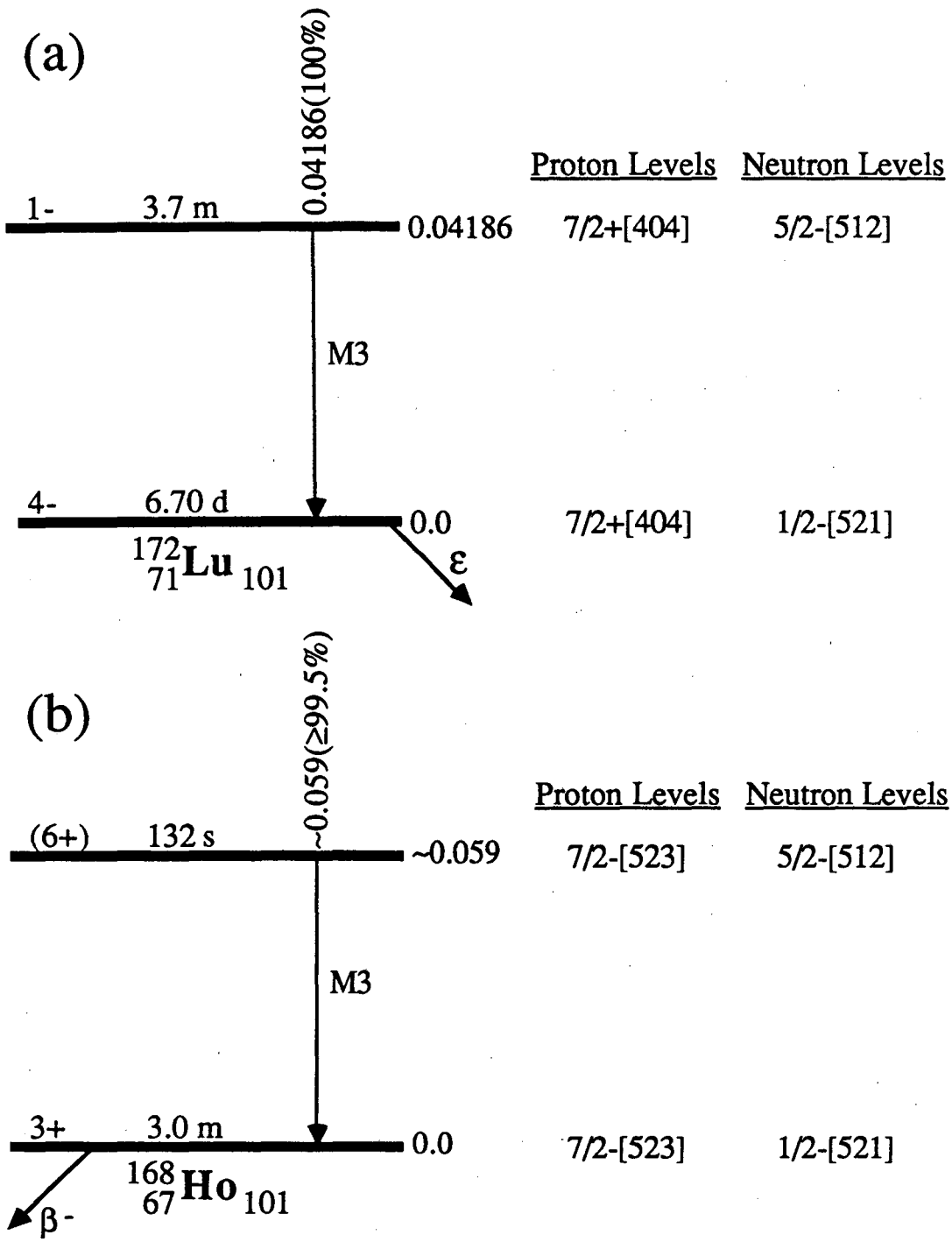

Figure 5.9. Level schemes of N=101 isomers and their proton and neutron level couplings; (a) Lu-172 and Lu-172m, and (b) Ho-168 and proposed Ho-168m.

If similar isomerism as ^{172}Lu is seen in ^{168}Ho, the level scheme and assignments shown in Figure 5.9b result. The 7/2-[523] spin and parity of the 67th proton level has been well established for this region [Led78] and other even-massed Ho isotopes [Kat78, Tuu78]. The ground state and isomeric levels result from couplings of the 7/2-[523] proton level with the 1/2-[521] and 5/2-[512] neutron levels. The assignment of the 6+ isomeric state is further justified by the ground state assignment of ^{170}Ho (67 protons and 103 neutrons) as 6+ consisting of couplings of the 7/2-[523] proton and 5/2-[512] neutron levels [Kat78, Tuu78]. It should be noted that the spin and parity assignments mentioned in this section are in agreement with predictions of Nilsson *et al.* [Nil69] using deformations predicted by Möller and Nix [Möl81].

The decay scheme in Figure 5.9b is the proposed scheme for the 132(4) s ^{168}Ho^{m} isomer. Assignments of the spin, parity and energy of the isomeric level are uncertain due to the possibility of the ~59 keV M3 transition feeding another level which deexcites by a γ ray with an energy too low (< 10 keV) to be detected by the measurement system or which is highly converted. However, due to similarities to ^{172}Lu^{m} decay, the proposed scheme in Figure 5.9b is highly probable.

5.1c. ^{168}Ho $Q\beta^-$ CORRECTIONS

The accepted $Q\beta^-$ value for the decay of 3.0-m ^{168}Ho has been reported as 2.74(10) MeV [Kaw73]. This result was obtained from endpoint measurements of β^- particles coincident with gamma rays depopulating the 821-keV level in ^{168}Er. Recalculations from their data indicated an average endpoint energy of 1.90(9) MeV for β^- particles in coincidence with 80-, 741-, and 821-keV gamma rays. Their reported $Q\beta^-$ value was determined using only the endpoint energy of the 821-keV

coincident β^- particles, 1.91(10) MeV. The beta endpoint of ^{168}Ho had also been measured prior to the results above [Kaw73] as ~2.2 MeV (with no reported error) [Tak61], however, this value was obtained with no gamma gating.

During the determination of the β telescope efficiency, section 4.3, endpoint energy problems were noted. The endpoint energies in Figures 4.2 and 4.3, 2.10(6) and 2.10(6) MeV, for β^- particles coincident with 741- and 821-keV gamma rays , do not agree with the accepted value [Kaw73], but are similar to the value measured by Takahashi *et al.* [Tak61]. An extensive study of the beta endpoints for the decay of ^{168}Ho was undertaken. Beta endpoints were determined for β^- feedings to levels at 821.1, 895.7, and 994.7 keV [Hau71]. These levels were chosen for their large β^- feedings and small feedings from more excited levels of ^{168}Er. Gates were set on the two strongest gamma transitions depopulating each level and their corresponding backgrounds in the 52% Ge detector. The beta spectra coincident with these gates were obtained. Beta spectra were generated by adding the two γ-gated β telescope spectra and subtracting the background-gated β telescope spectra for each level. Fermi-Kurie plots were calculated for each of the three beta spectra and their corresponding endpoints determined. Figures 5.10, 5.11, and 5.12 show the gamma-coincident β^- spectra, corresponding Fermi-Kurie plots and β^- endpoints. The results of this analysis are summarized in Table 5.3 which contains the level energy, γ-gates used, measured endpoints, and the calculated Q_{β^-} values. The beta endpoint found by Kawade *et al.* [Kaw73] for the 821-keV level is also listed in the table. A weighted average of 2.93(3) MeV was determined from the three Q_{β^-} values in Table 5.3, which gives 2.93(3) MeV as the Q_{β^-} value for the decay of 3.0-m ^{168}Ho^g. Comparisons of revised log *ft* values

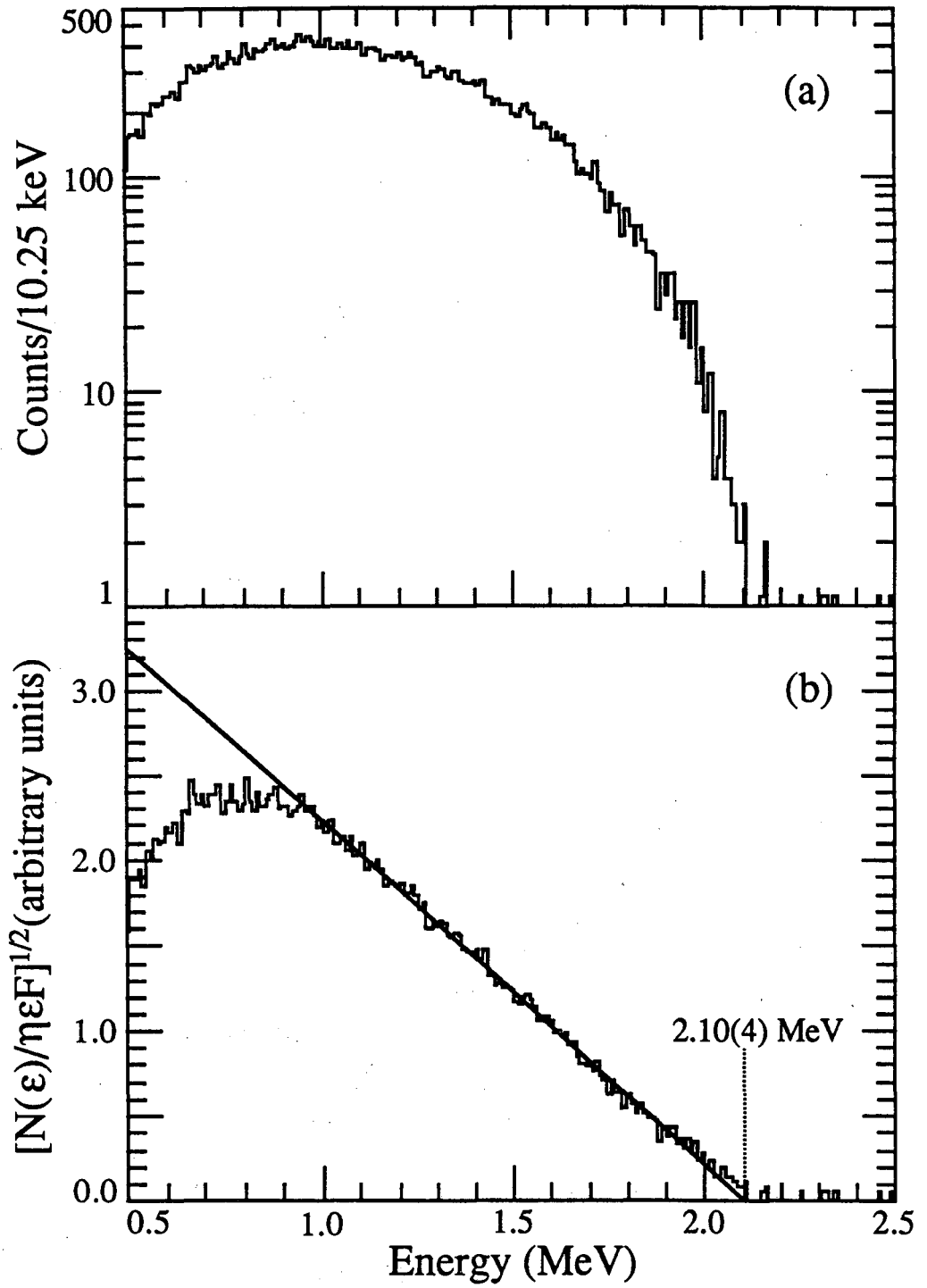

Figure 5.10. Beta decay data for β^-particles measured in the beta telescope coincident with gamma rays depopulating the 821-keV level (see Table 5.3) in the decay of 3.0-m Ho-168; (a) actual coincident beta spectrum and (b) Fermi-Kurie plot and endpoint energy.

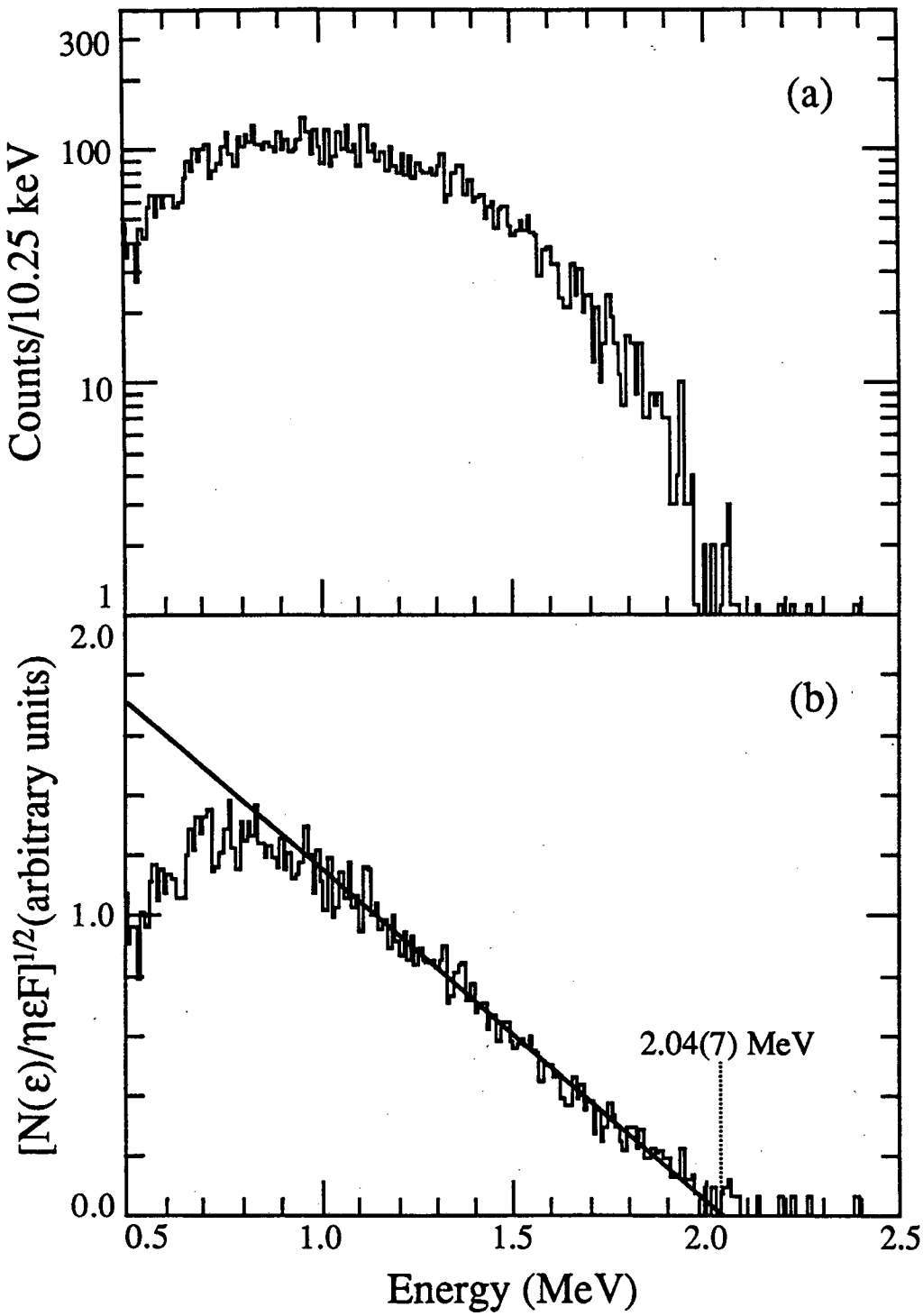

Figure 5.11. Beta decay data for β^-particles measured in the beta telescope coincident with gamma rays depopulating the 896-keV level (see Table 5.3) in the decay of 3.0-m Ho-168; (a) actual coincident beta spectrum and (b) Fermi-Kurie plot and endpoint energy.

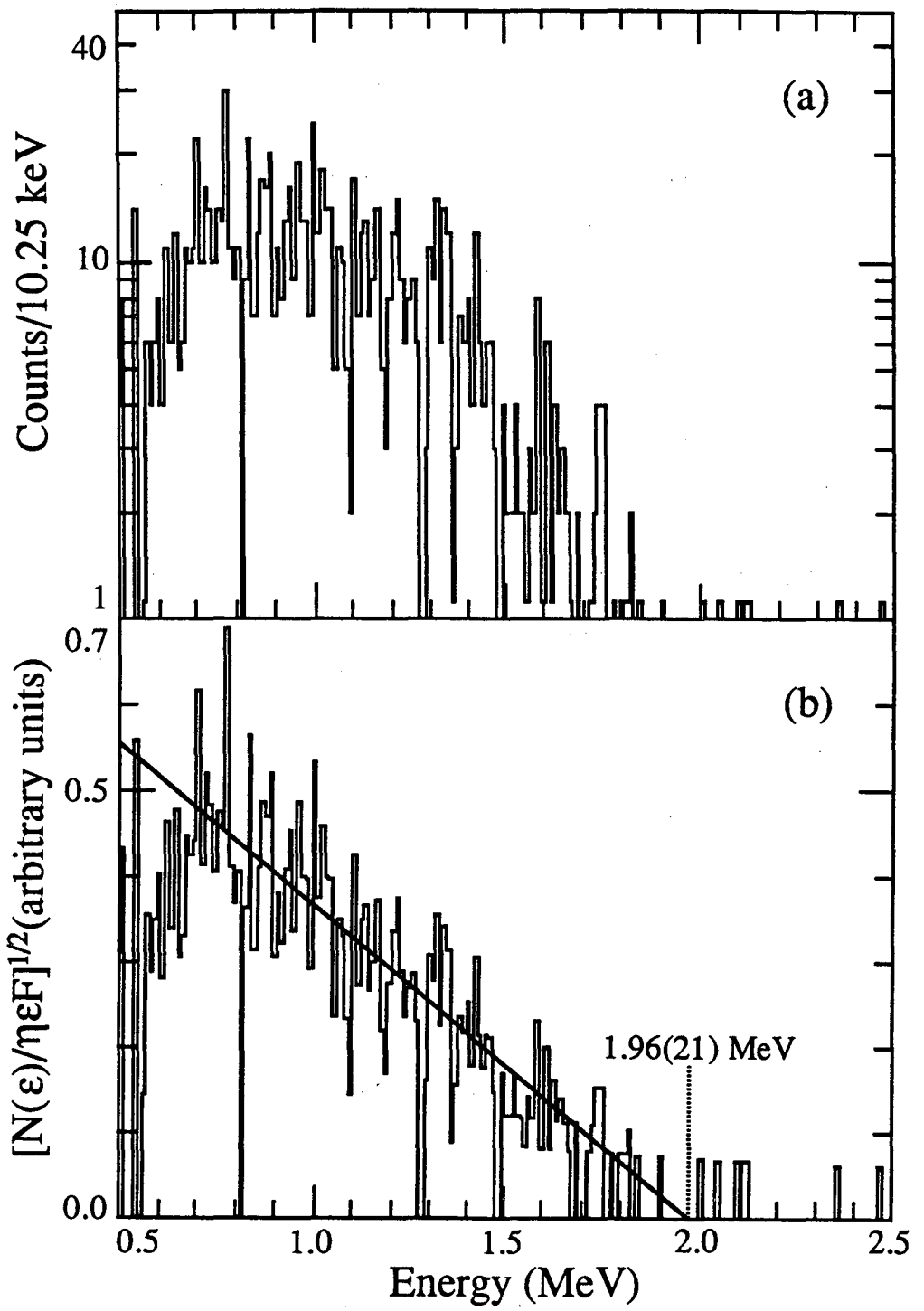

Figure 5.12. Beta decay data for β^-particles measured in the beta telescope coincident with gamma rays depopulating the 995-keV level (see Table 5.3) in the decay of 3.0-m Ho-168; (a) actual coincident beta spectrum and (b) Fermi-Kurie plot and endpoint energy.

Table 5.3. Beta endpoint data for Q_{β^-} value determinations for the decay of 3.0 m ^{168}Ho, and the previously measured endpoint energy.

Level Energy (keV)	γ-ray Gates Used (keV)	Measured β^- Endpoint (MeV)	Endpoint from [Kaw73] (MeV)	Calculated Q_{β^-} Value (MeV)
821.1	741, 821	2.10(4)	1.90(9)	2.92(4)
895.7	632, 816	2.04(7)	-	2.94(8)
994.7	731, 915	1.96(21)	-	2.96(21)

Table 5.4. Comparison of old log *ft* values [Led78] for the β^- decay of 3.0-m ^{168}Ho with revised values calculated with new Q_{β^-} value 2.93(3)MeV.

^{168}Er level (keV)[a]	β^- int. (%)[a]	Old log *ft*[a]	Revised log *ft*
821.1	71	5.3	5.4
895.7	18	5.8	6.0
994.7	2.0	6.6	6.8
1541.4	2.6	5.9	6.2
1569.5	0.15	7.1	7.4
1848.2	0.58	6.1	6.4
1915.3	0.13	6.6	7.0
1930.2	0.33	6.2	6.5
1994.6	0.19	6.3	6.7
2193.0	1.7	4.9	5.4
2254.7	0.38	5.3	5.9
2424.9	0.46	4.6	5.4
2484.6	0.072	5.1	6.0

[a] Values are from [Led78].

calculated using the new Q_{β^-} value with log *ft*'s [Led78] for the old Q_{β^-} value are listed in Table 5.4.

5.2. ^{169}Dy - NEW ISOTOPE

The A=169 mass chain was studied using ^{170}Er ions with the standard OASIS target/ion source geometry (capillaries, W endplate, no window) or sources with W electroplated on Ta endplates. Natural erbium or ^{170}Er enriched (~1.7 g ^{170}Er strip spot-welded to natural erbium closest to the plasma region of the SuperHILAC ion source) ion sources were used as the source material for the SuperHILAC to deliver beam intensities of 35 to 100 particle nanoamperes on target for ~57 hours. This experiment was performed to search for the new isotope ^{169}Dy. Using the mass prediction compilation [Hau88], a simple average Q_{β^-} value of 3.2 MeV was calculated for the decay of this isotope. Half-lives of 38 s [Kla84] and 64 s using the GTBD code [Tak88] and the Q_{β^-} value above were predicted for this isotope. A tape cycle time of 160 s was chosen to maximize the measured activity. A summary of half-lives, decay modes, and Q values of the other A=169 isobars [Bro86] that could be separated by OASIS is listed in Table 5.5. Actually, ^{169}Hf was not surface ionized well (~10^{-4} efficiency compared to Lu isotopes) in the OASIS ion source, due to its high first ionization potential (7.0 eV versus 5.4 eV for Lu).

High-energy singles β^- particles were measured in the beta telescope with energies beyond the β endpoints of the isotopes listed in Table 5.5 and are shown in Figure 5.13a. Because β^+ maximum energies are 1.022 MeV less than the decay energy, ^{169}Hf and ^{169}Lu endpoints were ruled out. The most energetic beta endpoint, 2.03 MeV, for ^{169}Ho results from a small, <5%, beta branch to a 91.9

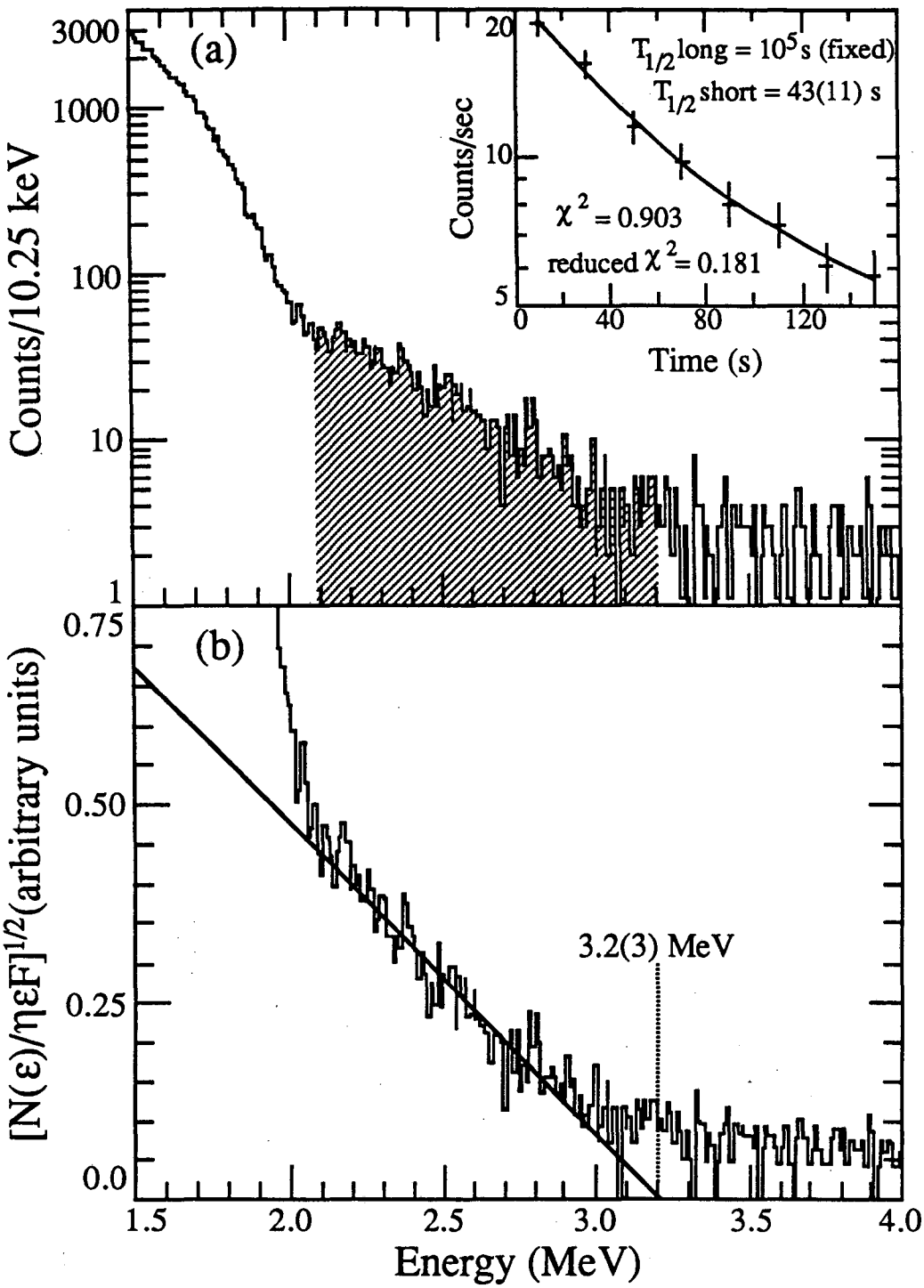

Figure 5.13. Beta decay data for A=169 mass chain; (a) beta particle spectrum measured in the beta telescope and (b) Fermi-Kurie plot and 3.2(3) MeV endpoint. The inset in (a) shows the two-component decay fit of the beta intensity from 2.1 to 3.2 MeV (shaded portion of the spectrum).

Table 5.5. Summary of A=169 isobar information [Bro86] for nuclei that can be separated in OASIS. ^{169}Hf (~10^{-4} ionization efficiency relative to the other elements) is listed since some of this isobar might have been separated.

Isotope	Half-life	Decay Mode	Q value (MeV)[a]
^{169}Hf	3.24 m	EC, β^+	3.35(10)
^{169}Lu	1.42 d, 2.7m[b]	EC, β^+, IT	2.293(3)
^{169}Yb	32.0 d, 46 s[c]	EC, IT	0.908(4)
^{169}Tm	stable	--	--
^{169}Er	9.40 d	β^-	0.3509(14)
^{169}Ho	4.7 m	β^-	2.125(20)
^{169}Dy	~38 s, ~64 s[d]	β^-	~3.2[e]

[a] Q value reported is for ground state decay.
[b] ^{169}Lu has an IT decaying isomer at 24.2 keV. Ground state half-life is listed first.
[c] ^{169}Yb has an IT decaying isomer at 29.0 keV. Ground state half-life is listed first.
[d] Listed $T_{1/2}$ values are predictions, [Kla84] and [Tak73] respectively.
[e] Q value is an average from mass tables compiled in [Hau88].

keV level in ^{169}Er [Hau71]. Beta particles with energies above the 2.03 MeV ^{169}Ho endpoint were seen clearly above the background (similar to the 3.5 to 4.0 MeV region in Figure 5.13a). The inset to Figure 5.13a shows the two-component decay fit of the background-subtracted beta intensity between 2.1 and 3.2 MeV (shaded region), with the long component held fixed at a very long half-life, 10^5 s, to represent background that wasn't completely subtracted. A half-life of 43(11) s was obtained for the short-lived activity, which again does not agree with any of the

listed radiations in Table 5.5. A Fermi-Kurie plot of the β particles measured is shown in Figure 5.13b. A β^- endpoint of 3.2(3) MeV was obtained from fitting the region from 2.1 to 2.9 MeV. Gamma coincidence spectra with these energetic β^- particles produced only background radiations. To check the β telescope energy calibration γ gates were set on γ radiations depopulating the 853-keV level in the decay of ^{169}Ho and a beta endpoint of 1.3(1) MeV was obtained, in excellent agreement with 1.3 MeV found in the literature [Hau71].

Close inspection of the γ-ray and x-ray singles data yielded only one short-lived gamma ray at 1578.2(4) keV. It decayed with a half-life of 35(11) s as shown in the two-component decay fit in Figure 5.14. Holding the long-component fixed at a long half-life, 10^5 s, produced the best chi-squared value for this decay. No Ho K x rays were observed and all other γ rays measured were longer lived. The beta particle spectrum gated by this 1578-keV γ ray is shown in Figure 5.15. Statistics were too poor to obtain a beta endpoint, but visual inspection of the spectrum indicates an endpoint of ~1.5 MeV, which is consistent with a total decay energy of 3.2 MeV. The time histogram of the 38 beta particles in coincidences with 1578-keV γ rays is shown in Figure 5.16a. A maximum likelihood fit of these data is shown in Figure 5.16b. (Details on the maximum likelihood formulae and computer code used are given in Appendix B.) The likelihood calculation reached a maximum at 58 s and dropped to 50% of this maximum (68% confidence limits) at 42 and 90 s which gave a half-life of $58\binom{+32}{-16}$ s.

These results indicated a beta decaying isotopes with a 39(8) s half-life, obtained from a weighted average of the high-energy β^- particle and 1578-keV γ-ray half-lives, which decays to the ground state, with a maximum β^- energy of 3.2(3) MeV, or to a 1578.2(4)-keV level which deexcites directly to the ground state.

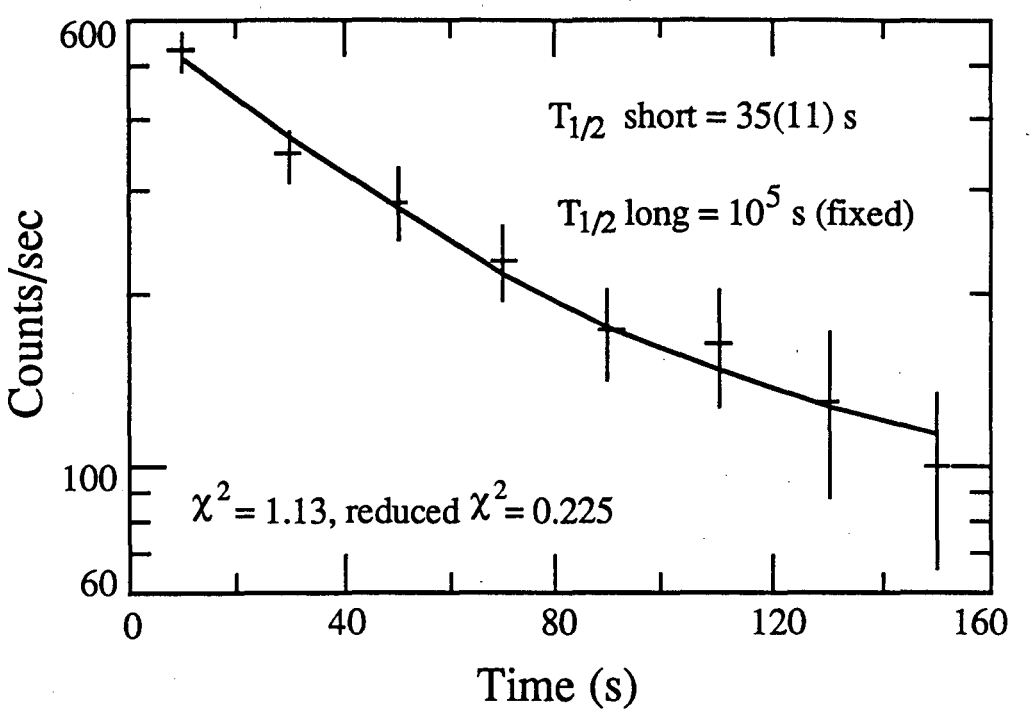

Figure 5.14. Two-component decay curve fit to the intensity distribution of the 1578.2(4) keV gamma rays measured in the 52% Ge detector for the A=169 mass chain.

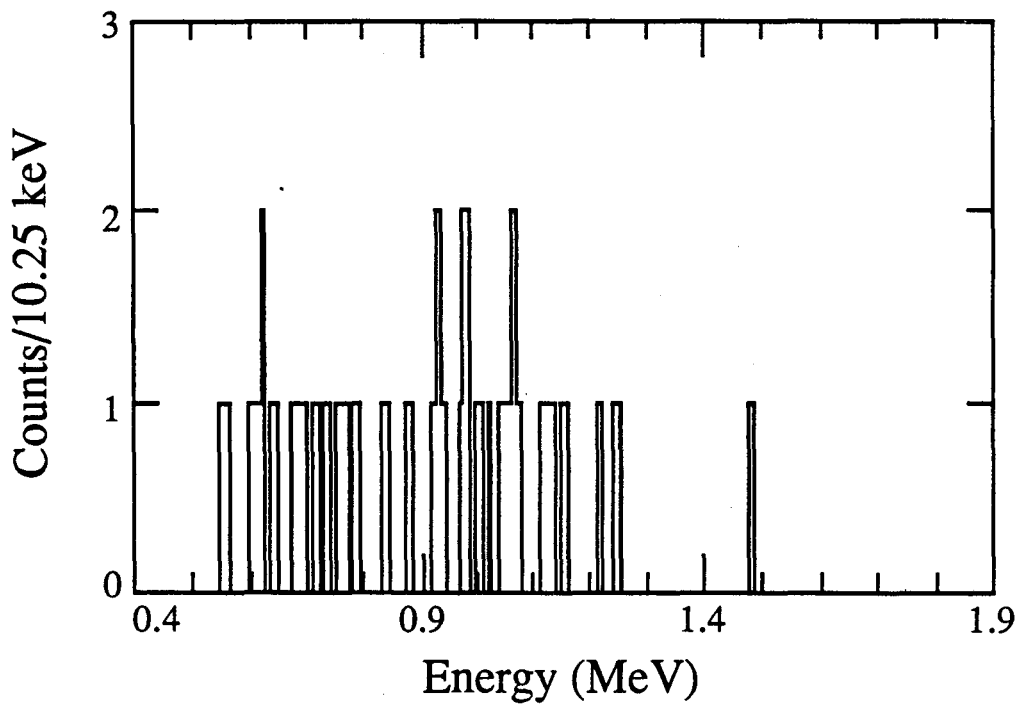

Figure 5.15. Beta particle spectrum measured in coincidence with 1578-keV gamma rays in the A=169 mass chain.

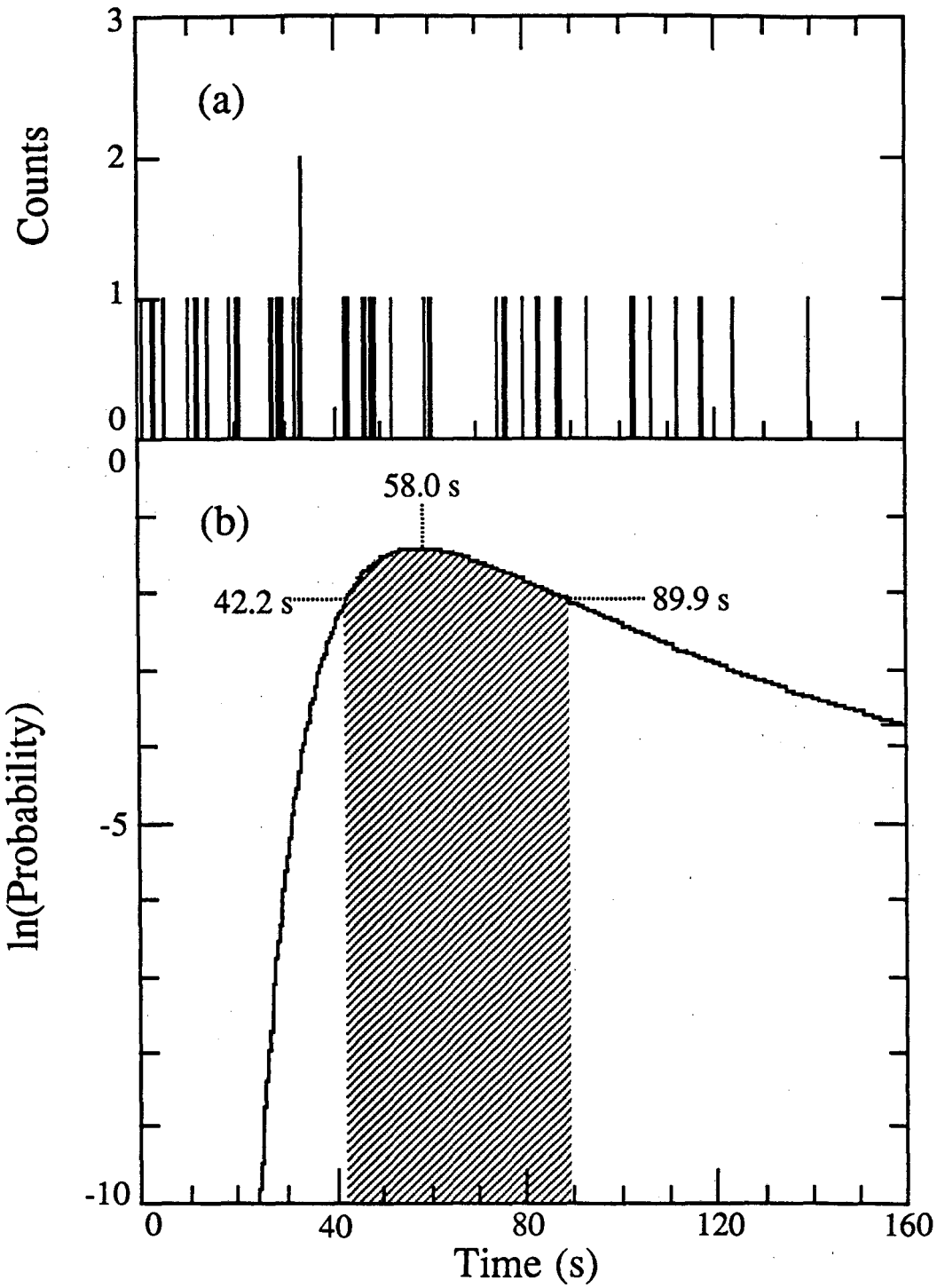

Figure 5.16. Time information of the beta particles measured in coincidence with 1578-keV gamma rays in the A=169 mass chain; (a) time distribution and (b) maximum likelihood calculation showing the probabilty of the time being the correct half-life to fit the time distribution. Shaded region shows where the probability drops to 50% of the maximum value (68% confidence limits).

Based on the agreement of the measured beta endpoint to the predicted Q_{β^-} value for ^{169}Dy and of the measured half-life with the predicted values, the discovery of the new isotope ^{169}Dy is suggested. The intensity of the ground state beta branch was determined by calculating a β^- spectrum with a 3.2 MeV endpoint as was done for the β telescope calibration, section 4.3. This calculated spectrum was normalized to the measured β spectrum in the 2.3 to 3.0 MeV interval. The measured and calculated β spectra are shown in Figure 5.17. The integral of the calculated β^- spectrum was corrected for the β telescope efficiency to determine the ground state β^- intensity. The 1578 keV γ-ray's intensity was determined from the 52% Ge detector because the statistics were poor in the 24% Ge detector (low efficiency at this energy, see Figure 4.1) and summing was not a problem since there were no other gamma rays in coincidence. Ground state and 1578-keV beta branches of 0.78 and 0.22, respectively, were determined. Estimated errors on these quantities are ~20% due to uncertainties in the method to determine the ground state β^- intensity and possible missed weak γ rays.

The tentative decay scheme proposed for ^{169}Dy is shown in Figure 5.18. This scheme is consistent with the lack of x rays since there would be very little internal conversion. The assignments of the 103rd neutron (odd particle in ^{169}Dy) and the 67th proton (odd particle in ^{169}Ho), 5/2-[512] and 7/2-[523], respectively, are well established for this region [Led78 and discussion in section 5.1b]. The measured log ft = 5.4 for the ground state beta branch is consistent with the log ft = 5.8 for the 7/2-[523] proton to 5/2-[512] neutron transition reported in the decay of ^{167}Ho, but it is lower than the log ft = 6.4 for the 5/2-[512] neutron to 7/2-[523] proton transition previously measured in ^{171}Er decay [Led78]. The log ft = 4.8 for the β^- feeding to the 1578-keV level is faster than any known β transition involving

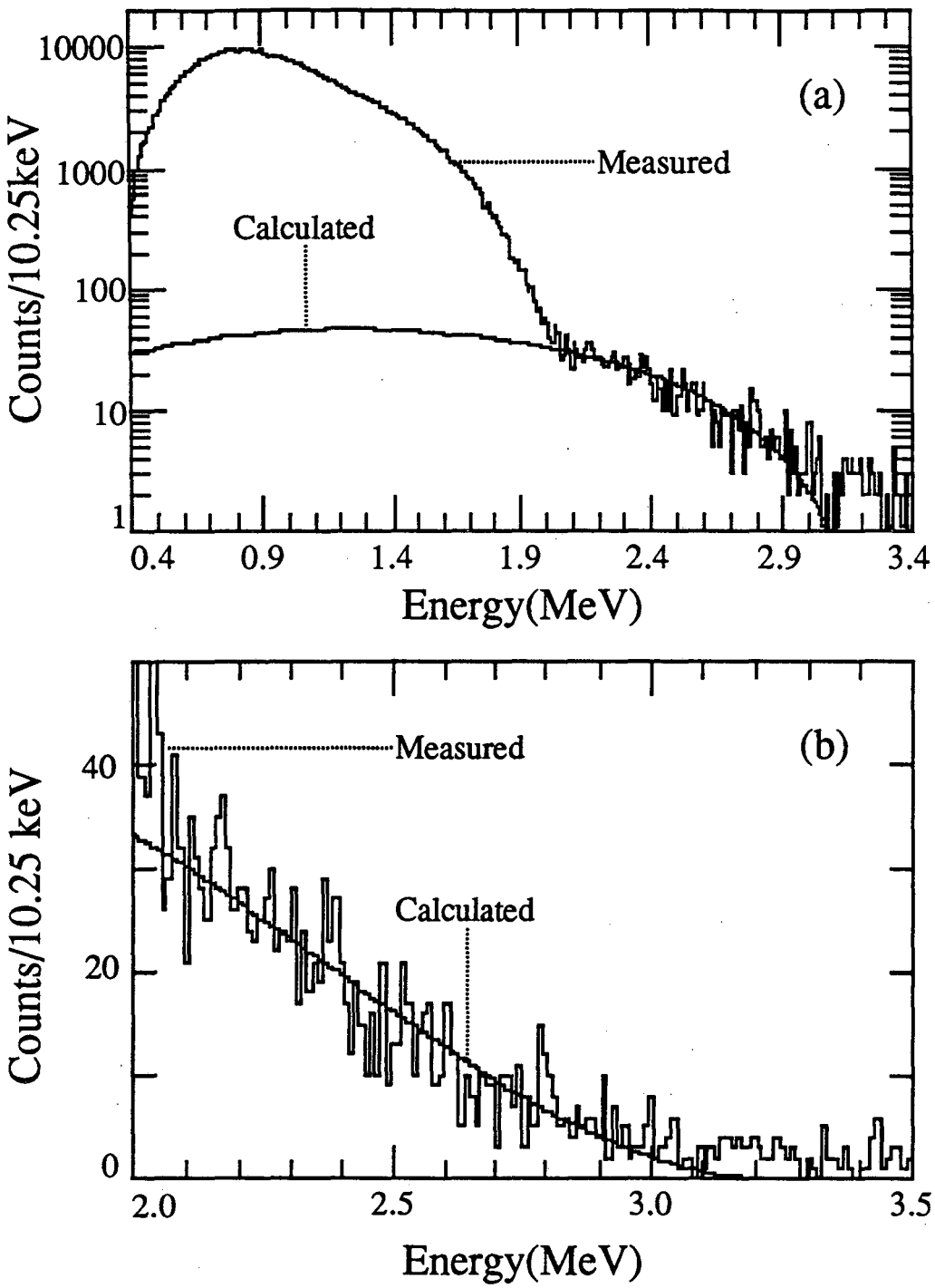

Figure 5.17. Fit of the measured A=169 beta spectrum with the calculated β^- spectrum with a 3.2 MeV endpoint, normalized to the 2.1 to 2.9 MeV interval; (a) entire spectrum and (b) the 2.0 to 3.5 MeV region of the spectrum.

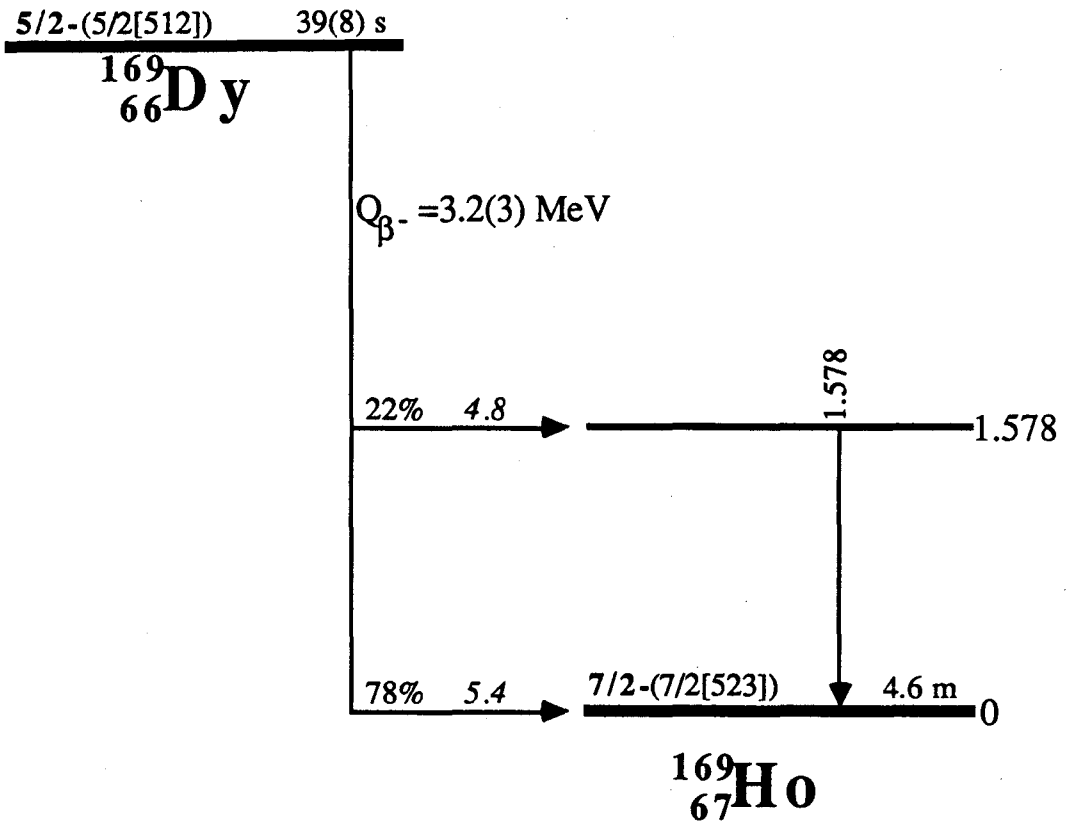

Figure 5.18. Proposed tentative decay scheme for 39 s Dy-169. Log*ft* 's are in italics. All energies are in MeV. The Q value was determined in the experiment.

the 5/2-[512] neutron level. A three quasiparticle state could be a possible assignment of this level composed of 7/2-[523] proton and 5/2-[512] neutron particle states and a 5/2-[523] neutron hole state. This assignment would have a resulting 7/2- spin and parity which permits allowed beta feeding ($\Delta I=1$, $\Delta\pi$=no) and strong ground state γ feeding. The assignment of the 5/2-[512] neutron level to the 39-s ^{169}Dy parent and the 7/2-[523] proton orbital to the measured ^{169}Ho ground state are tentatively proposed and in agreement with nuclear level predictions of Nilsson *et al.* [Nil69]. The 1578-keV level has been left unassigned.

5.3. ^{171}Ho DECAY SCHEME

The A=171 mass chain was studied in both the ^{176}Yb and ^{170}Er beam experiments. Natural ytterbium ion sources were used in the SuperHILAC to deliver beam intensities of 18 to 27 particle nanoamperes of ^{176}Yb ions on target for ~30 hours. This experiment was performed to look for ^{171}Ho which was thought to be an undiscovered isotope. Half-life predictions were 72.4 [Kla84] and 84.7 s [Tak73], so a tape cycle time of 256 s was chosen. The production rate for this (3p2n) out reaction channel was extremely low, but Er K x rays were seen to decay on-line with a half-life of ~50 s. At this point, a tape cycle time of 64 s was used to try to maximize the coincidence information. Due to limited ^{176}Yb beam time and the low production rate, very little data on ^{171}Ho decay were actually obtained.

After the experiment, it was found in two annual reports from GSI [Ryk84] and Mainz [Ryk88] that the A=171 mass chain had been studied before. Both papers refer to the same experiment performed by a GSI collaboration where they reported a 45(5) s component in the electron spectrum recorded with a thin plastic scintillator and weak erbium K x rays in coincidence with them. The authors made a

tentative assignment of this activity to either the β^- decay of the new isotope ^{171}Ho or the IT decay of the new isomer ^{171}Er^m, both decaying by strongly converted transitions. Discrimination between the two tentative assignments was not possible from their data since the plastic scintillator used could not distinguish between high energy beta particles and conversion electrons.

The data from the ^{176}Yb beam experiments were analyzed, but the low production rate yielded little information. Erbium K x rays were detected which decayed with a half-life of 49(5) s. These x rays were seen in coincidence with β^- particles in the β telescope having energies up to ~2.5 MeV and in weak coincidence with the known 198- and 280-keV γ transitions in ^{171}Er [Shi84]. These results unambiguously assigned the new activity detected in this research and in previously reported results [Ryk84, Ryk88] to the β^- decay of ^{171}Ho. These results have been published [Cha89]. Later in 1989, Rykaczewski *et al.* formally published their A=171 mass chain findings [Ryk89]. They assigned the 49 s activity to ^{171}Ho using half-life and systematic arguments to eliminate the ^{171}Er^m possibility. No further findings were reported.

During the ^{170}Er beam experiments, the A=171 mass chain was studied to obtain more decay data and try to assemble a decay scheme. Natural erbium and ^{170}Er enriched ion sources were used by the SuperHILAC to deliver beam intensities of 30 to 82 particle nanoamperes on target for ~45 hours. A tape cycle time of 128 s was used this time since the 49 s half-life was known. The production rate of ^{171}Ho was much greater during this experiment, due to much larger beam intensities and probably due to the more favorable three nucleon transfer reaction ((2n) in, (1p) out) relative to the five nucleon transfer reaction ((3p,2n) out) for the ^{176}Yb experiment. However, other A=171 isotopes, mainly ^{171}Er and ^{171}Lu, were

Table 5.6. Summary of A=171 isobar information [Shi84] for nuclei that can be separated in OASIS.

Isotope	Half-life	Decay Mode	Q value (MeV)[a]
^{171}Hf	12.1 h	EC, β^+	2.4(2)
^{171}Lu	8.24 d, 1.32 m[b]	EC, β^+, IT	1.480(2)
^{171}Yb	stable	--	--
^{171}Tm	1.92 y	β^-	0.0964(10)
^{171}Er	7.52 h	β^-	1.4907(13)
^{171}Ho	72.4 s,83.0 s[c]	β^-	3.16[d]

[a] Q value reported is for ground state decay.
[b] ^{171}Lu has an IT decaying isomer at 71.1 keV. Ground state half-life is listed first.
[c] Listed $T_{1/2}$ values are predictions, [Kla84] and [Tak73] respectively.
[d] Q value is an average from tables compiled in [Hau88].

made with even larger cross sections than ^{171}Ho. A summary of the half-lives, decay modes, and Q values of the A=171 isobars [Shi84] that could have been produced in the experiment are listed in Table 5.6. The Q_{β^-} value for ^{171}Ho is an average from the mass compilation of Haustein [Hau88]. The maximum β energy obtainable for the other A=171 isotopes results from ^{171}Er decay with 2.3% of its β^- intensity feeding the ground state or the 5.03-keV level in ^{171}Tm. The main β^- branch (94%) of ^{171}Er feeds a level at 425 keV in ^{171}Tm giving a maximum beta energy of 1.065(94) MeV [Shi84].

The beta spectrum measured in the ^{170}Er experiment for the A=171 mass chain is shown in Figure 5.19a. The high-energy β^- particles, 1.0 to 3.0 MeV, were seen to decay with a half-life of 56(4) s after background subtraction (see inset

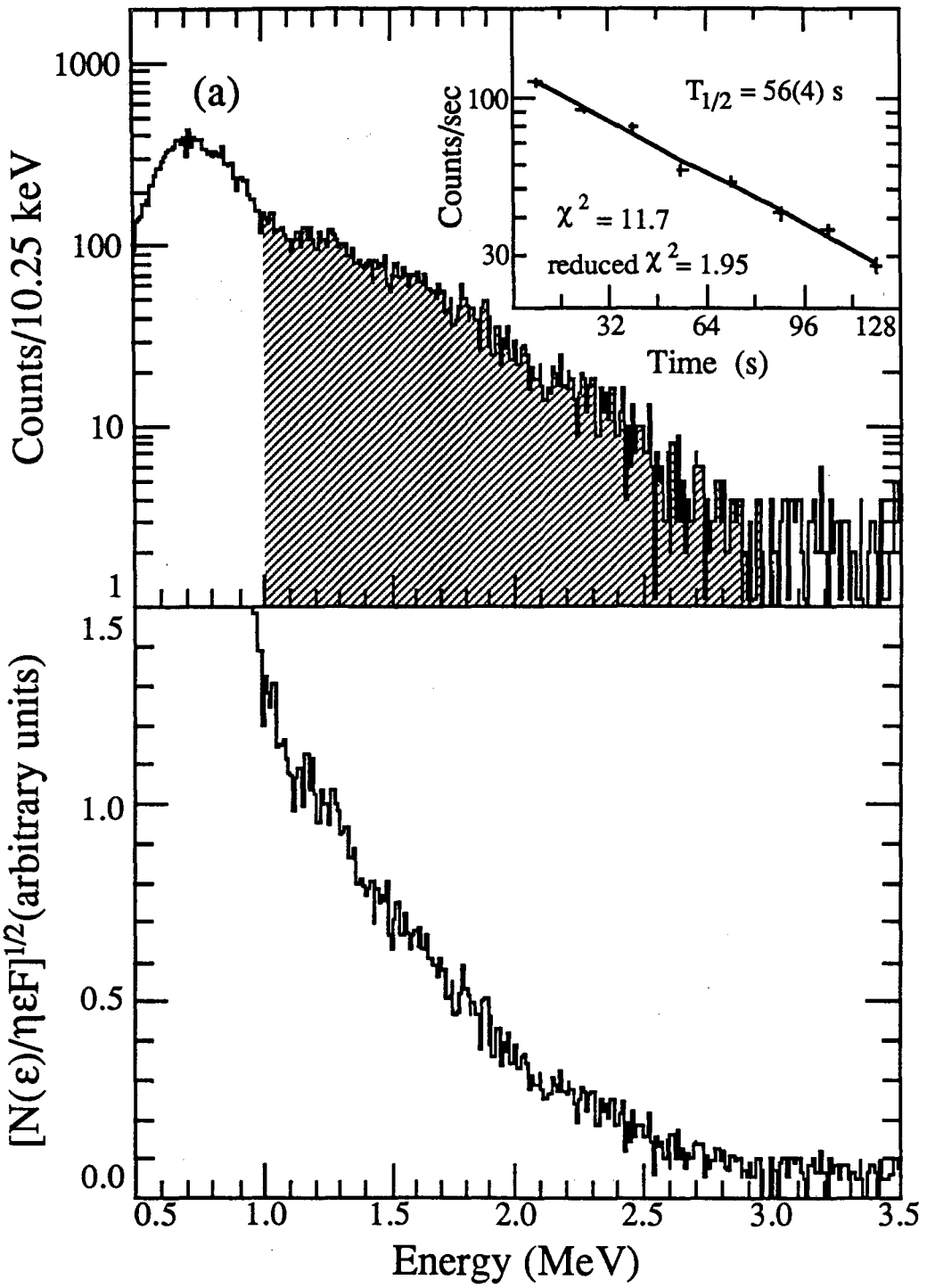

Figure 5.19. Beta decay data for A=171 mass chain; (a) beta particle spectrum measured in the beta telescope and (b) Fermi-Kurie plot. The inset in (a) shows the decay of 1.0 to 3.0 MeV beta particles (shaded portion of spectrum), after subtraction of background.

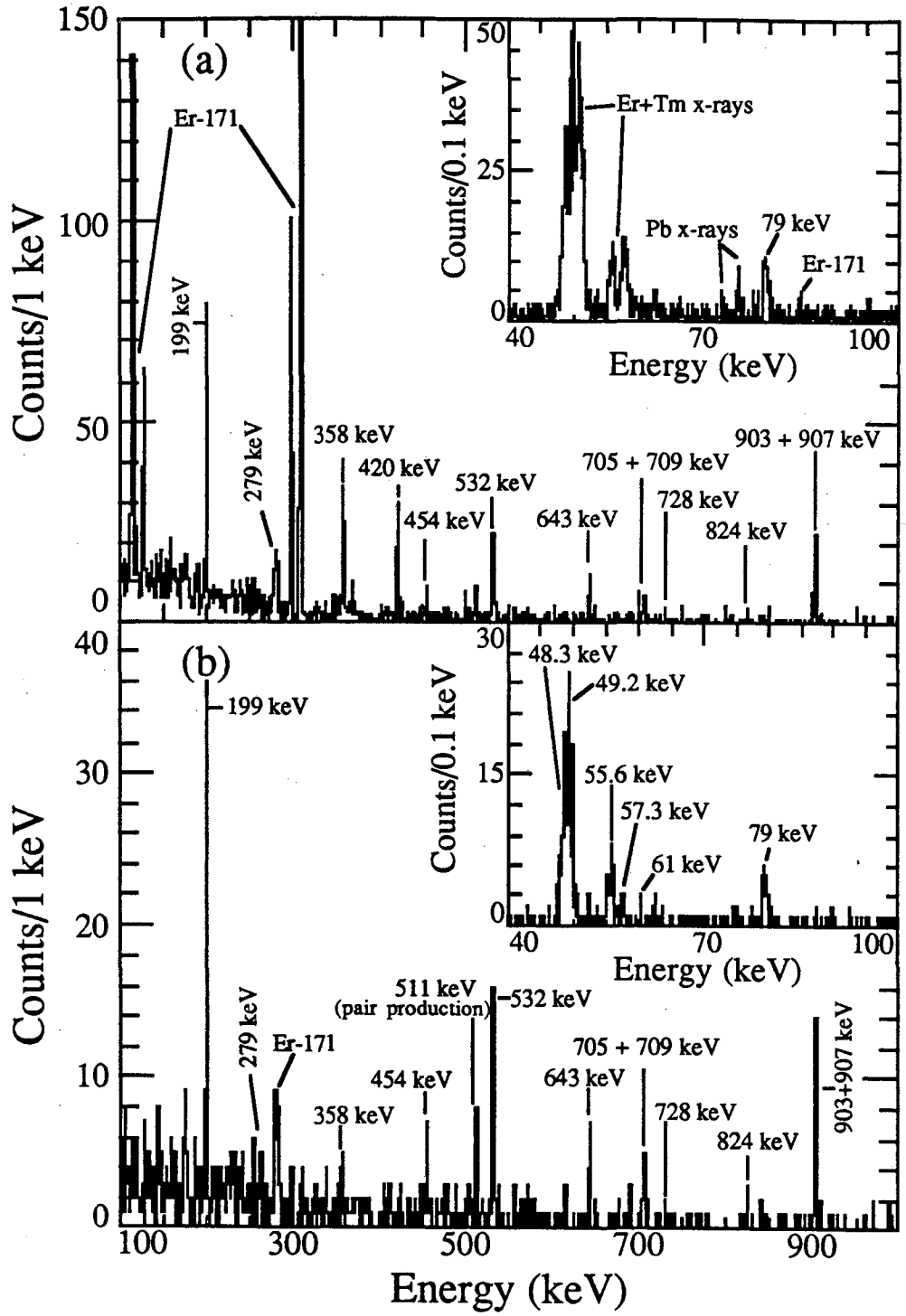

Figure 5.20. Gamma spectra in coincidence with beta particles measured in the beta telescope for the A=171 mass chain; (a) for betas with E≥0.3 MeV and (b) for betas with E≥1.0 MeV. The insets show the x-ray region for each beta gate.

to Figure 5.19a). A Fermi-Kurie analysis was performed on this beta data, but it did not show a single β^- component in the high-energy region, see Figure 5.19b. Spectra of the γ rays measured in the beta telescope in coincidence with beta particles with energies ≥0.3 MeV are shown in Figure 5.20a and its inset. The labeled γ lines were previously unobserved. Contamination from ^{171}Er γ rays at ~120 keV, ~300 keV and Tm K x-ray energies is indicated. Looking at γ rays coincident with β^- particles with energies ≥1.0 MeV produced much cleaner spectra as shown in Figure 5.20b and its inset. This gate removed all of the Tm K x rays and left only a small contamination from the strongest (65.6% absolute intensity) γ transition of ^{171}Er decay at 308 keV [Gra72].

The γ rays seen in coincidence with the high-energy beta particles (Figure 5.20b) were analyzed in the singles data. Difficulties arose for the analysis of the 199- and 279- keV γ rays due to interfering radiations at these energies induced in the detectors by the neutron background. Analysis of the 358-keV γ-ray was complicated by a sum peak from the 308-keV γ ray and the Tm K_α x rays in ^{171}Er decay [Gra72]. The 61-keV γ-ray could not be identified in the singles data due to Lu K_β x rays at this energy. These γ rays were all short-lived with an error-weighted average half-life of 54(3) s. Table 5.7 lists the Er K x rays and fifteen γ rays assigned to the decay of ^{171}Ho with their measured relative intensities and γ-ray coincidences. The 61.2-keV γ-ray intensity was determined relative to the 79-keV γ ray in a γ spectrum measured in coincidence with beta signals in the plastic scintillator. The 1687-keV γ ray was first noted in the coincidence spectra with x rays and the 79-keV γ ray and was later seen in coincidence with β^- particles. Six of the γ rays listed in Table 5.7 (79, 199, 279, 358, 705, and 903 keV) were observed previously in the adopted level scheme for ^{171}Er [Shi84].

Table 5.7. Gamma-ray energies, E_γ, intensities, I_γ(rel.), and γ coincidences measured in the decay of ^{171}Ho.

E_γ (keV)	I_γ (rel.)[a]	Coincident γ-rays (X=Er K x rays)
48.2 Er $K_{\alpha 2}$	51(8)	X, (61), 199, 279, (454), (642), (708), (903), (907), (1687)
49.1 Er $K_{\alpha 1}$	106(7)	b
55.7 Er $K_{\beta 1}$	34(3)	X, 199, 279, (358), (454), (824)
61.2(5)	4(2)	X, 199, 642
79.1(1)	25(2)	X, 279, (454), (824), (1687)
198.6(1)	88(23)	X, 61, 642, 705, (708)
279.2(4)	60(9)	X, 79
358.3(3)	49(33)	X
453.8(3)	13(4)	X, 79
532.2(1)	58(4)	X
642.5(2)	39(5)	X, (61), 199
704.7(3)	27(5)	X, 199
708.5(1)	34(19)	X, 199
727.6(1)	44(5)	X
823.9(5)	30(6)	X, 79
903.3(4)	100(6)	c
907.2(2)	57(6)	(X)
1687.1(10)	25(8)	X, (79)

[a] Intensities are relative to 100 for the 903.3-keV gamma transition.
[b] Clean coincidence gate could not be set due to interferences of Tm $K_{\alpha 2}$ x rays.
[c] No coincidences were observed.

The proposed decay scheme for ^{171}Ho, based on the γ-ray coincidence and intensity information and the adopted level scheme [Shi84], is shown in Figure 5.21. This decay scheme is consistent with decay via many beta groups and the observation of a multi-component high-energy beta spectrum in Figure 5.19b. A half-life of 200(30) ns, Figure 5.22, was measured for the 199-keV level, in good agreement with previously published results of 210(10) ns [Shi84]. The placement of the level at 841-keV is uncertain because of the possible reversal of the order of the 61- and 641-keV γ-cascade and could alternatively be placed at 259.8 keV. There is no indication of direct β^- feeding to this level. The beta intensities and log *ft*'s listed in Figure 5.21 are based on no ground-state feeding. Since β transitions have been measured between the 7/2-[523] proton and the 5/2-[512] neutron states [Led78], ground-state feeding is expected in ^{171}Ho decay, but could not be determined. The spin and parity assignments for the ^{171}Er levels in the decay scheme are from the adopted level scheme [Shi84]. The assignment of the ^{171}Ho parent state (the 67th proton) as 7/2-[523] was discussed in section 5.1b. The upper-limit, assuming no ground-state feeding, for beta feeding of the 199-keV level is ≤2%, but because decay to this level would be highly forbidden (ΔI=3, Δπ=no), no beta feeding to this level is proposed. A half-life of 55(3) s was determined as a weighted average from all the available gamma and beta decay information.

The beta spectrum measured in coincidence with 199-, 643-, 705-, 709-, 824-, 903-, and 907-keV γ rays, and hence feeding the 903- and 907-keV levels, is shown in Figure 5.23a. The Fermi-Kurie plot of this spectra is shown in Figure 5.23b with an endpoint of 2.3(6) MeV. This is consistent with the predicted average Q_{β^-} value of 3.2 MeV [Hau88]. A Q_{β^-} value of 3.2(6) MeV is assigned to this isotope.

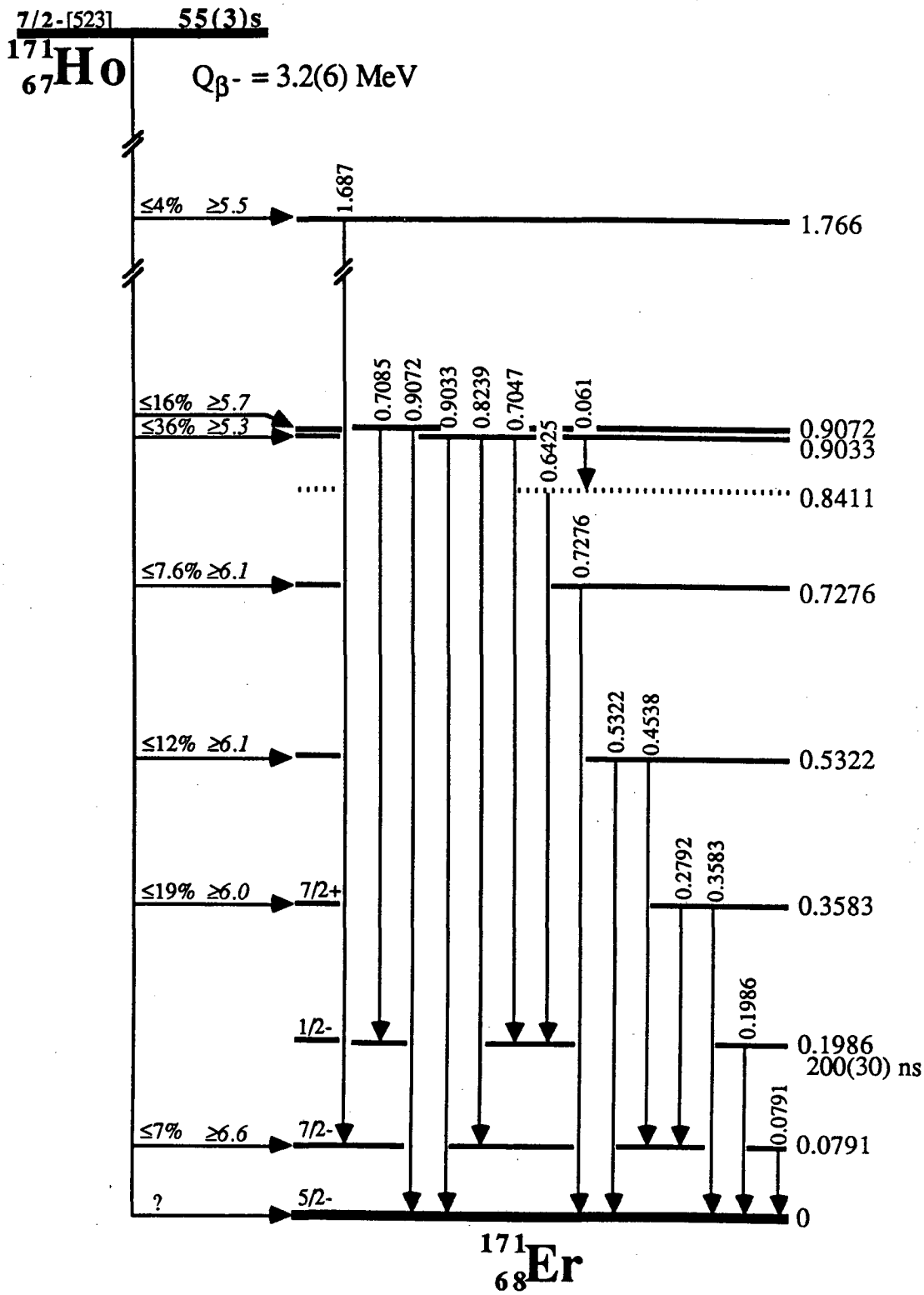

Figure 5.21. Proposed decay scheme for 55-s Ho-171. All energies are in MeV. Beta branches and log*ft*'s are based on no ground-state beta branch.

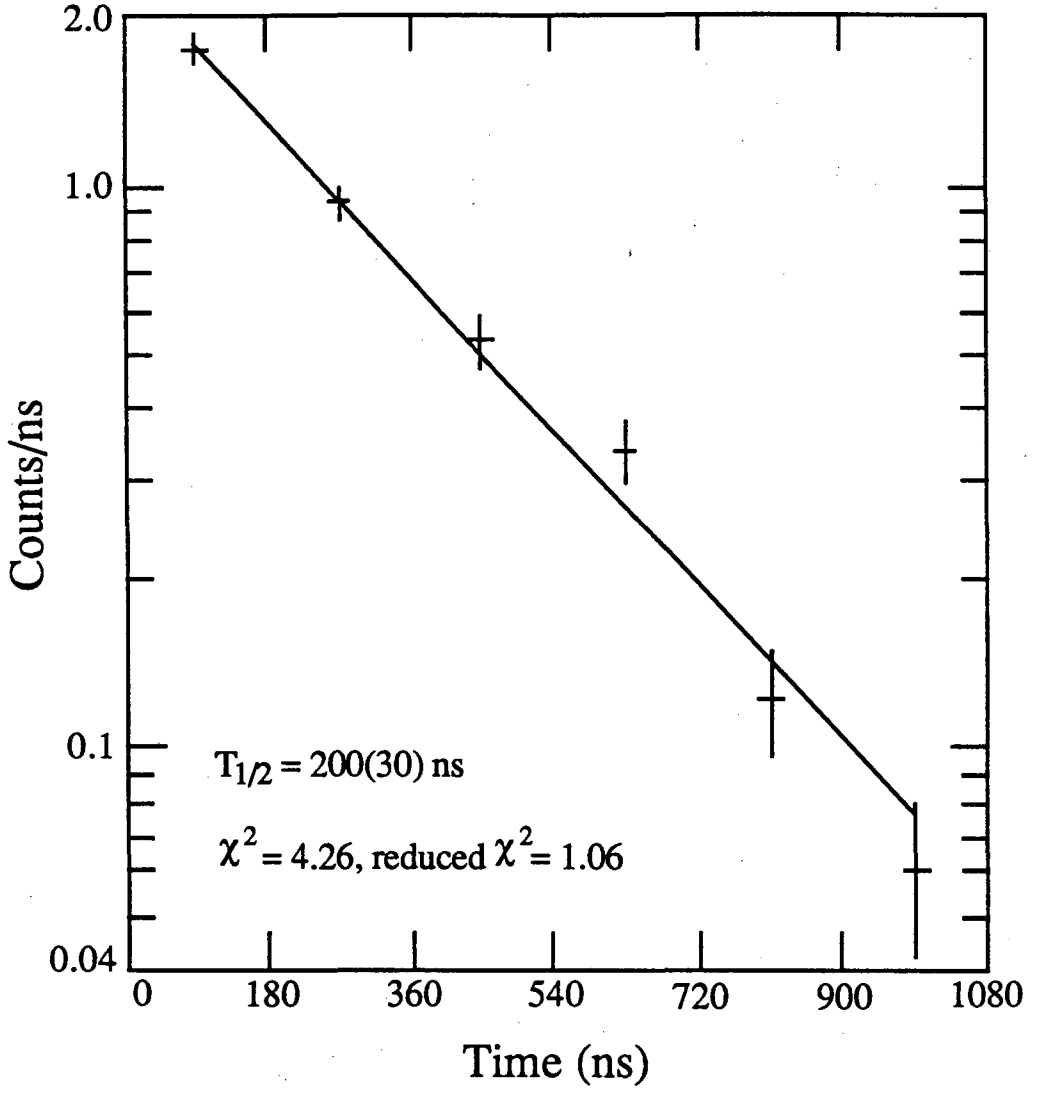

Figure 5.22. Single-component decay fit to the timing information between 199-keV gamma rays and radiations feeding the 199-keV level in Er-171.

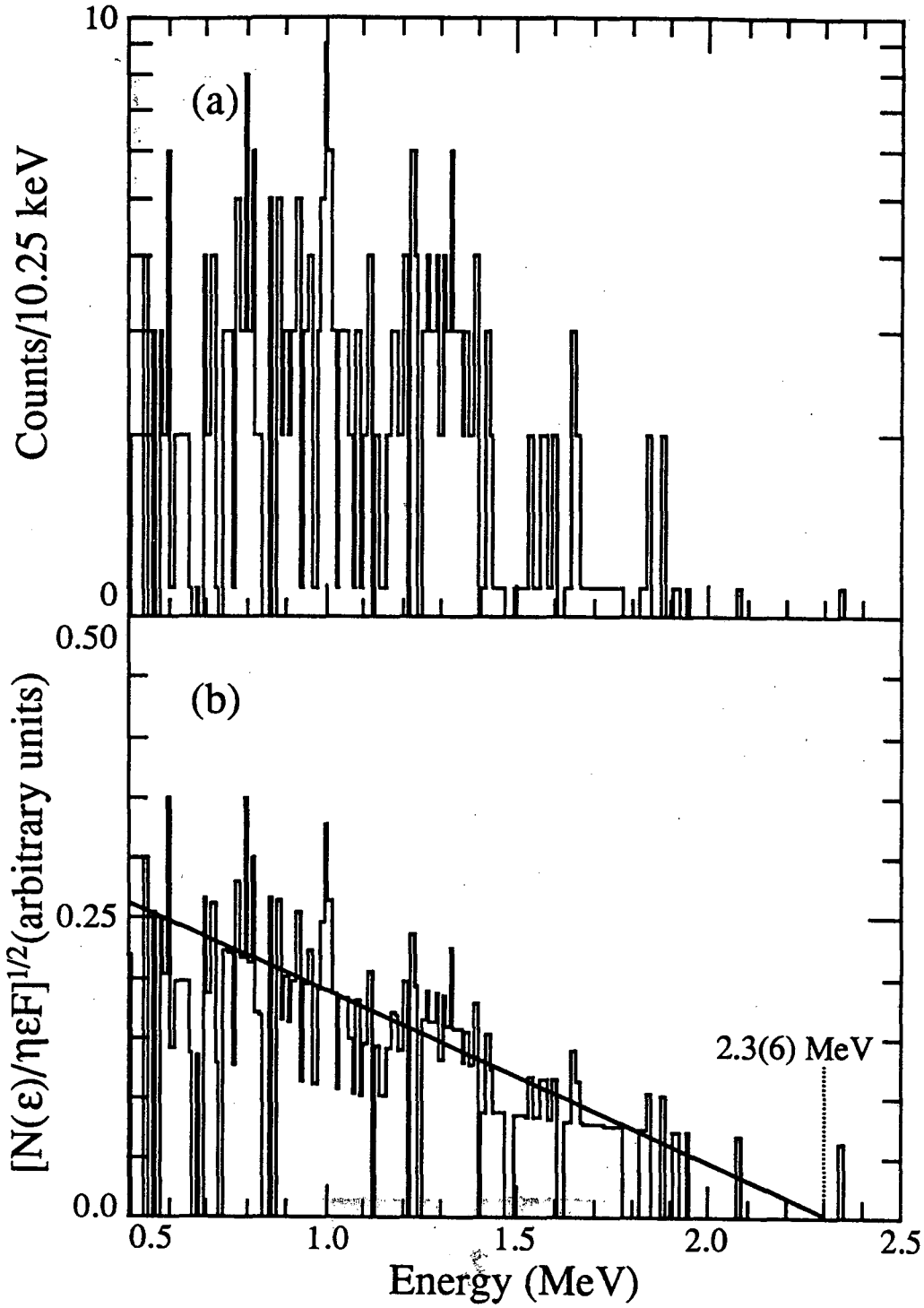

Figure 5.23. Beta decay data measured in coincidence with 199, 642, 705, 708, 824, 903, and 907 keV gamma rays (gamma transitions associated with beta decay to the proposed 903 and 907 keV levels of Er-171) of Ho-171 decay; (a) beta particle spectrum and (b) Fermi-Kurie plot with a 2.3(6) MeV endpoint.

5.4. ^{174}Er - NEW ISOTOPE

The A=174 mass chain was the first multinucleon transfer reaction experiment performed with OASIS. Event descriptions and parameters were not optimum for β^- decaying isotopes for the half-lives in this region. The lessons learned from this ^{176}Yb beam experiment gave information which allowed the design of the successful ^{170}Er beam experiment in which almost all of the results mentioned in the previous sections were obtained in only two weeks of beam time. Even though the detection system was not optimized for neutron-rich nuclides in this experiment, useful new results were obtained for the A=174 mass chain. Natural ytterbium ion sources were used in the SuperHILAC to deliver beam intensities of 5 to 24 particle nanoamperes of ^{176}Yb ions on target in OASIS for ~60 hours. The experiment was performed to search for the new isotope ^{174}Er. Mass predictions compiled by Haustein [Hau88] gave an average Q_{β^-} value of 1.7 MeV (the value given by Comay *et al.* [Com88] was excluded because it was drastically different from the other eight values listed for this isotope). The half-life predictions were 80 s [Kla84] and 15 m [Tak73]. A half-life of 395 s was calculated using the GTBD code [Tak88] and the 1.7 MeV Q_{β^-} value above. A tape cycle time of 512 s was chosen initially, and when Tm K x rays (from the decay of either ^{174}Er or a ^{174}Tm isomer) were seen to decay with ~175 s half-life on-line, the tape cycle time was continued. The information on ^{174}Er decay contained below has been previously published [Cha89] unless otherwise noted.

The twelve gamma rays and three Tm K x rays with energies, relative intensities, and gamma coincidences listed in Table 5.8 are assigned to the decay of the isotope ^{174}Er. These gamma rays decayed with a half-life of 3.3(2) m which did

Table 5.8. Gamma-ray energies, E_γ, intensities, I_γ(rel.), and coincidences assigned to the decay of 3.3 m ^{174}Er.

E_γ (keV)[a]	I_γ (rel.)[b]	Gamma Coincidences[c]
49.7 Tm$K_{\alpha 2}$	137(5)	X, (58.5), 71.7, 100, 122, (130), 152, 637, 642
50.7 Tm $K_{\alpha 1}$	263(9)	d
57.4 Tm $K_{\beta 1}$	67(3)	X, 71.7, 100, (122), 152, (637), (642)
58.5[e]		
71.7	15(1)	X, (58.5), (122), 637, 643
100.4	100(1)	X, 152
121.8	39(6)	X, (58.5), (71.7), 130
130.4	42(8)	122, 637, 643
151.8	91(15)	X, 100.4
636.7	27(5)	X, (58.5), (71.7), 130
642.7	25(2)	X, (58.5), (71.7), 130
708.4	93(7)	(58.5)
714.4	56(6)	(58.5)
766.9	92(9)	f
772.9	75(8)	f

[a] The uncertainty in the γ-ray energies is $\pm$ 0.2 keV.

[b] Intensities are relative to 100 for the 100.4-keV γ transition.

[c] X = Tm K x rays. ( ) denotes a weak coincidence.

[d] Clean coincidence gate could not be set.

[e] Not seen in the singles data. See text.

[f] No coincidences measured.

not match any of the known half-lives of this isobaric chain. All of the γ rays were seen in coincidence with β^- particles in the β telescope and plastic scintillator and were not in coincidence with any of the known γ rays from the decay of ^{174}Tm [Bro84]. Some of the gamma rays were seen in coincidence with Tm K x rays as indicated in Table 5.8. The first and last points (new half-life and Tm K x-ray coincidences) are either consistent with a possible isomer of ^{174}Tm or the new isotope ^{174}Er; however the ^{174}Tm isomer is ruled out by points two and three (β^- coincidences and absence of ^{174}Tm γ coincidences). The 58.5-keV gamma transition was not seen in the HPGe singles data due to interfering x-ray activity (Yb Kβ x rays from ^{174}Tm decay and Tm Kβ x rays from the decay of ^{174}Er itself!) at that energy, but was clearly identified in the coincidence spectra. The low energy part of the HPGe detector singles spectrum is shown in Figure 5.24 with all pertinent peaks labelled.

Based on the coincidence and intensity information, the decay scheme in Figure 5.25 has been proposed for ^{174}Er. The even-even isotope, ^{174}Er has a 0+ ground state. The two strong β^- transitions to the 766.9- and 772.9-keV levels are similar to the 0+ to 1+ and (1)- β^- transitions in ^{172}Er decay [Led78]. Assuming then a spin difference of one unit between the ^{174}Er ground state and the 770-keV levels, the observed strong γ transitions to the proposed ^{174}Tm ground state are inconsistent with a tentative 4- assignment for the ^{174}Tm ground state [Bro84]. This discrepancy can be explained by an isomer in either ^{174}Tm or ^{174}Er which would change the spins of the parent or daughter ground states. Even-even isotopes, such as ^{174}Er, rarely have isomers, but for N=106 isotopes, isomers of even-even ^{176}Yb and ^{178}Hf do exist. However, their isomers both decay by intense isomeric transitions [Led78]. Isomers are highly probable for the odd-odd isotope

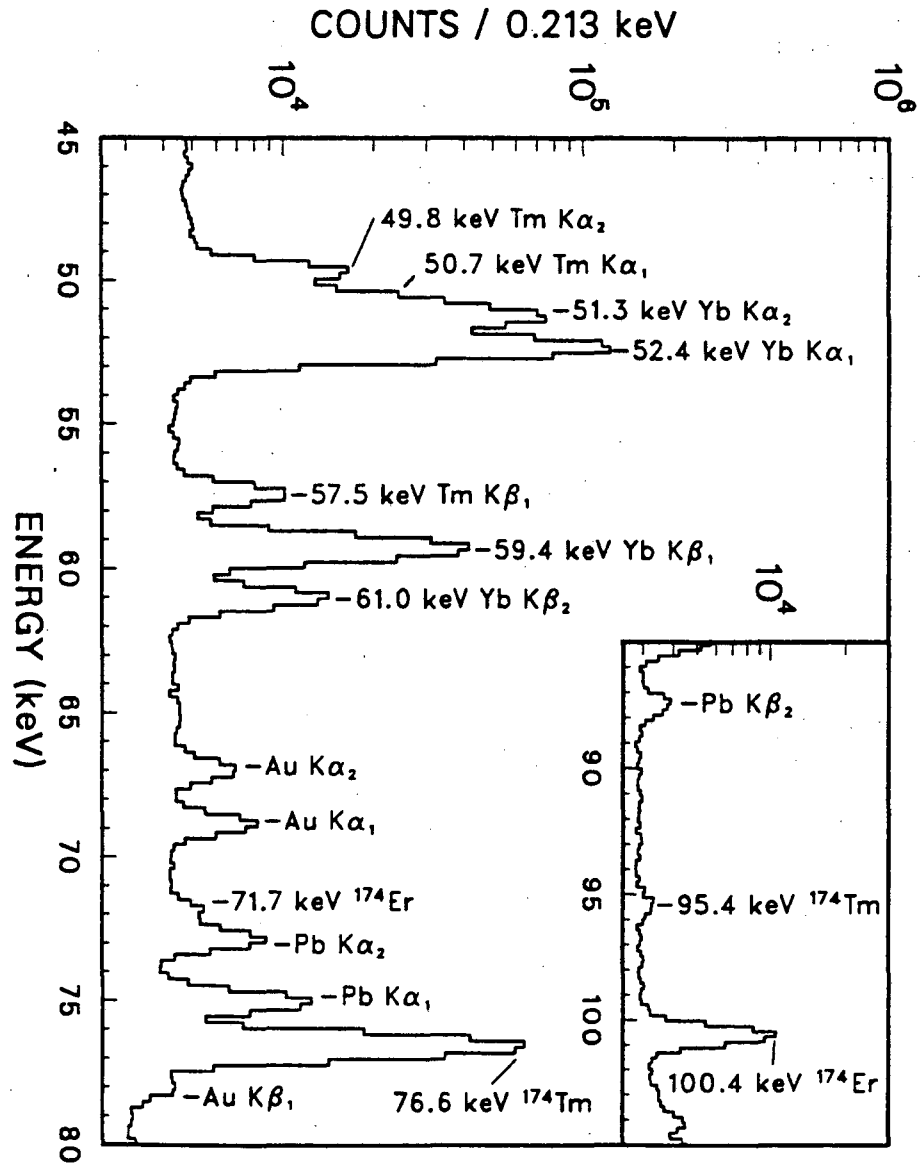

Figure 5.24. Low-energy part of the gamma-ray singles spectrum measured in the 52% Ge detector in the A=174 mass chain experiment.

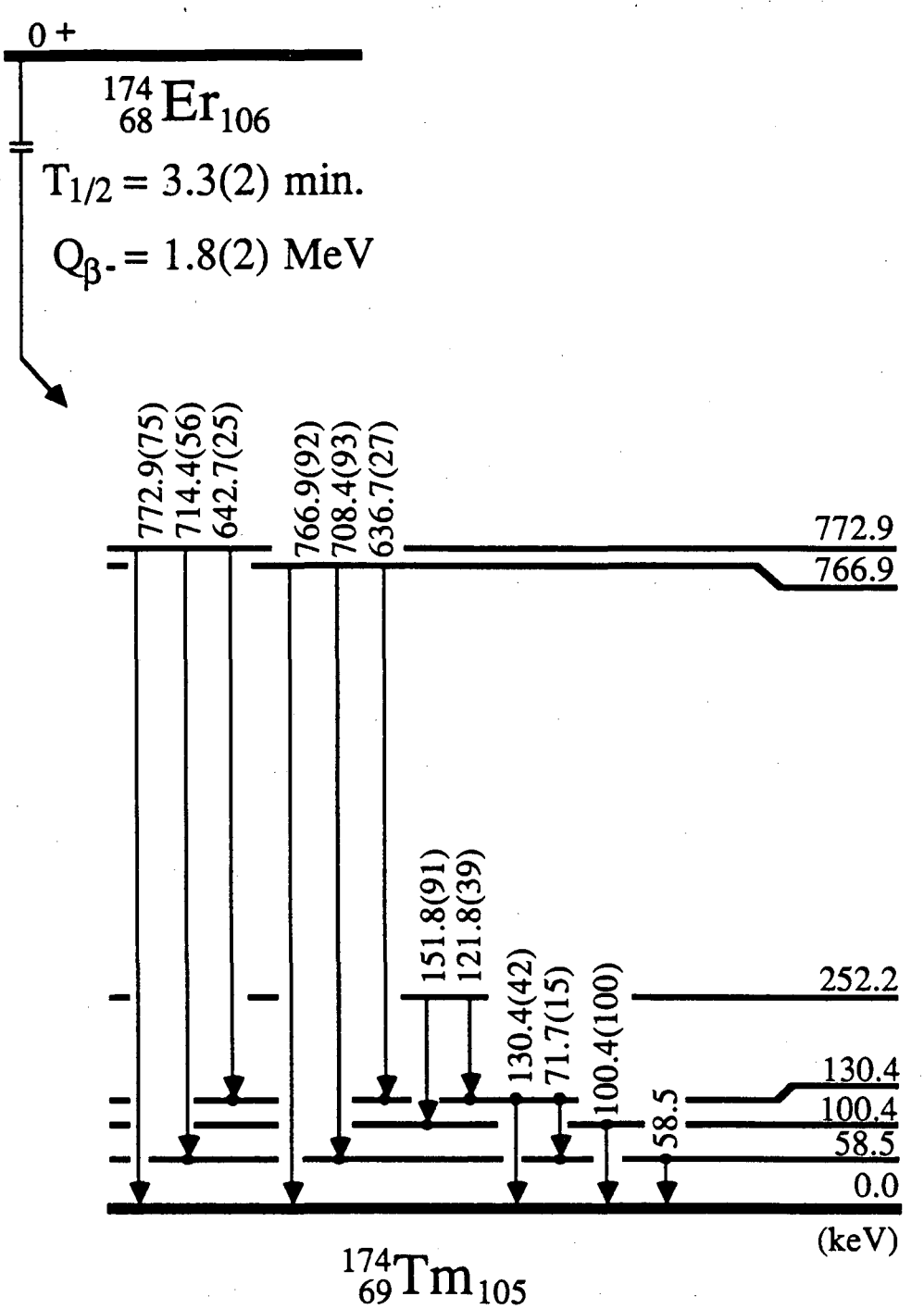

Figure 5.25. Proposed decay scheme for Er-174. Intensities are relative to the 100.4-keV transition.

^{174}Tm. Consequently, spin and parities of the ^{174}Tm levels in Figure 5.25 have not been proposed.

After the β^- spectrum analysis programs were written and used with excellent success on the ^{170}Er beam experiment data, the beta data for the A=174 mass chain was reanalyzed using similar techniques. The β^- spectrum feeding the 767- and 773-keV levels in ^{174}Tm, shown in Figure 5.26a, was generated by gating with the 637, 643, 708, 714, 767, and 773 keV gamma rays. The Fermi-Kurie plot and endpoint of 1.05(23) MeV are shown in Figure 5.26b. The Q_{β^-} value of 1.8(2) MeV is suggested for the decay of 3.3-m ^{174}Er, in good agreement with average predicted value of 1.7 MeV. The β telescope calibration for the ^{176}Yb experiment was checked by measuring the β^- particle spectrum in coincidence with 366-keV γ rays from the decay of ^{174}Tm , shown in Figure 5.27a. A β^- endpoint of 1.22(5) MeV was obtained from the Fermi-Kurie plot in Figure 5.27b, in good agreement with the value of 1.21(5) MeV reported in the literature [Bro84]. The β^- endpoint results reported here were not published in the ^{174}Er discovery paper [Cha89].

5.5. TARGET/ION SOURCE TESTS

The normal target/ion source geometry of OASIS was designed to optimize production and ionization of compound nucleus recoiling products. The target was placed immediately upstream of narrow capillary tubes with small acceptance angles to selectively allow the compound nucleus recoils (small lab frame angle) to pass and discriminate against other transfer reaction products. (See Figure 3.4) For the multinucleon transfer reactions studied in this research, large recoil angles were expected (see discussion in chapter 2). During the first ^{176}Yb beam experiment, modifications to the anode of the ion source were made as shown in Figure 5.28a.

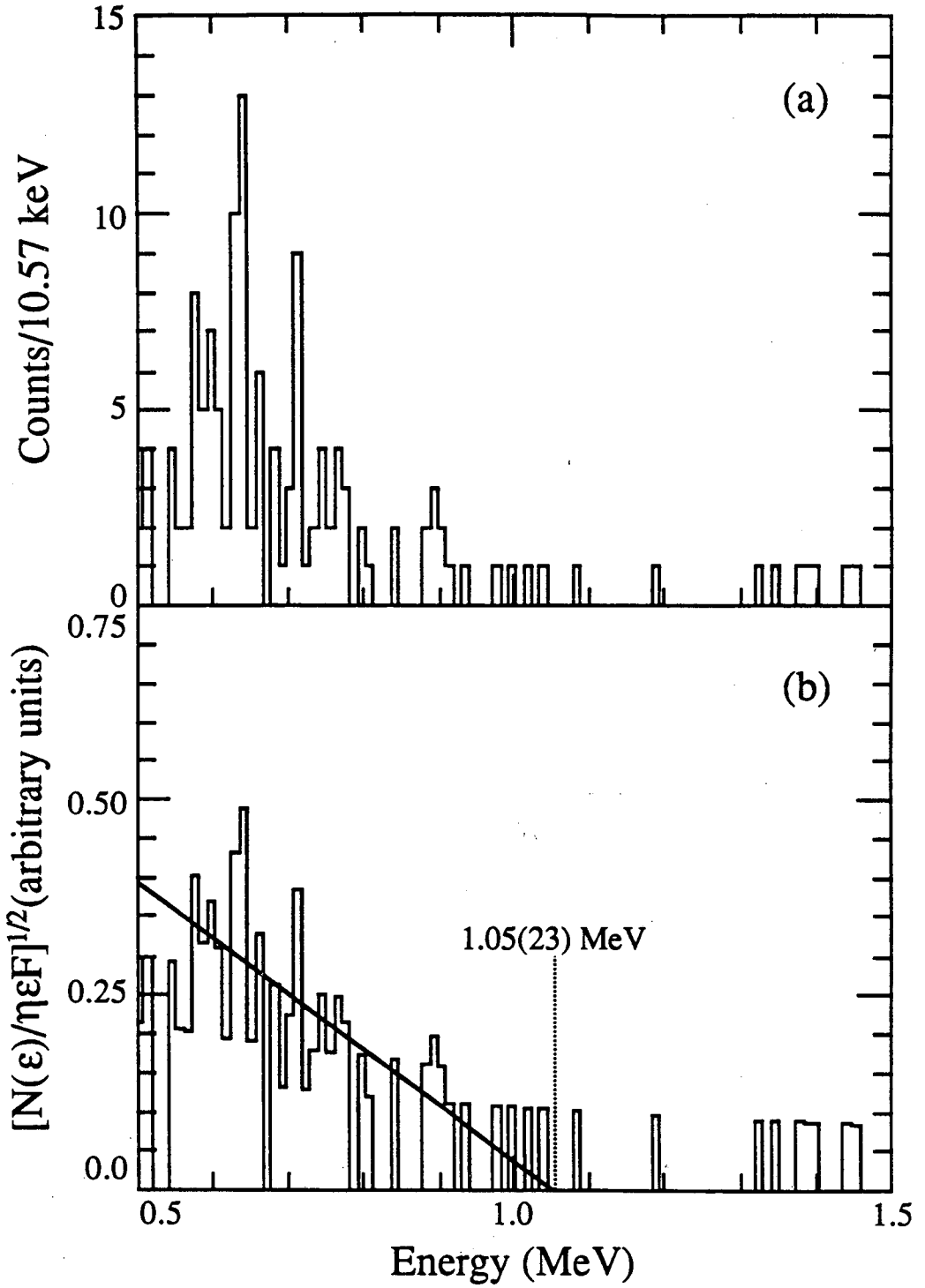

Figure 5.26. Beta particle data measured in coincidence with 637, 643, 708, 714, 767, and 773 keV gamma rays in the A=174 mass chain; (a) beta particle spectrum and (b) Fermi-Kurie plot and 1.05(23) MeV endpoint.

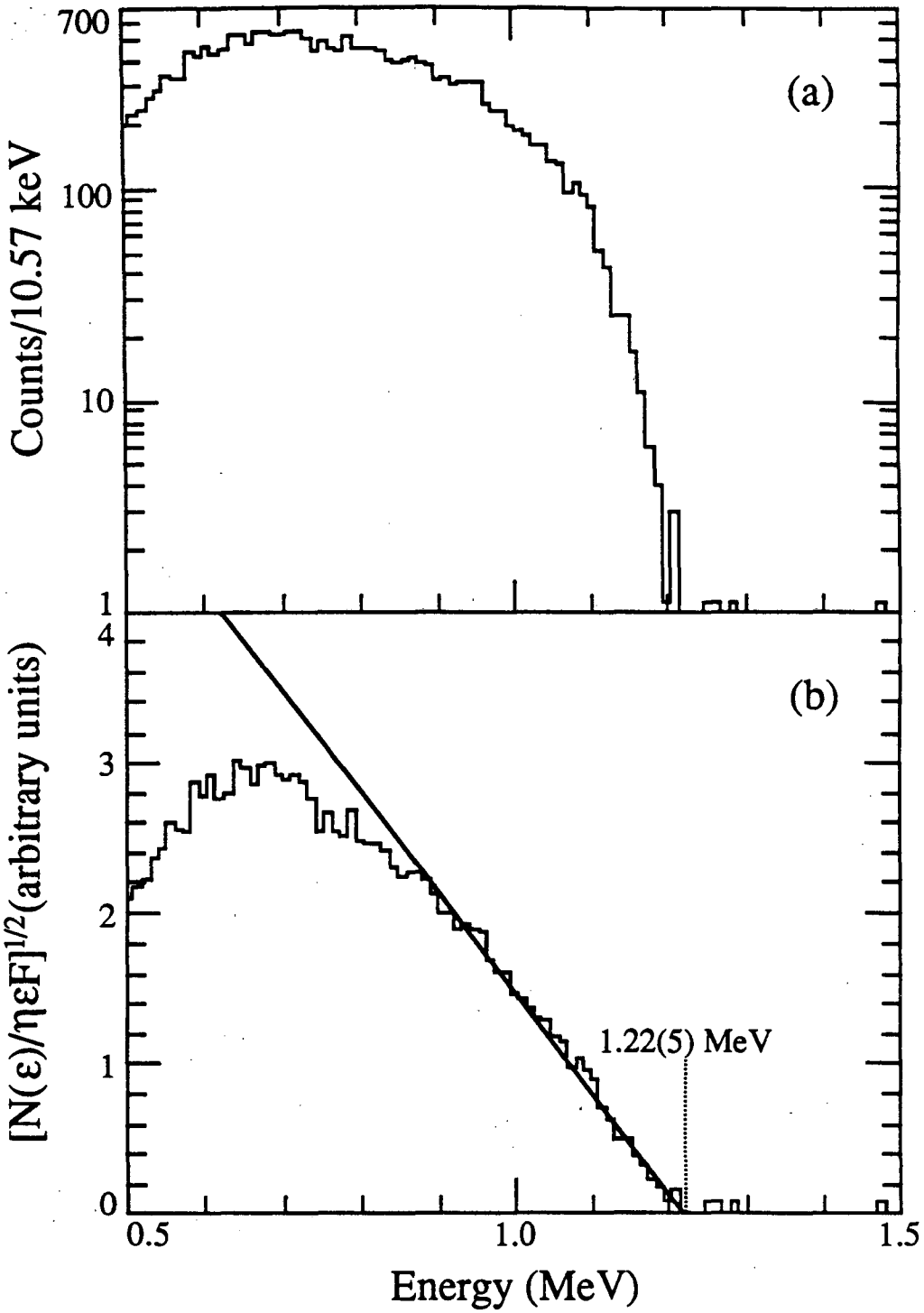

Figure 5.27. Beta particle data measured in coincidence with 366-keV gamma rays from the decay of Tm-174; (a) beta particle spectrum measured in the beta telescope and (b) Fermi-Kurie plot and beta endpoint of 1.22(5) MeV.

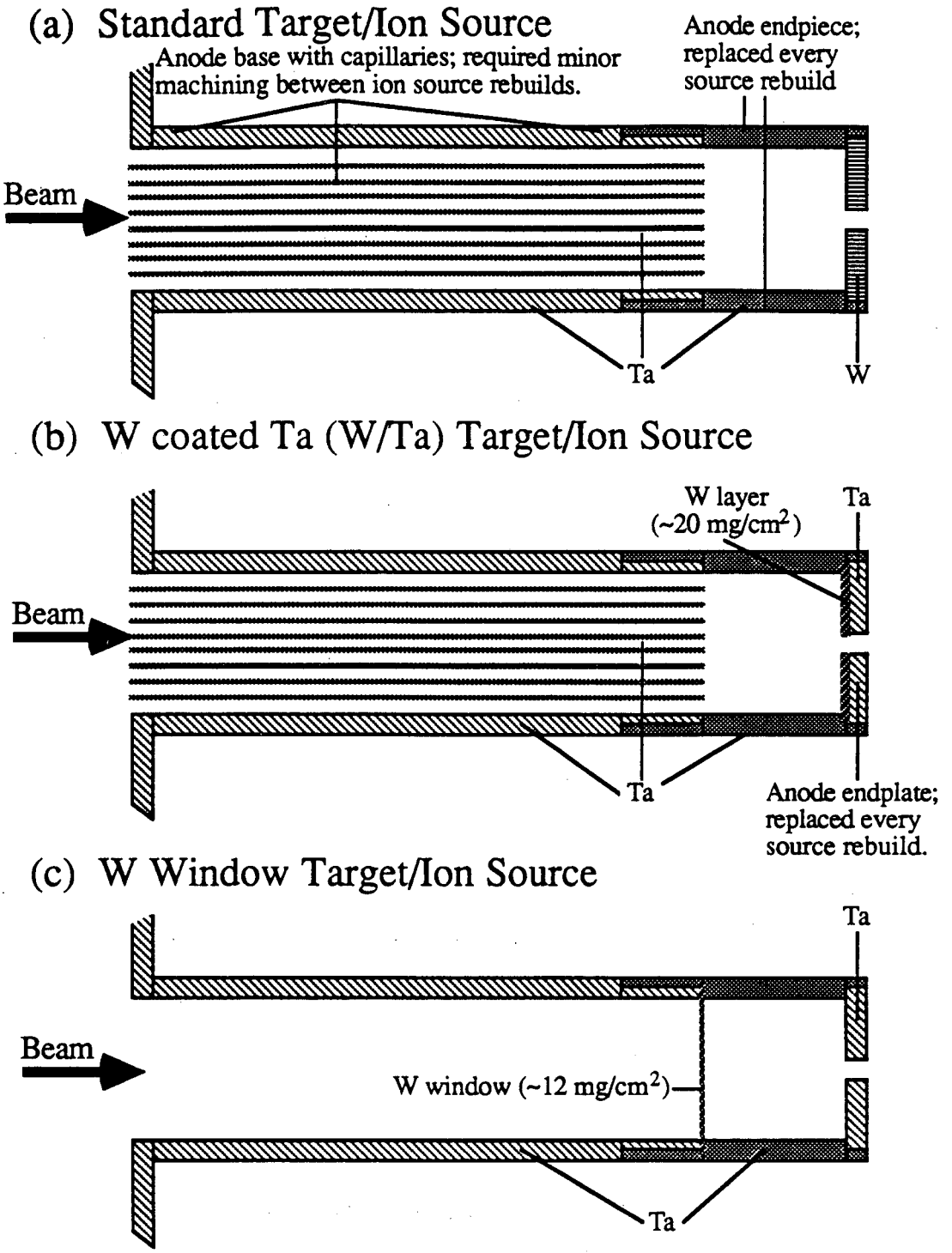

Figure 5.28. Target/ion source geometries used in the Er-170 beam experiments; (a) standard target/ion source, (b) W/Ta target/ion source, and (c) W window target/ion source.

The anode (anode base, capillaries, anode endpiece and endplate) was normally made entirely of Ta because of its high temperature stability and good diffusion and surface ionization properties. For this research, the target was removed and the Ta endpiece was replaced with W. This endpiece served as the target, recoil catcher, and to some degree as ionizer. Since the target was removed, the ion source was open to the SuperHILAC vacuum. Only the capillaries stopped the recoils, once in a gaseous state, from migrating back into the vacuum of the SuperHILAC. During the ^{176}Yb beam experiment, one other target/ion source geometry was tried; where a Ta endpiece was used and a ~17 mg/cm^2 W foil was placed just downstream of the capillaries. This foil was thicker than the calculated ~11.5 mg/cm^2 of W necessary to slow the ^{176}Yb beam below the Coulomb barrier. This source showed almost a two-fold increase in the production rate, but no quantitative results were obtained.

During the ^{170}Er beam experiment attempts were made to quantify the differences in various target/ion source geometries. The three geometries tested are shown in Figure 5.28. The W coated (W/Ta) geometry (Figure 5.28b) was used since Ta shows better diffusion than W and is much easier to machine. The ~20-mg/cm^2 W layer was actually evaporated onto both sides of the endplate and was thicker than the ~12.6 mg/cm^2 necessary to slow the ^{170}Er beam below the Coulomb barrier. The W window geometry (Figure 5.28c) was a modification of the W foil source used in the ^{176}Yb beam experiment where the capillaries were removed to allow the full beam to hit the W window. The 12-mg/cm^2 thickness was chosen on the following criteria: maximize the amount of W encountered by beam with energy greater than the Coulomb barrier, and yet keep it thin enough to allow the recoils to exit the window even at large multinucleon transfer reaction angles. A computer code was written to determine the optimum target thickness. The code

assumed the recoils emerged at the quarter-point angle [Wil80] (an over-estimate for all of the recoils, but a good average), calculated the recoil energy for a binary reaction, and, using range and stopping power tables [Hub80], determined if the target-like recoil had enough energy to exit the foil. Using the above criteria, it was determined that the maximum effective target thickness occurred at the Coulomb barrier thickness, 12.6 mg/cm^2, and that ~99% of the recoils would leave the window/target. A 12-mg/cm^2 W foil was used since this was the closest commercially available thickness.

The tests of the three target/ion source geometries were performed with the A=168 mass chain and measuring the production rate of detected ^{168}Ho and ^{168}Lu gamma radiations. For ^{168}Ho, γ transitions at 741, 815, and 821 keV were used, and for ^{168}Lu, gamma transitions at 511 (from positron annihilation), 896, and 979 keV were used. Peaks were integrated on-line using the 52% Ge singles data, background was subtracted, and the results were normalized by dividing by the integrated beam intensity. Tests were performed for ~6 hours on each target/ion source geometry to obtain good average relative intensities (number of background-corrected γ rays detected in a set time divided by the beam integral) for each γ ray. The results of the tests are listed in Tables 5.9 and 5.10 where the results are also normalized to the standard target/ion source geometry. The W/Ta target/ion source showed ~25% increase versus the standard geometry for the production of ^{168}Ho and ^{168}Lu, and the W window geometry had a 110% increase in the production of ^{168}Ho and a 40% increase in the production of ^{168}Lu. The differences between the increases of the ^{168}Ho and ^{168}Lu production for the W window source is not understood, but might have something do with a different reaction to produce

Table 5.9. Results of the target/ion source tests on the production of ^{168}Ho. Errors are estimated as ~10%.

Target/Ion Source	Relative Intensities of ^{168}Ho γ Rays			Ave. Normalized to Standard
	741 keV	815 keV	821 keV	
Standard	3.5	1.64	3.4	1.0
W/Ta	4.5	2.2	4.3	1.3
W Window	7.2	3.4	7.0	2.1

^{168}Lu, a (3p) in, (5n) out reaction channel, versus the (pn) out reaction for ^{168}Ho production. The W window geometry was clearly the best one to use, but lasted only ~6 hours at which point the window melted due to beam heating. The W/Ta target ion source geometry was used the most after the tests due to its increase in yield over the standard source, durability (it lasted ~24 hours like the standard ion/target source), and the ease of machining Ta versus W endplates.

Table 5.10. Results of target/ion source test on the production of ^{168}Lu. Errors are estimated as ~10%.

Target/Ion Source	Rel. Intensities of ^{168}Lu Radiations			Ave. Normalized to Standard
	511 keV	896 keV	979 keV	
Standard	1.21	0.76	0.95	1.0
W/Ta	1.45	0.93	1.1	1.2
W Window	1.6	1.1	1.3	1.4

6. CONCLUSIONS

Neutron-rich rare-earth nuclides were produced using multinucleon transfer reactions between ^{170}Er and ^{176}Yb ion beams and ^{nat}W targets. Two new isotopes and one new isomer were discovered in this study. Decay schemes were determined for these three nuclides and also for two previously discovered isotopes. A brief summary of the results for these nuclides will be discussed in the following paragraphs.

The ^{176}Yb beam experiment produced the new isotope ^{174}Er [Cha89], which had a measured half-life of 3.3(2) min.. Fifteen x rays and γ rays (Table 5.8) were assigned to the decay of this isotope and were placed in the tentative decay scheme shown in Figure 5.25. The strong beta branches to the 767- and 773-keV levels in ^{174}Tm, which both have strong ground state γ transitions, are inconsistent with a 0+ assignment for ^{174}Er and a 4- assignment for the measured ^{174}Tm ground state. An isomer of the odd-odd ^{174}Tm could explain the measured results. Another possible explanation would be an isomer of even-even ^{174}Er which has an expected 0+ ground state. Though even-even isomers are rare for this region, even-even N=106 isomers exist for both ^{176}Yb and ^{178}Hf. These isomers seem to result from the unpairing of the neutrons in the last neutron level, 7/2-[514], and with one neutron remaining in that level and one in the next neutron level, 9/2+[624], resulting in the 8- assignments for both of the ^{176}Yb and ^{178}Hf isomers. However, an 8- assignment for ^{174}Er is inconsistent with the proposed decay scheme and the ^{174}Tm ground state assignment. For the same reasons, a 0+ assignment for ^{174}Er is inconsistent. Also, the 8- isomers of ^{176}Yb and ^{178}Hf both decay by strong IT branches [Led78]. This research suggests that the measured ^{174}Er parent state has a

0+ spin and parity assignment. Attempts to solve the problems of the parent and daughter spins would require source intensities at least an order of magnitude greater than produced in this study since no evidence of isomers were seen using the 512 s tape cycle time. The SuperHILAC could possibly give a factor of 2 to 5 times greater beam intensities with ^{176}Yb enriched ion sources and an optimally running accelerator, but this would not be efficient enough. However, using the 2 to 5 times more intense 11.4 MeV/u ^{176}Yb beams obtainable at the UNILAC accelerator at GSI, would allow use of twice the previous target thickness. Yields of ~10 times the source intensities of this study then could be obtained, which might give new information.

In the A=168 mass chain, studied during the ^{170}Er beam experiment, the decay scheme of 8.8(3)-m ^{168}Dy was determined, Figure 5.4. Gamma- and x-ray intensities were obtained for the five previously identified γ transitions [Geh82] plus two new γ transitions and the two Ho K_α x rays, Table 5.2. During the analysis of the ^{168}Dy data, a new isomer, ^{168}Ho^m, was identified. The isomer had a measured half-life of 132(4) s from Ho K x rays, but the proposed IT γ transition was not measured due to its large internal conversion coefficient. The proposed decay scheme for ^{168}Ho^m, Figure 5.9b, is consistent with similar isomerism seen in ^{172}Lu [Val62], Figure 5.9a. Also during the data analysis for this mass chain, the Q_{β^-} value for 3.0-m ^{168}Ho^g [Kaw73] was determined. Gamma-ray coincident beta spectra were generated and Kurie plots calculated to determine β^- endpoints to three ^{168}Er levels, Figures 5.10-5.12. A Q_{β^-} value of 2.93(3) MeV is proposed for ^{168}Ho^g.

The new isotope, ^{169}Dy, was identified during the ^{170}Er beam experiment. High-energy β^- particles, with a 3.2(3) MeV endpoint, were observed to decay with

a 43(11) s half-life and showed no coincidences above background. Only a 1578-keV γ ray decayed with a short half-life of 35(11) s, while all other γ rays decayed with longer half-lives. Absence of Ho K x rays indicates that there was no internal conversion of γ rays from Dy β^- decay. The assignment of these activities to the decay of ^{169}Dy was based on the agreement of the experimental half-life, 39(8) s, and Q_{β^-} value, 3.2(3) MeV, with theoretical half-life predictions, 38 s [Kla84] and 64 s [Tak73], and mass table calculations for decay energies, 3.2 MeV [Hau88]. The proposed decay scheme for ^{169}Dy is shown in Figure 5.18.

The A=171 mass chain was studied in both the ^{176}Yb and ^{170}Er beam experiments in hopes of determining the decay scheme for ^{171}Ho [Ryk84, Ryk88, Ryk89]. The ^{176}Yb beam experiment yielded only enough information to confirm the discovery [Ryk84, Ryk88]. During the ^{170}Er beam experiment, 18 x rays and γ rays (see Table 5.7) were measured to decay with a 55(3) s half-life. A partial decay scheme, Figure 5.21, was devised for the decay of ^{171}Ho. Beta particle decay data for this mass chain had high-energy β^- particles that decayed with the correct half-life. Kurie analysis of β^- particles coincident with γ rays depopulating the 900-keV levels yielded a β^- endpoint of 2.3 (6) MeV and a Q_{β^-} value of 3.2(6) MeV.

The beta telescope used on OASIS, 718 μm Si/HPGe, produced very useful beta spectra for determining decay energies. Comparisons of the measured Q_{β^-} values with those calculated from nuclear mass tables has always been a goal of this research. The most recent nuclear masses calculations have been compiled by Haustein [Hau88] and made available on magnetic tape for ease of computer usage. Throughout this thesis, an average of the Q_{β^-} values calculated using all the mass tables was used. An average was chosen over using a particular mass formula for the following reasons: the region studied was close to β stability where most

formulae should predict masses well, and selecting a formula by its fit to known masses in this region would be biased towards formulae that used a large number of known masses in determining their calculation parameters. It was also believed by the author of this thesis that the mass formulae would scatter about the real masses, such that an average would yield reasonable values. The mass formula of Pape and Antony [Pap88] did not calculate masses for this region and the mass table of Wapstra *et al.* [Wap88] was a compilation of known masses with an occasional extrapolated mass. Neither of these two were used in the average calculations. Occasionally, the Q_{β^-} value calculated with the mass formula of Comay *et al.* [Com88] was 1/2 of all the other values calculate and would be excluded from the average. Table 6.1 shows the comparison of the Q_{β^-} values measured in this research and the average values calculated using the mass tables [Hau88]. The errors listed in Table 6.1 indicate that averaging the Q_{β^-} values calculated from the mass

Table 6.1. Comparison of measured Q_{β^-} values with theoretical values calculated using the nuclear mass tables [Hau88 and references therein].

Nuclide	Experimental Q_{β^-} Value (MeV)	Ave. Theoretical Q_{β^-} Value[a] (MeV)	Error (Theory - Exp.) (MeV)
^{168}Ho	2.93(3)	2.97 [9]	0.04(3)
^{169}Dy	3.2(3)	3.19 [9]	-0.01(30)
^{171}Ho	3.2(6)	3.16 [9]	-0.04(60)
^{174}Er	1.8(2)	1.[illegible] [8][b]	-0.09(20)

[a] Reported value is an average of the calculated Q_{β^-} values. The number of mass tables used in the calculation is in [ ].

[b] The Q_{β^-} value calculated using the mass table in reference [Com88] was not used in determining the average for this isotope due to it's large discrepancy with the other values calculated.

tables works well for this region.

The production of more undiscovered neutron-rich rare-earth nuclides by the methods of this research is not a very likely proposition. The actual experimental time required for identifying the new isotopes ^{169}Dy and ^{174}Er was approximately 3 days running time for each. Due to the fact that the cross sections drop off by an order of magnitude for each neutron added, producing new Dy, Ho, and Er isotopes would require ~30 days of experiments at similar source intensities. Since the most neutron-rich isotopes of Er and Yb were already used for this research, no gain can be obtained by changing the target/projectile selection. Increases in the beam intensity could help; however, the SuperHILAC was running extremely well during the ^{170}Er beam experiments, and probably only a factor of two increase could be obtained. Performing this research at the UNILAC accelerator in GSI would allow use of 11.4 MeV/u ion beams, with similar intensities as those from the SuperHILAC. This increase in beam energy would allow for more than twice the target material to be traversed before the ion beam energy dropped below the Coulomb barrier. With both an increase in the target thickness, due to increased beam energy, and the beam intensity, the new isotopes might be extended one more neutron in this region by multinucleon transfer reactions.

Production of these isotopes by other reaction mechanisms might be a more feasible possibility. Production of actinium and thorium isotopes using proton spallation reactions on ^{238}U yielded strong sources [Chu83]. Cross-sections were calculated in this research for ^{231}Ac, ^{233}Ac, ^{231}Th, and ^{233}Th. The same isotopes were produced in multinucleon transfer reactions of ^{238}U on ^{nat}W targets at GSI [Gip86]. The cross-sections for ^{231}Ac, ^{233}Ac, ^{231}Th, and ^{233}Th in the GSI study were approximately the same as those found in the proton spallation of ^{238}U.

However, due to differences in the beams used, protons at 28 GeV/u versus ^{238}U at 11.4 MeV/u, much more target material was subtended by the protons (~2 to 10 times thicker targets were used). Also, proton beams are easier to accelerate than heavy-ion beams, so ~100 times more intense beams were used. Both of these factors resulted much higher yields, of the order of 10^3 times more, from spallation of uranium with protons than from multinucleon transfer reactions of ^{238}U projectiles on ^{nat}W targets [Gip86]. There is a drawback to the proton spallation reactions in that most of the recoils stop in the target. Chemical separations of the uranium targets used in the proton spallation reactions [Chu83] were performed approximately every eight minutes to separate the actinium and thorium isotopes from the uranium.

APPENDIX A

COMPUTER CODE FOR ANALYSIS OF BETA SPECTRA

Variables involving 'SPEC' in their title deal with the binary file saving format also used when storing other spectra generated in this study.

```
C
C=====================================================================
      PROGRAM BETA
C=====================================================================
C
C                THIS PROGRAM CALCULATES THE THEORECTICAL BETA
C                SPECTRUM, FOR AN ALLOWED DECAY, GIVEN THE END
C                POINT ENERGY E0 IN MEV--THERE IS AN APPROXIMATION
C                TO THE RELATIVISTIC FERMI FUNCTION.
C
      IMPLICIT REAL*8( A-H,O-Z )
      REAL*4 Z,A,PH
      REAL*4 NB( 0:4095 )
      COMMON Z,A,PH
      INCLUDE 'SPEC_ID.TXT'
      RECORD /SPEC_ID/SPEC
C
C                SET ARRAY TO ZERO
C
      DO 933 I = 0,4095
            NB( I ) = 0
 933  CONTINUE
C
C                GET THE NECESSARY INFO
C
      TYPE '(A,$)',' ENTER THE Z AND A OF THE DAUGHTER NUCLEUS => '
      ACCEPT *,Z,A
      TYPE '(A,$)',' ENTER +1 FOR B- OR -1 FOR B+ => '
      ACCEPT *,PH
C
C                GET THE ENDPOINT AND ENERGY RANGE
C
      TYPE '(A,$)',' ENTER LOW ENERGY AND ENDPOINT IN keV => '
      ACCEPT *, RKEV1,RKEV0
 701  E1 = RKEV1 / 1000.0
      E0 = RKEV0 / 1000.0
      DD = 0.0102496
      GAM  =  ( Z / 137.0 ) * PH
      ILOW = E1 / DD
      IHIGH = E0 / DD
C
C                GET THE NORMALIZATION FACTOR
C
      TYPE '(A,$)',' ENTER THE NORMALIZATION FACTOR => '
      ACCEPT *, RNORM
```

```
      RNORM1 = 1E6
      ISTART = ILOW
      IF( ISTART .EQ. 0 ) ISTART = 1
      DO 1 K = ISTART, IHIGH
            E = DD * FLOAT( K )
            ETA = ( DSQRT( E * ( E + 1.022 ) ) ) / 0.511
            W = DSQRT( ETA**2 + 1.0 )
            W0 = ( DSQRT( E0 * ( E0 + 1.022 ) + 0.261 ) ) / 0.511
            CALL FERMI( E,F1 )
            PZAE = F1 * ETA * W * ( ( W0 - W )**2 )
C
C                 CALCULATE THE NORMALIZATION FACTOR
C
            CALL FERMI( E1,FMIN )
            ETMN = ( DSQRT( E1 * ( E1 + 1.022 ) ) ) / 0.511
            WMIN = DSQRT( ETMN**2 + 1.0 )
            PMIN = FMIN * ETMN * WMIN * ( ( W0 - WMIN )**2 )
            FAC = RNORM1 / PMIN
            NB( K ) = PZAE * FAC
 1    CONTINUE
C
C                 NOW REALLY CALCULATE THE NORMALIZATION
C
      SUM = 0.0
      DO I = ILOW, IHIGH
            SUM = SUM + NB(I)
      END DO
      DO I = ILOW, IHIGH
            NB(I) = ( NB(I) *( RNORM / SUM ) ) + 0.5
      END DO
      CALL SPIDZ1(SPEC)
      SPEC.NWORDS=8192
      SPEC.XMAX=4095
      SPEC.TYPE=R4D1
      SPEC.XLOW=0
      SPEC.XHIGH=SPEC.XMAX
      SPEC.SPID=1
      SPEC.SPLOC=RAM
      SPEC.BEGIN=0
      SPEC.END=SPEC.XMAX
      CALL SPEDIT1(SPEC)
      CALL SPWRIT1(SPEC,NB)
      STOP
      END
C
C=====================================================================
      SUBROUTINE KURIE( E,NC,FKUR )
C=====================================================================
      IMPLICIT REAL*8( A-H,O-Z )
      REAL*4 Z,A,PH
      COMMON   Z,A,PH
C
C                 THIS SUBROUTINE TAKES THE ENERGY E IN MEV,
C                 THE NUMBER OF COUNTS AT ENERGY E, NC, AND
C                 RETURNS THE KURIE PLOT FKUR.
C
```

```
      NW = NC
      ETA = ( DSQRT( E * ( E + 1.022 ) ) ) / 0.511
      W = DSQRT( ETA**2 + 1.0 )
      CALL FERMI( E,FZA )
      FKUR = DSQRT( NW / ( FZA * ETA * W ) )
      RETURN
      END
C
C=====================================================================
      SUBROUTINE FERMI( E,FF )
C=====================================================================
C
C                THIS ROUTINE ACCEPTS THE PHASE PH(+1 FOR
C                NEGATRONS AND -1 FOR POSITRONS), THE ATOMIC
C                NUMBER Z, OF THE RESIDUAL NUCLEUS, THE
C                KINETIC ENERGY E OF THE BETA PARTICLE (IN
C                MEV); AND RETURNS FF, THE VALUE OF THE FERMI
C                FUNCTION F(ZAE).
C
      IMPLICIT REAL*8( A-H,O-Z )
      REAL*4 Z,A,PH
      COMMON  Z,A,PH
C
      GAM = PH * Z / 137.0
      W = ( E + 0.511 ) / 0.511
      ETA = DSQRT( W**2 - 1.0 )
      Y = GAM * ( DSQRT( 1.0 + ETA**2 ) ) / ETA
      S = DSQRT( 1.0 - GAM**2 ) - 1.0
      FN = 2.0 * 3.14159 * Y / ( 1.0 - DEXP( -2.0 * 3.14159 * Y ) )
      F1 = 4.0 * ( 1.0 + S / 2.0 )
      X = 3.0 + 2.0 * S
      CALL GAMMA( X,GX,IER )
      GF = GX
      F2 = GF**2
      EX = 2 * S
      RHMC = 0.0062144 * ( A**0.33333 )
      F3 = RHMC**EX
      F4 = ( 1.0 + ETA**2 ) * ( 1.0 + 4.0 * ( GAM**2 ) ) - 1.0
      F4 = ( F4 / 4.0 )**S
      FF = F1 * F3 * FN * F4 / F2
      RETURN
      END
C
C=====================================================================
      SUBROUTINE GAMMA( XX,GX,IER )
C=====================================================================
      IMPLICIT REAL*8( A-H,O-Z )
C
C                THIS SUBROUTINE CALCULATES A SIMPLE GAMMA FUNCTON
C
      IF( XX - 34.5 ) 6,6,4
 4    IER = 2
      GX = 1.E38
      RETURN
 6    X = XX
      ERR = 1.0E-6
```

```
      IER = 0
      GX = 1.0
      IF ( X - 2.0 ) 50,50,15
 10   IF ( X - 2.0 ) 110,110,15
 15   X = X - 1.0
      GX = GX * X
      GOTO 10
 50   IF ( X - 1.0 ) 60,120,110
C
C                  SEE IF X IS NEAR NEGATIVE INTEGER OR ZERO
C
 60   IF ( X - ERR ) 62,62,80
 62   K = X
      Y = FLOAT( K ) - X
      IF ( DABS( Y ) - ERR ) 130,130,64
 64   IF ( 1.0 - Y - ERR ) 130,130,70
C
C                    X NOT NEAR A NEGATIVE INTEGER OR ZERO
C
 70   IF ( X - 1.0 ) 80,80,110
 80   GX = GX / X
      X = X + 1.0
      GOTO 70
 110  Y = X - 1.0
      GY = 1.+Y*(-.5771017+Y*(.9858540+Y*(-.8764218+Y*(.8328212+
     $      Y*(-.5684729+Y*(.2548205+Y*(-.05149930))))))))
      GX = GX * GY
 120  RETURN
 130  IER = 1
      RETURN
      END
```

APPENDIX B

MAXIMUM LIKELIHOOD COMPUTER CODE

On-line data measured in this research contained timing information with resolution equal to the tape cycle time divided by 4k (a 4096-channel LeCroy scaler was used). Time binning this data and using a least-squares decay fitting program does not extract all possible information. A maximum likelihood code was written to determine half-lives from these data. The code used assumes only one radioactive substance is being measured and no background radiations. The probability for observing decay between time t and $t + dt$ during measuring interval T is:

$$G(\lambda, t)\, dt = \lambda\, e^{-\lambda t} \left(1 - e^{-\lambda T}\right)^{-1} dt \qquad (1)$$

Now, the probability for observing M decays at times $t_1, t_2, \ldots, t_M$, is proportional to:

$$G(\lambda, t_1, t_2, \ldots, t_M) = \lambda^M \prod_{i=1}^{M} e^{-\lambda t_i} \left(1 - e^{-\lambda T}\right)^{-1} \qquad (2)$$

The probability, G, is a function of λ, and the procedure involves finding the value of λ which maximizes $G(\lambda)$ [or $\ln(G(\lambda))$]:

$$\ln\left(G(\lambda, t_1, t_2, \ldots, t_M)\right) = -M \ln\left(1 - e^{-\lambda T}\right) + M \ln \lambda - \sum_{i=1}^{M} \lambda t_i \qquad (3)$$

Using the relation between λ and $t_{1/2}$, $\lambda = \ln(2)/t_{1/2}$, $\ln(G(t_{1/2}))$was calculated by the code listed below. The output file was examined to determine the channel, or time, with the maximum probability. This time value corresponded to the maximum

likelihood half-life. A simple error procedure was used where the probability histogram was examined to ascertain the two time values where the probability dropped to 50% of the maximum value. The range of these two values has been found to correspond to 68% confidence limits [Lyo86]. However, since the ln of the probability was calculated, one looked to determine where the probability decreased by 0.693, i.e., -ln(1/2).

Variables involving 'SPEC' in their title deal with the binary file saving format also used when storing other spectra generated in this study. Formulae (1-3) above and the full details of their derivation can be found in Segré [Seg77].

```
C
C     ================================================================
      Program Maximumlikelihood
C     ================================================================
C
C     This program will read an SP format time spectra and will
C     preform a single component maximum likelihood fit.  It will
C     output a file of the probability for each channel(i.e.
C     half-life in same units as time spectra)..  Obviously the
C     maximum is the best half-life.
C
      dimension rdata1(0:16383),rdata2(0:16383)
      character*80 label
      character*30 infile,outfile
      include 'spec_id.txt'
      record /spec_id/spec
C
      type *, 'Program MAXILIKE.  Version 1.0 7/6/89.'
      type *, 'Preforms a single component maximum likelihood fit'
      type *, 'on an SP formatted time spectra.'
C
C     Get the spectra in question
C
      type '(a$)', ' filename of time spectra =>'
      accept '(a)', infile
      call spread1(infile,spec,rdata1)
      call spinfo(spec)
C
C     Get more info for the max-like-fit.
C
      type '(a$)', ' Enter the beginning and ending channels => '
      accept *,ilo,ihi
C
C     zero the output spectrum
C
```

```
      do i=0,spec.xmax
            rdata2(i)=0.0
      end do
C
C     Now do the fit!!!
C
      itot=0
      do i=ilo,ihi
            itot=itot+rdata1(i)
      end do
      type '(a$,i4)', ' Total number of events in window = ',itot
      ttot=ihi-ilo+1.0
      do i=ilo,ihi
            rlam=0.69314718/(i-ilo+1.)
            tlam=rlam*ttot
            tone=itot*alog(1-exp(-tlam))
            ttwo=itot*alog(rlam)
            tthree=0.0
            do j=ilo,ihi
                  if (rdata1(j).gt.0.0) then
                        l=rdata1(j)
                        do k=1,l
                              tthree=tthree+(rlam*(j-ilo+1.))
                        end do
                  end if
            end do
            rdata2(i)=(ttwo-tone-tthree)
      end do
C
C     Now save the probability spectrum
C
      type '(a$)', ' Filename for the output => '
      accept '(a)', outfile
      open(2,file=outfile,status='new')
      write(2,200)ilo,ihi
 200  format(1x,'Beginning channel = ',i4,' End channel = ',i4)
      do i=0,spec.xmax,5
            write(2,300)i,(rdata2(j),j=i,(i+4))
 300        format(1x,i4,5(1x,f14.6))
      end do
      stop
      end
```

REFERENCES

[Avi81] F.T. Avignone, H. Noma, D.M. Moltz, and K.S. Toth, Nucl. Instrum. & Methods **189**, 453 (1981).

[Bel86] R.A. Belshe and M.K. Lee, Nucl. Instrum. & Methods in Physics Research **A253**, 65 (1986).

[Bel87a] R.A. Belshe, EVA Reference Manual, Engineering Division PUB-3062, Lawrence Berkeley Laboratory (1987).

[Bel87b] R.A. Belshe, SUSIE Reference Manual, Engineering Division PUB-3061 Rev., Lawrence Berkeley Laboratory (1987).

[Bla52] J.M. Blatt and V.F. Weisskopf, *Theoretical Nuclear Physics*, (John Wiley and Sons, New York, 1952) p.627.

[Bos88] U. Bosch, W.-D. Schmidt-Ott, E. Runte, P. Tidemand-Petersson, P. Koschel, F. Meissner, R. Kirchner, O. Klepper, E. Roeckl, K. Rykaczewski, and D. Schardt, Nucl. Phys. **A477**, 89 (1988).

[Bro84] E. Browne, Nucl. Data Sheets **41**, 511 (1984).

[Bro86] E. Browne and R.B. Firestone, *Table of Radioactive Isotopes*, (John Wiley & Sons, Inc., 1986).

[Cha89] R.M. Chasteler, J.M. Nitschke, R.B. Firestone, K.S. Vierinen, P.A. Wilmarth, and A.A. Shihab-Eldin, Z. Phys. A **332**, 239 (1989).

[Chu83] Y.Y. Chu and M.L. Zhou, Phys. Rev. C **28**, 1379 (1983).

[Com88] E. Comay, I. Kelson, and A. Zidon, At. Data Nucl. Data Tables **39**, 235 (1988).

[Cow70] G.A. Cowan, "Heavy Element Synthesis by Prompt Multiple Neutron Capture", in *Proceedings of The Robert A. Welch Foundation*

Conferences on Chemical Research, XIII. The Transuranium Elements - The Mendeleev Centennial, edited by W.O. Milligan (Houston, Texas, 1970) p. 291.

[Dus88] G. Dussel, E. Caurier, and A.P. Zuker, At. Data Nucl. Data Tables **39**, 205 (1988).

[Geh82] R.J. Gehrke, R.C. Greenwood, J.D. Baker, and D.H. Meikrantz, Z. Phys. A **306**, 363 (1982).

[Gip86] K.-L. Gippert, E. Runte, W.-D. Schmidt-Ott, P. Tidemand-Petersson, N. Kaffrell, P. Peuser, R. Kirchner, O. Klepper, W. Kurcewicz, P.O. Larsson, E. Roeckl, D. Schardt, and K. Rykaczewski, Nucl. Phys. **A453**, 1 (1986).

[Gra84] R.L. Graham, J.S. Geiger, and M.W. Johns, Can. J. Phys. **50**, 513 (1972).

[Gre85] K.E. Gregorich, *Actinide Production in ^{136}Xe Bombardments of ^{249}Cf*, Ph.D. Thesis, LBL-20192 (1985).

[Gre87] R.C. Greenwood, R.A. Anderl, J.D. Cole, and H. Willmes, Phys. Rev. C **35**, 1965 (1987).

[Hau71] P.E. Haustein and A.B. Tucker, Nucl. Phys. **A173**, 321 (1971).

[Hau88] P.E. Haustein, At. Data Nucl. Data Tables **39**, 185 (1988). Nuclear mass tables referenced therein: [Pap88], [Dus88], [Möl88a], [Möl88b], [Com88], [Sat88], [Tac88], [Spa88], [Jän88], [Mas88], and [Wap88].

[Hub80] F. Hubert, A. Fleury, R. Bimbot, and D. Gardes, Supplément aux *Annales de Physique* **5**, 1 (1980).

[Hyd71] E.K. Hyde, *The Nuclear Properties of the Heavy Elements III, Fission Properties*, (Dover Publications, Inc., New York, 1971) p. 128.

[Jän88] J. Jänecke and P.J. Masson, At. Data Nucl. Data Tables **39**, 265 (1988).

[Kat78] R. Katajanheimo, T. Tuurnala, and E. Hammarén, Z. Phys. A **286**, 57 (1978).

[Kaw73] K. Kawade, H. Yamamoto, K. Tsuchiya and T. Katoh, J. Phys. Soc. Jpn **34**, 857 (1973).

[Kaw88] Y. Kawase and K. Okano, Z. Phys. A **330**, 231 (1988).

[Kla84] H.V. Klapdor, J. Metzinger, and T. Oda, At. Data Nucl. Data Tables **31**, 81 (1984).

[Kra79] J.V. Kratz, W. Brüchle, G. Franz, M. Schädel, J. Warnecke, G. Wirth, and M. Weis, Nucl. Phys. **A332**, 477 (1979).

[Led78] *Table of Isotopes, 7th Edition*, edited by C.M. Lederer and V.S. Shirely (John Wiley & Sons, Inc., New York, 1978).

[Lyo86] L. Lyons, *Statistics for nuclear and particle physicists*, (Cambridge University Press, Cambridge, 1986) p. 88-90.

[Mac86] H. Mach, A. Piotrowski, R.L. Gill, R.F. Casten, and D.D. Warner, Phys. Rev. Lett. **56**, 1547 (1986).

[Mas88] P.J. Masson and J. Jänecke, At. Data Nucl. Data Tables **39**, 273 (1988).

[Mei89] F. Meissner, K. Becker, W.-D. Schmidt-Ott, U. Bosch, V. Kunze, H. Salewski, E. Roeckl, H. Keller, R. Kirchner, O. Klepper, and D. Schardt, *GSI Scientific Report 1988, ISSN 0174-0814*, p. 32, (1989).

[Möl81] P. Möller and J.R. Nix, At. Data Nucl. Data Tables **26**, 165 (1981).

[Möl88a] P. Möller and J.R. Nix, At. Data Nucl. Data Tables **39**, 213 (1988).

[Möl88b] P. Möller, W.D. Myers, W.J. Swiatecki, and J. Treiner, At. Data Nucl. Data Tables **39**, 225 (1988).

[Möl89] P. Möller and J. Randrup, *Lawrence Berkeley Laboratory Report No. 27504* (1989), to be published in Nucl. Phys. A.

[Mor81] L.G. Moretto and R.P. Schmitt, Rep. Prog. Phys. **44**, 533 (1981).

[Nil69] S.G. Nilsson, C.F. Tsang, A. Sobiczewski, Z. Szymanski, S. Wycech, C. Gustafson, I.-L. Lamm, P. Möller, and B. Nilsson, Nucl. Phys. **A131**, 1 (1969).

[Nit83] J.M. Nitschke, Nucl. Instrum. & Methods **206**, 341 (1983).

[One72] R.A. O'Neil and D.G. Burke, Nucl. Phys. **A195**, 207 (1972).

[Pag72] L. Pages, E. Bertel, H Joffre, and L. Sklavenities, Atomic Data **4**, 1 (1972).

[Pap88] A. Pape and M.S. Antony, At. Data Nucl. Data Tables **39**, 201 (1988).

[Rös78] F. Rösel, H.M. Fries, K. Adler, and H.C. Pauli, At. Data Nucl. Data Tables **21**, 91 (1978).

[Rou69] J.T. Routti and S.G. Prussin, Nucl. Instrum. & Methods **72**, 125 (1969).

[Run85] E. Runte, K.-L. Gippert, W.-D. Schmidt-Ott, P. Tidemand-Petersson, L. Ziegeler, R. Kirchner, O. Klepper, P. O. Larsson, E. Roeckl, D. Schardt, N. Kaffrell, P. Peuser, M. Bernas, P. Dessagne, M. Langevin, and K. Rykaczewski, Nucl. Phys. **A441**, 237 (1985).

[Ryk84] K. Rykaczewski, P.O. Larsson, R. Kirchner, O.Klepper, E. Roeckl, D. Schardt, K.L. Gippert, E. Runte, W.-D. Schmidt-Ott, P. Tidemand-Petersson, N. Kaffrell, P. Peuser, W. Kurcewicz and J. Zylicz, Institut für Kernchemie Universität Mainz, Jahresbericht 1983, IKMz 84-1, p. 72, (1984).

[Ryk88] K. Rykaczewski, K.-L. Gippert, N. Kaffrell, R. Kirchner, O. Klepper, V.T. Koslowsky, W. Kurcewicz, W. Nazarewicz, E. Roeckl, E. Runte, D. Schardt, W.-D. Schmidt-Ott, and P. Tidemand-Petersson, GSI Scientific Report 1987, ISSN 0174-0814, p. 30 (1988).

[Ryk89] K. Rykaczewski, K.-L. Gippert, N. Kaffrell, R. Kirchner, O. Klepper, V.T. Koslowsky, W. Kurcewicz, W. Nazarewicz, E. Roeckl, E. Runte, D. Schardt, W.-D. Schmidt-Ott, and P. Tidemand-Petersson, Nucl. Phys. **A499**, 529 (1989).

[Sat88] L. Satpathy and R.C. Nayak, At. Data Nucl. Data Tables **39**, 241 (1988).

[Sch76] W.U. Schröder, J.R. Birkelund, J.R. Huizenga, K.L. Wolf, J.R. Unik, and V.E. Viola, Jr., Phys. Rev. Lett. **36**, 514 (1976).

[Sch77a] W.U. Schröder and J.R. Huizenga, Ann. Rev. Nucl. Sci. **27**, 465 (1977).

[Sch77b] W.U. Schröder, J.R. Birkelund, J.R. Huizenga, K.L. Wolf, and V.E. Viola, Jr., Phys. Rev. C **16**, 623 (1977).

[Seg77] E. Segré, *Nuclei and Particles, Second Edition*, (W.A. Benjamin, Inc., Massachusetts, 1977) p. 193.

[Shi84] V.S. Shirley, Nucl. Data Sheets **43**, 127 (1984).

[Spa88] L. Spanier and S.A.E. Johansson, At. Data Nucl. Data Tables **39**, 259 (1988).

[Tac88] T. Tachibana, M. Uno, M. Yamada, and S. Yamada, At. Data Nucl. Data Tables **39**, 251 (1988).

[Tak61] K. Takahashi, T. Kuroyanagi, H. Yuta, K. Kotajima, K. Nagatani, and H. Morinaga, J. Phys. Soc. Jpn **16**, 1664 (1961).

[Tak73] K. Takahashi, M. Yamada, and T. Kondoh, At. Data Nucl. Data Tables **12**, 101 (1973).

[Tak88] K. Takahashi, private communication (1988).

[Tuu78] T. Tuurnala, R. Katajanheimo, and O. Heinonen, Phys. Scripta **18**, 31 (1978).

[Val62] J. Valentin, D.J. Horen, and J.M. Hollander, Nucl. Phys. **31**, 373 (1962).

[Van76] R. Vandenbosch, M.P. Webb, and T.D. Thomas, Phys. Rev. Lett. **36**, 459 (1976).

[Wap88] A.H. Wapstra, G. Audi, and R. Hoekstra, At. Data Nucl. Data Tables **39**, 281 (1988).

[Wil60] R.G. Wille and R.W. Fink, Phys. Rev. **118**, 242 (1960).

[Wil80] W.W. Wilcke, J.R. Birkelund, H.J. Wollersheim, A.D. Hoover, J.R. Huiznega, W.U. Schröder, and L.E. Tubbs, At. Data Nucl. Data Tables **25**, 389 (1980).

[Wil88] P.A. Wilmarth, *Beta-Delayed Proton Emission in Neutron-Deficient Lanthanide Isotopes*, Ph.D. Thesis, LBL-26101 (1988).

[Wol84] H.-J. Wollersheim, GSI Preprint GSI-84-34 (1984).

[Zyc83] I. Zychor, K. Rykaczewski, H. Ahrens, H. Folger, W. Kurcewicz, K. Sümmerer, N. Kaffrell, and N. Trautmann, Radiochim. Acta **33**, 1 (1983).

LAWRENCE BERKELEY LABORATORY
UNIVERSITY OF CALIFORNIA
INFORMATION RESOURCES DEPARTMENT
BERKELEY, CALIFORNIA 94720